General Disclaimer

One or more of the Following Statements may affect this Document

- This document has been reproduced from the best copy furnished by the organizational source. It is being released in the interest of making available as much information as possible.

- This document may contain data, which exceeds the sheet parameters. It was furnished in this condition by the organizational source and is the best copy available.

- This document may contain tone-on-tone or color graphs, charts and/or pictures, which have been reproduced in black and white.

- This document is paginated as submitted by the original source.

- Portions of this document are not fully legible due to the historical nature of some of the material. However, it is the best reproduction available from the original submission.
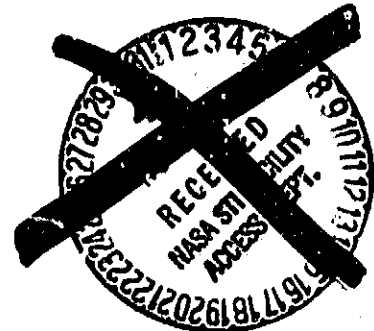
**PHASE AVERAGED MEASUREMENTS OF THE COHERENT STRUCTURE
OF A MACH NUMBER 0.6 JET**

A Thesis

by

SAIED EMAMI

Submitted to the Graduate College of
Texas A&M University
in partial fulfillment of the requirements for the degree of

MASTER OF SCIENCE

DEC 1983

Major Subject: Mechanical Engineering

PHASE AVERAGED MEASUREMENTS OF THE COHERENT STRUCTURE
OF A MACH NUMBER 0.6 JET

A Thesis

by

SAIED EMAMI

PHASE AVERAGED MEASUREMENTS OF THE COHERENT STRUCTURE
OF A MACH NUMBER 0.6 JET

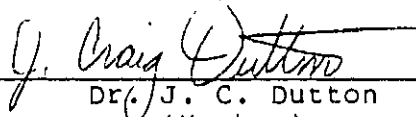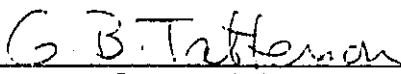A Thesis

by

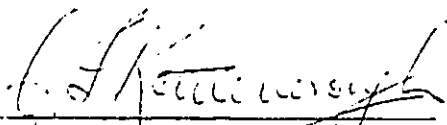SAIED EMAMI

Approved as to style and content by:

_____
Dr. G. L. Morrison
(Chairman of committee)

_____
Dr. J. C. Dutton
(Member)

_____   _____
Dr. G. B. Tatterson   Dr. G. R. Hopkins
(Member)   (Head of Department)

Dec 1983

ABSTRACT

Phase Averaged Measurements of the Coherent Structure

of a Mach Number 0.6 Jet.   (Dec 1983)

Saied Emami, B.S., Texas A&M University

Chairman of Advisory Committee: Dr. Gerald L. Morrison

The existence of a large scale structure in a Mach
number 0.6, axisymmetric jet of cold air has been proven by
previous work. In order to further characterize the
coherent structure, phase averaged measurements of the axial
mass velocity, radial velocity, and the product of the two
have been made. These measurements yield information about
the percent of the total fluctuations contained in the
coherent structure. These measured values were compared to
the total fluctuation levels for each quantity and the
result expressed as a percent of the total fluctuation level
contained in the organized structure at a given frequency.
These measurements were performed for five frequencies (St=
0.16, 0.32, 0.474, 0.95, and 1.26). All of the phase
averaged measurements required that the jet be artificially
excited.

The fluctuating profiles showed that the axial mass
velocity fluctuation maximized when excited at a frequency
of St = 0.474. The radial velocity fluctuations had a lower
amplitude for both the full wave and phase averaged

fluctuations compared to the axial mass velocity fluctuation. The Reynold's stresses tended to decay faster in amplitude than the axial mass velocity and radial velocity fluctuations for both the full wave and phase averaged components.

The coherence contours showed that the radial velocity fluctuations possessed higher levels of coherence than the axial mass velocity fluctuation and the Reynold's stresses.

The temporal and spectral content of the phase averaged radial velocity fluctuations showed that when the jet was excited at the frequency of St = 0.474, a high amplitude component at that frequency dominated the entire flowfield from X/D = 1 to 10. This fundamental frequency was accompanied by several relatively high amplitude harmonics. These harmonics were more dominant for the radial velocity fluctuations.

ACKNOWLEDGEMENTS

I wish to express my gratitude and sincere appreciation to Dr. G. L. Morrison for his constant assistance and encouragement during the course of this research which without his assistance, completion of my research objectives would have been impossible. I am also grateful to Dr. J. C. Dutton and Dr. G. B. Tatterson for the honor of having them on my committee. Special thanks to Mr. Eddie Denk for his assistance at the Turbomachinery Laboratories.

Finally, I would to acknowledge the financial support provided by NASA Langley through grant number (NAG1-11?).

TABLE OF CONTENTS

LIST OF FIGURES

LIST OF FIGURES (Continued)

LIST OF FIGURES (Continued)

LIST OF FIGURES (Continued)

LIST OF FIGURFS (Continued)

NOMENCLATURE

ALS   – arbitrary linear scale

A_m – mass velocity fluctuation sensitivity coefficient

A_T – stagnation temperature fluctuatuation sensitivity coefficient

A_v – radial velocity fluctuation sensitivity coefficient

D   – diameter of the jet

e' – fluctuating hot-wire voltage

e   – fluctuating hot wire voltage

$\overline{E}$ – mean hot-wire voltage

E_b – hot-wire bridge

f   – frequency (Hz)

G   – amplitude

m   – mass velocity

$\widetilde{m}$ – mass velocity fluctuation ($(\widetilde{\rho u})$) nondimensionalized by the mean value of the mass velocity $(\overline{\rho U})_e$ at the jet exit

R_w – hot wire resistance

St   – strouhal number (fD/U)

T   – stagnation temperature

T   – mean stagnation temperature

$\overline{U}_e$ – mean centerline jet velocity at the exit

$(\widetilde{\rho uv})$ – the Reynold stress was nondimensionalized by the mean mass velocity $(\overline{\rho U})_e$ and mean axial velocity $(\overline{U})_e$ at the jet exit

$\widetilde{v}$ – radial velocity fluctuation ($(\widetilde{v})$) nondimensionalized by the mean value of the axial velocity (U) at the jet exit

X   – downstream distance from the nozzle exit

z - radial distance from the jet centerline

α - yaw angle of crossed hot-wire probe relative to the local flow angle

ρ - density

CHAPTER I

INTRODUCTION

1.1 introduction

At the present time, jet exhaust noise is one of the
major noise problems challenging scientists and engineers.
With the development of large jet engines for use in high
speed commercial and military aircraft, high exhaust
velocities have made the jet noise problem very critical due
to environmental noise pollution, especially during the
aircraft's take off from metropolitan airports. Many
investigations have been performed in order to determine
ways to reduce this noise. In order to effectively reduce
noise from a jet of air, sufficient knowledge about noise
production mechanisms and noise source locations inside the
jet is desirable.

During the last three decades, there have been many
theories presented that mathematically describe the noise
generation of a jet of air. The works of Lighthill [1,2],
Ffowcs William [3], Ribner [4], Phillips [5], Pao [6],
Lilley [7], and Doak [8] are all capable of predicting the
noise radiated from a jet of air with some degree of
accuracy. However, in order to calculate the noise, all

The format and style of this thesis follows that of the ASME
Journal of Fluids Engineering.

of these works must use empirical information about flow fluctuations in the jet. Therefore, the only way to determine the source functions is to experimentally measure the flow fluctuations required to calculate them. In jet flows, this is an almost insurmountable task due to the complexity of the source terms and direct measurement of the noise is much easier. However, by using dimensional analysis with the theories [1-8], it is possible to approximate the directivity of the acoustic field and the dependence of the sound intensity upon the velocity of the jet.

During the past several years, a new class of jet noise theories has been developed [9-17]. These theories are based upon the experimental evidence that there is a large scale organized structure in turbulent free shear flows [18-20]. This organized structure starts as an instability wave on the shear layer, is amplified and finally decays.

According to the theories, this organized structure in the jet is of prime importance in the noise production mechanism in both subsonic and supersonic flows. Because of these theories, a new range of noise reduction and suppression techniques might become available. The important inference is that the development of the large scale coherent structure (organized structure) might be controlled through the modification of initial conditions

and hence the noise which is generated by this organized structure might be reduced.

For low Reynolds number, transonic and supersonic jets [21-2` , a large scale organized structure which causes a major portion of the noise radiation has been experimentally confirmed. In subsonic jets, many experiments have been performed in order to determine the noise production mechanism. Mollo-Christensen [28] first discovered the coherent structure in subsonic jets for Mach numbers greater than 0.15 and less than 0.9 by using space-time correlations of the near pressure field. He also measured far field noise spectra and directivity patterns. It was believed that the coherent structure radiated acoustic energy more efficiently than a random structure.

Crow and Champagne [19] examined the organized structure in very low speed jets of air (Mach numbers less than 0.1) by using a speaker to excite the jets in the axisymmetric mode (n=0 mode number). They used both hot-wire anemometry and flow visualization to identify the flowfield. It was concluded that there was an orderly structure in the jets and this structure could be approximately characterized by a linear stability theory. They observed an instability wave in the shear layer leaving the nozzle exit. Further downstream there was a puff formation involving the whole jet column which scaled on the jet's diameter.

Chan [14], Lau, Fisher and Fuchs [20], and Moore [29]
furthered the investigation of the orderly structure in
subsonic jets. Chan [14] artificially excited a subsonic
jet and measured the wave properties of three different
modes having azimuthal mode numbers of n=0, 1, and 2. The
structure was modeled by a wave theory, and a linear
stability solution of a divergent shear flow was found to
adequately describe the local properties of the waves.
Thus, in subsonic jets, an orderly structure has been
observed and measured.

Experiments [21-25] have shown that for low Reynolds
number transitional supersonic jets there are instability
waves present which can be characterized by a linear
stability theory for the first several diameters of flow.
It was also shown that this instability produces a major
portion of the noise radiated by the jet. The instability
waves generate sound pressure level contours which are very
close in shape and amplitude to those generated by the high
Reynolds number jet. It was shown that it was highly
probable that the noise production mechanism in the low
Reynolds number jets and other high Reynolds number jets was
the same. If so, the theoretical approach taken by Tam
[9-12], Liu [15], Morris [17], and Chan [14] was
appropriate.

Morrison and Whitaker [30] measured the axial wave
number of the coherent structure in a Mach number 0.6 jet

for several frequencies. It was found that the axial wave number frequency relationship for their jet and those of several other investigators for both natural and excited jets with Mach number greater than 0.3 remained the same. For these jets, the Reynolds numbers ranged from 3,700 to over 500,000, the Mach number ranged from 0.3 to 2.5, and some of the shear layers were laminar and others were turbulent with various thickness. Therefore, in these compressible jets, the importance of initial shear layer thickness, whether the shear layer was initially laminar or turbulent, Mach number, or Reynolds number did not matter. These measurements were only for the axial fluctuations.

The overall noise level radiated by a Mach number 0.6 jet studied by Whitaker and Morrison [35] was observed to reach a maximum value around 30 degrees from the jet axis. It was found that the frequency content of this radiated noise was dependent upon the angle from the jet axis. As the angle from the jet axis increased, the spectra of the noise shifted to higher frequencies. When the jet was artificially excited, the noise production mechanism in the jet was found to be more responsive to mid-band excitation frequencies $(0.474 \leqslant St \leqslant 0.632)$.

This work will further identify the coherent structure in this Mach number 0.6 jet by determining the percent of the total flow fluctuations that are contained in the coherent structure at the various frequencies studied for

the axial mass flux $(\widetilde{\rho u})$, the radial velocity $(\widetilde{v})$, and the product of the two $(\widetilde{\rho uv})$.

.

CHAPTER II

MEASUREMEMENT PROCEDURE AND EXPERIMENTAL FACILITY

2.1 Measurement Precedure

The phase averaged[*]flow quantities were recorded by a computer based data acqusition system. This system recorded the artificial exciter signal input and the two hot-wire signals from the crossed hot-wires. The artificial exciter signal was used as a phase reference for phase averaging the hot-wire signals. The resulting wave form was spectrum analyzed. The spectral analysis indicated the presence of any harmonic components in the signal. The production of subharmonics, either half or two-thirds may indicate vortex pairing as shown by Browand and Laufer [31]. By monitoring these spectra at different axial locations, the possibility of vortex pairing and nonlinear interaction was investigated.

The crossed hot-wire measurements were performed using matched crossed hot-wires. The matching of the hot-wires was essential since it allowed instantaneous addition and subtraction of the voltages from the hot-wires using analog techniques. In this manner, two signals, one proportional

---

*The phase average signal is $q(t) = \lim_{N \to \infty} 1/N \sum_{n=0}^{N} q(t + n\tau)$ where τ is the period of the coherent structure in the jet.

to the axial mass velocity fluctuation and the other proportional to the radial velocity fluctuations were obtained. In addition, these two signals were multiplied together after being digitally recorded by a computer system in order to obtain a voltage that was proportional to the product of axial mass velocity fluctuations and radial velocity fluctuations.

All of the hot-wire data were decomposed into axial mass velocity, radial velocity and total temperature fluctuations using techiques outlined by Horstman and Rose [33] and Johnson and Rose [34] (see appendix A). In addition, a conditional sampling technique (phase averaging) was used to measure the phase averaged axial mass velocity, radial velocity and correlation of axial mass velocity and radial velocity. By obtaining phase averaged quantities, a comparison between full and phase averages of fluctuating components was made. It was experimentally determined that four hundred averages were required to accuratly evaluate the phase averaged quantities. The programs for the data acquisition and analysis ara in Appendix B.

2.2 Experimental Facility

The experiments were performed in a free jet test facility shown schematically in Figure 1. A round

ORIGINAL PAGE IS
OF POOR QUALITY
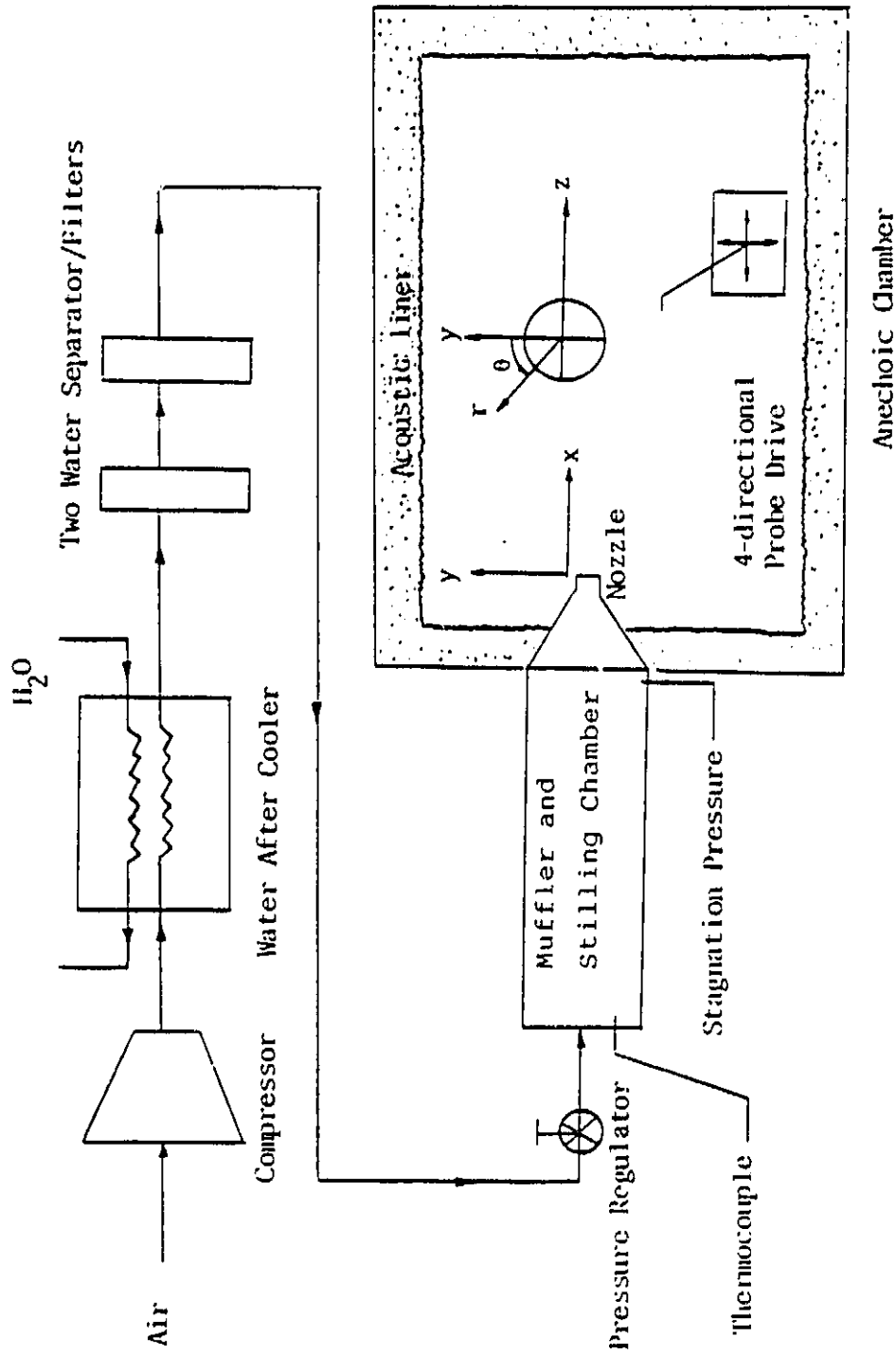
Fig. 1. Schematic diagram of jet test facility.

axisymmetric jet of air with exit diameter of 1.25 cm. was exhausted at atmospheric pressure into an anechoic chamber which had a free interior with dimensions of 2m * 2m * 2m. The walls of the anechoic chamber were lined with 23 cm thick fiberglass wedges. The air was supplied by a reciprocating compressor by way of a storage tank, water aftercooler, water separator/filters, an electronic pressure regulator, an acoustic muffler, and a 15 cm. diameter stilling chamber. The stilling chamber consisted cf a section of foam rubber followed by several perforated plates, a section of honeycomb and several fine screens. The flow was then accelerated through a nozzle whose contour is described by a third order polynomial. The contraction ratio for the nozzle was over 100:1. Previous measurements have shown that this flow facility produces a jet with a uniform exit velocity profile and a very low level of turbulence on the centerline of the jet.

Spectra of fluctuating quantities were obtained by using a Fast Fourier Transform algorithm on the data acquisition system. This system consists of a graphic video terminal, a digital plotter and a dot matrix printer connected to a Z80 based S100 microprocessor system. Analog data was recorded two ways. DC voltages were digitally recorded using a 12 bit analog to digital computer and AC voltages were digitally recorded by a high speed digital recorder interfaced to the computer.

The hot-wire probes which were custom manufactured were operated by a four channel TSI model 1050 anemometer system. A four degree of freedom (three linear and one rotation) probe drive system was used to traverse a hot-wire probe. The rotational degree of freedom was used for yawing the crossed hot-wire probes for calibration.

The method of excitation in this study was the same as the method used by Morrison and Wattanachayakul [36]. A function generator was used to provide square wave signals as input for the artificial excitation electronics. The device operated by generating sufficient voltage to create a spark across a 1.5 mm gap between two electrodes. This spark effectively put a small controlled disturbance in the jet. Electrodes for the excitation device consisted of 1/16 inch diameter, two percent thoriated tungsten rods. In order to stablize the spark at one location, the tips of the electrodes were ground into sharp points. These electrodes were mounted on the bottom of the jet nozzle ($\theta = 180^c$) placing them right at the exit of the jet (X/D=0). The electrode points were put into the shear layer with one electrode further into the jet than the other so that the spark would jump across the shear layer.

CHAPTER III

DISCUSSION OF RESULTS

3.1 Full Wave and Phase Averaged Flow Quantities

Radial distributions of the root mean square value of the axial mass velocity fluctuation, the radial velocity fluctuation and one component of the Reynold stress tensor were measured. These measurements were performed at axial locations of X/D = 1, 2, 3, 5, 7 and 10. Full wave and phase averaged fluctuation levels were measured for five excitation frequencies. The distribution of axial mass velocity for full wave and phase averaged fluctuations are presented in Figures 2 through 6. Note that in these figures, the mass velocity fluctuation $(\widetilde{\rho u})$ has been nondimensionlized by the exit value of the mean mass velocity $(\overline{\rho U})_e$, thus allowing comparisons between Figures 2-6 to be made.

These figures show that the maximum fluctuation levels initially occurred in the center of the shear layers where there was an inflection in the mean velocity profile. Morrison and Wattanachayakul [36] showed that the mean mass velocity profiles did not change when the jet was excited. However, the fluctuation profiles varied when the jet was excited at different frequencies. For the lower frequency of excitation, the radial location of the maximum amplitude fluctuation at X/D = 1 occurred at a radial position of 0.4. This radial position of maximum fluctuation level shifted
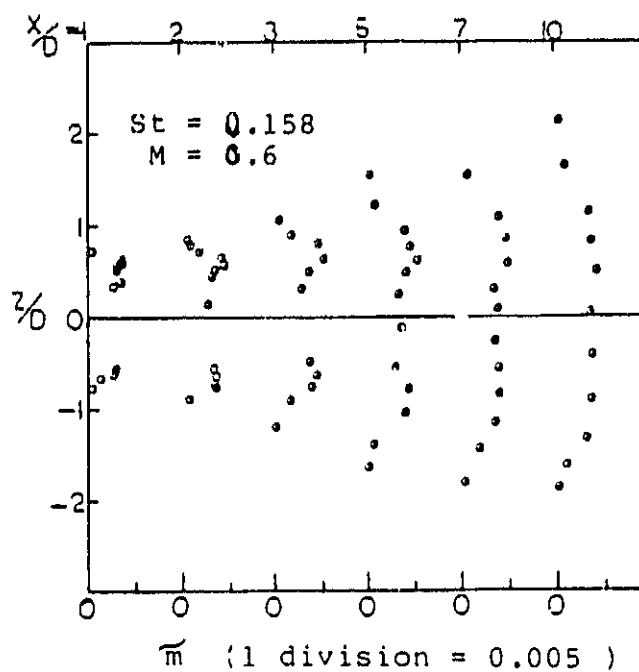
(a) Radial distribution of phase averaged mass velocity fluctuation
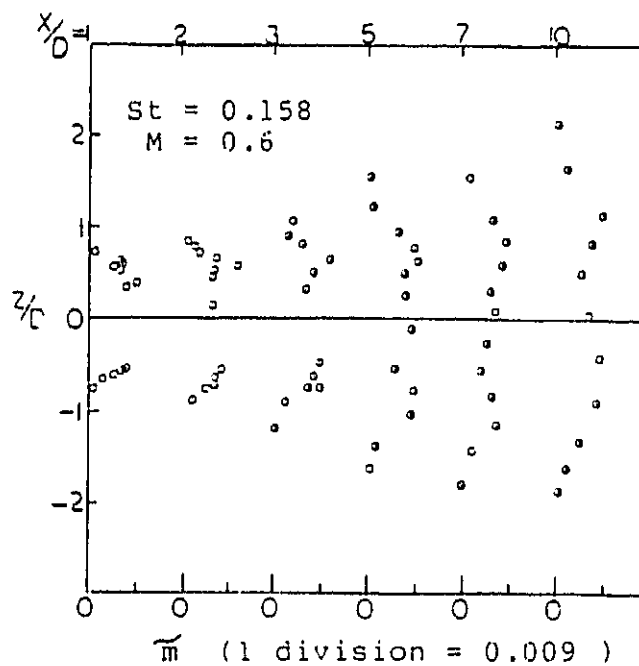
Fig. 2(b). Radial distribution of mass velocity fluctuation full spectrum
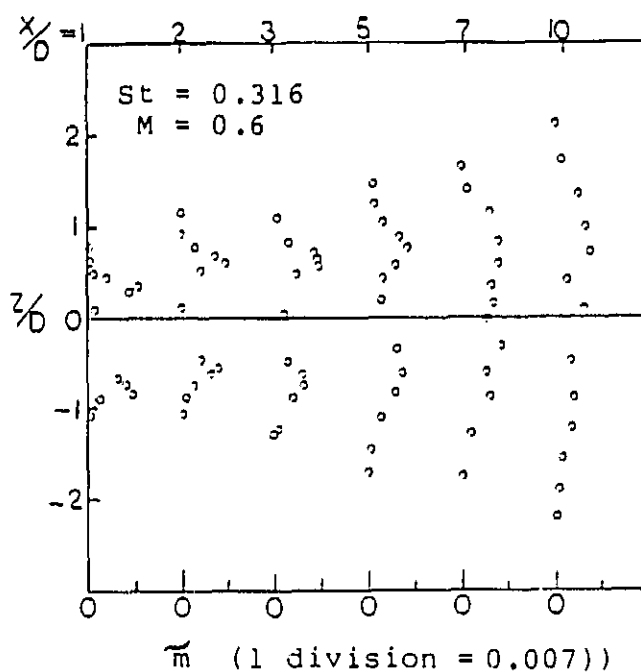
(a) Radial distribution of phase averaged mass velocity fluctuation
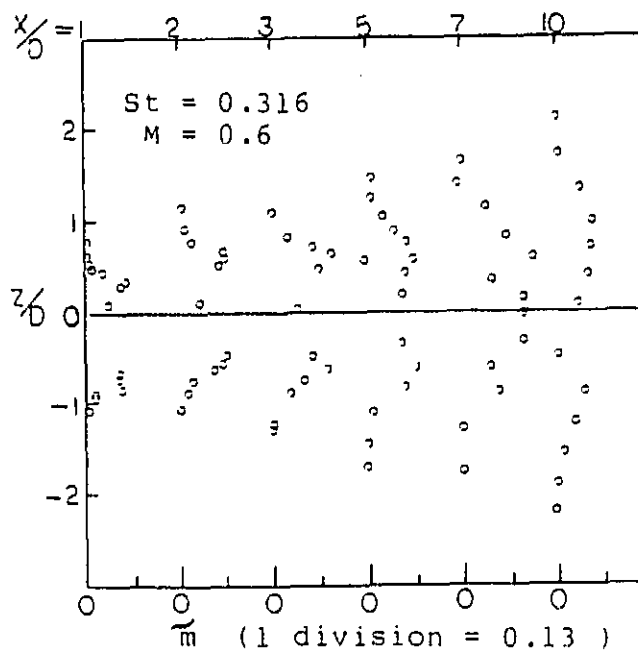
Fig. 3(b). Radial distribution of mass velocity fluctuation full spectrum
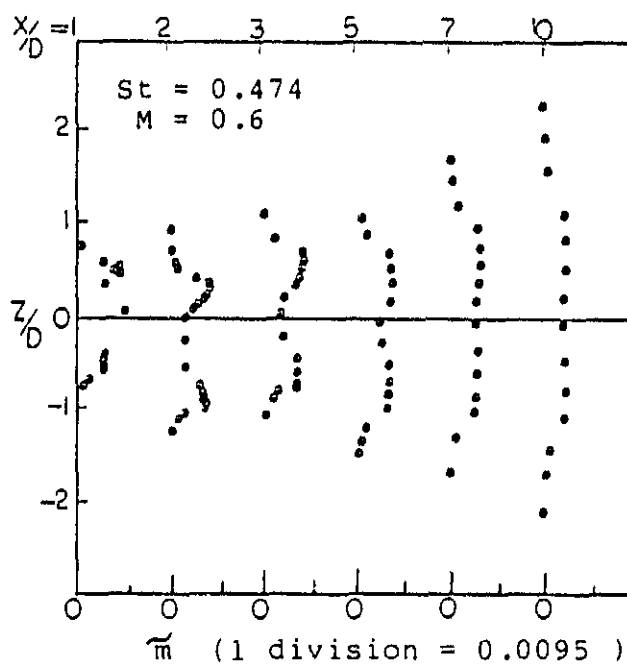
(a) Radial distribution of phase averaged mass velocity fluctuation
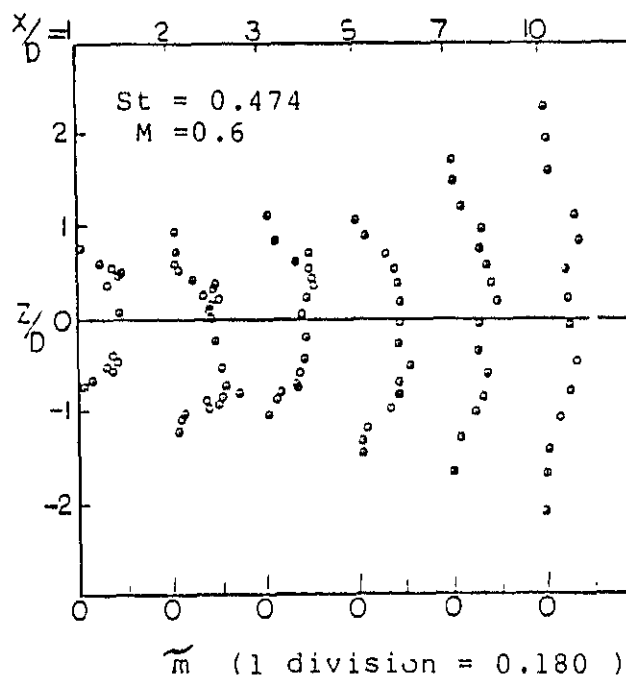
Fig. 4(b)· Radial distribution of mass velocity fluctuation full spectrum
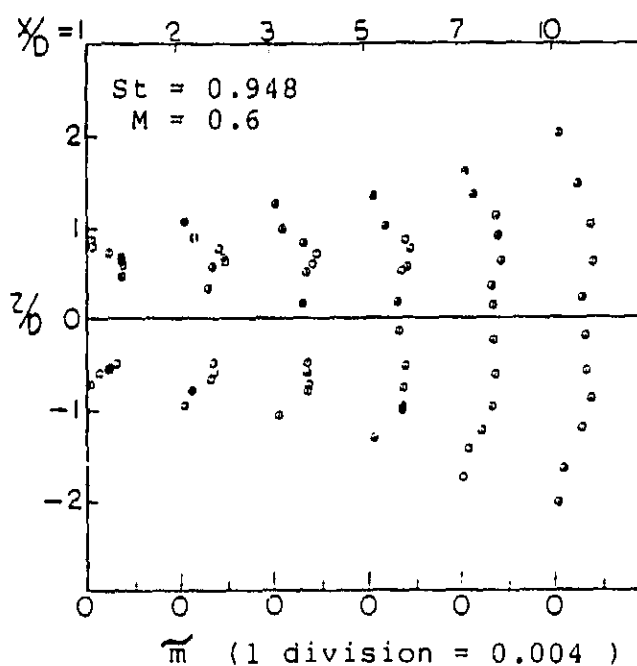
(a) Radial distribution of phase averaged mass velocity
    fluctuation
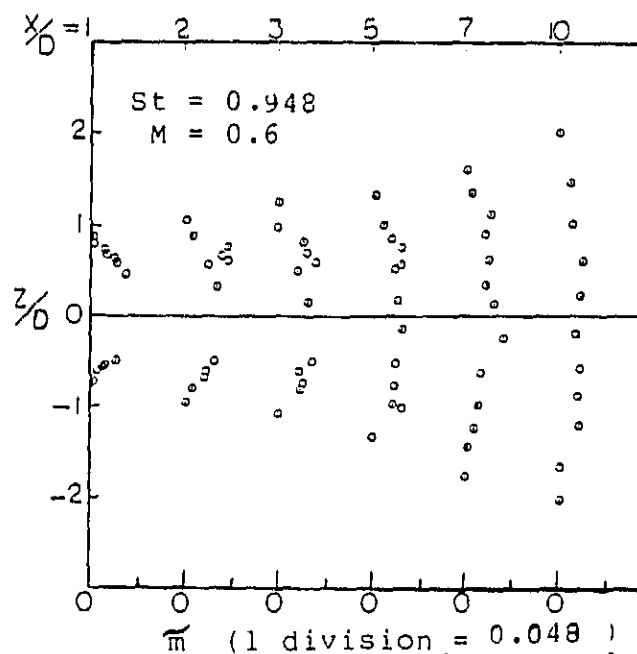
Fig. 5(b). Radial distribution of mass velocity fluctu-
           ation full spectrum
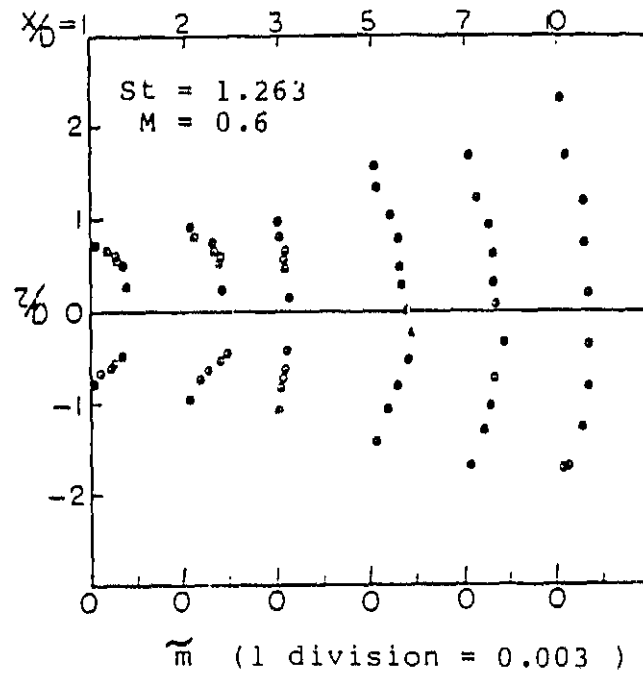
(a) Radial distribution of phase averaged mass velocity fluctuation
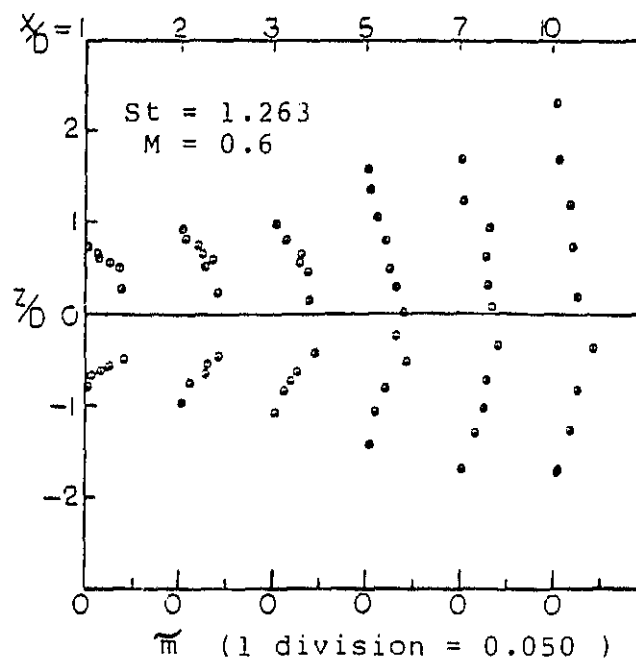
Fig. 6(b). Radial distribution of mass velocity fluctuation full spectrum

from Z/D = 0.4 to 0.6 for axial locations from X/D = 2 to X/D = 5 for both the full wave and the phase averaged fluctuations. Past X/D = 5, where the potential core of the jet ends and the mean velocity profiles become fully developed and self similar, the maximum amplitude of the flow fluctuations shift toward the centerline as the flow progressed downstream for both the full wave and the phase averaged components.

Figures 2 and 3 illustrate that for the low excitation frequencies, the full wave fluctuations of the mass velocity profile did not develop into self similar profiles. (become fully developed) by X/D = 10. However, the phase averaged component of the axial mass velocity had developed into a self similar profile at X/D = 7. Profiles with the maximum fluctuation level on the jet centerline and a Gaussian distribution were defined to be a fully developed profile.

Figure 4 shows that as the excitation frequency increased from St = 0.158 to St = 0.474, the amplitude of the fluctuation level increased for the phase averaged and the full wave components. The location of maximum fluctuation level was similar to the lower excitation frequency case. However, the higher the excitation frequency was, the sooner the profiles become self similar (fully developed). Figure 4 shows that the full wave and phase averaged mass velocity fluctuation profiles were similar to each other at an excitation frequency of St =

0.474, and was a fully developed fluctuation profile at X/D=6.

As the excitation frequency increased (Figure 5-6) from St = 0.948 to 1.263, the amplitude of the maximum fluctuation level decreased and the mass velocity profiles developed in a shorter axial space than the low excitation frequency case. Since the power input into the exciter remained constant for all excitation frequencies and (u) maximized at St = 0.474, the jet was more responsive to excitation at this frequency. This explains why Morrison and Whitaker [35] observed that more noise was radiated by this jet when excited at this frequency. Therefore, the Mach 0.6 jet is more responsive to mid-range frequency excitation of St= 0.316 t0 0.632 for both full wave and phase averaged components.

Figures 7 and 8 show the radial velocity profiles for the radial velocity fluctuations at excitation frequencies of St = 0.158 and 0.316. These figuresillustrate that the radial velocity fluctuations wore fully developed at X/D=5. However, as the frequency of excitation was increased above St = 0.316 (Figures 9-11), the radial velocity profile did not become fully developed until X/D=7 for both full wave and phase averaged fluctuations. The radial velocity fluctuation $(\widetilde{V})$ was nondimensionlized using the exit value of axial velocity $(\overline{U})_e$.

Figures 4 and 9 show that the radial profiles for the
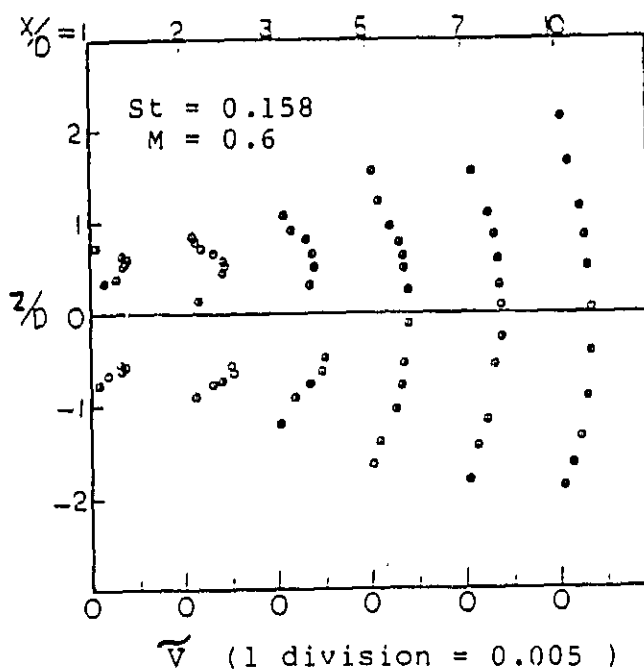
(a) Radial distribution of phase averaged radial velocity fluctuation
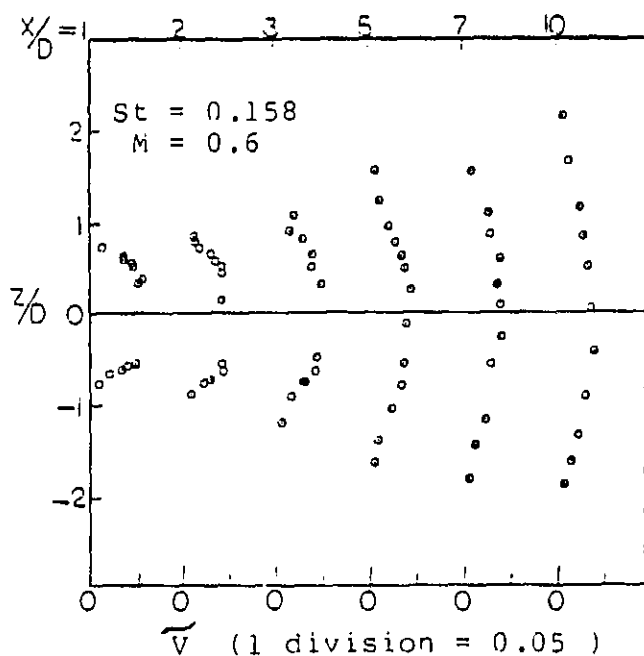
Fig. 7(b). Radial distribution of radial velocity fluctuation full spectrum
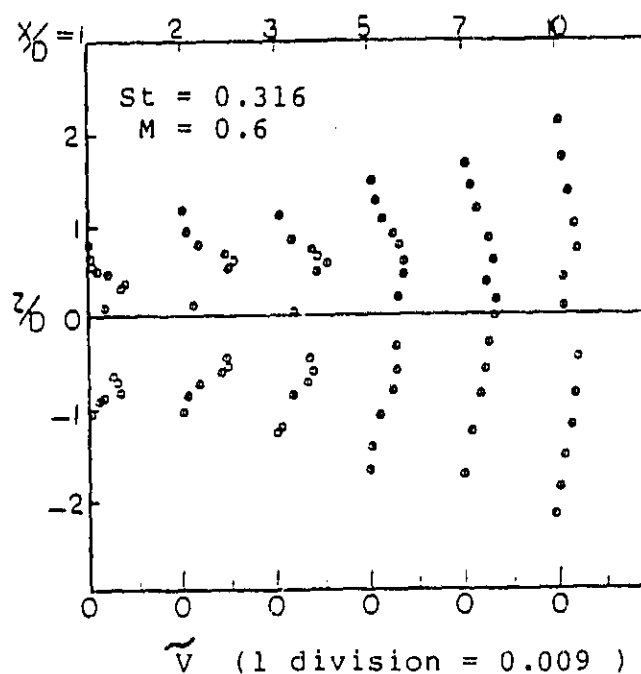
(a) Radial distribution of phase averaged radial velocity fluctuation
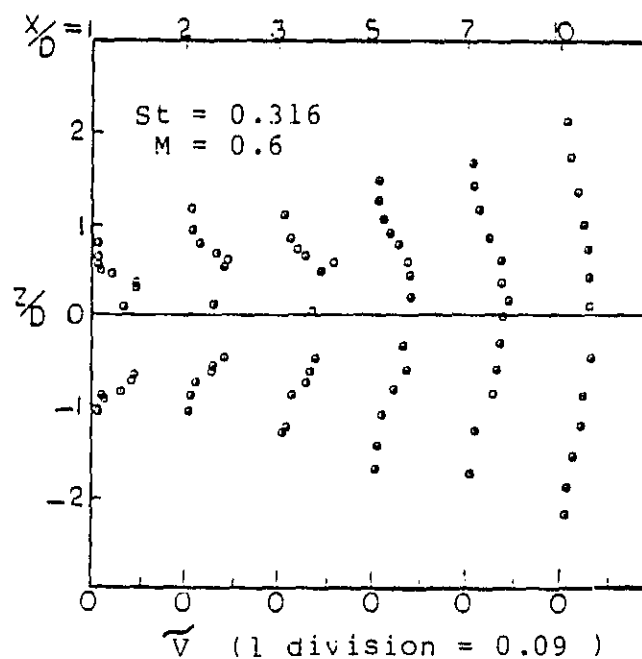
Fig. 8(b). Radial distribution of radial velocity fluctuation full spectrum
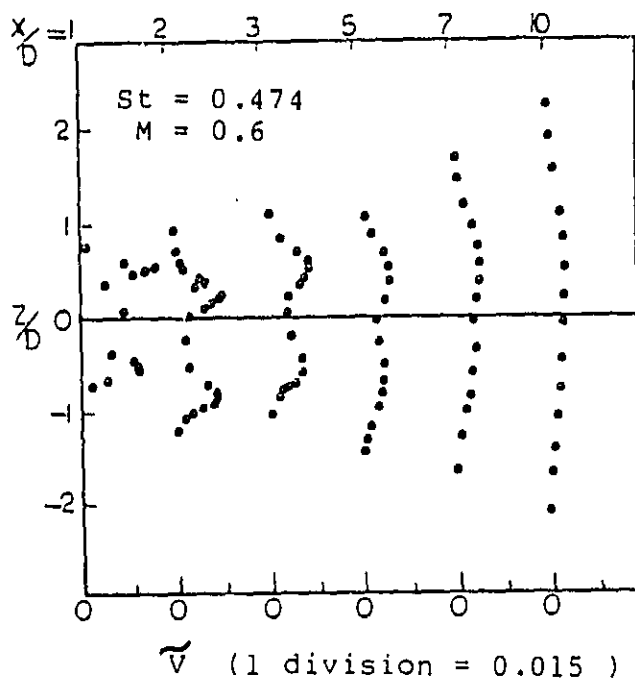
(a) Radial distribution of phase averaged radial velocity fluctuation
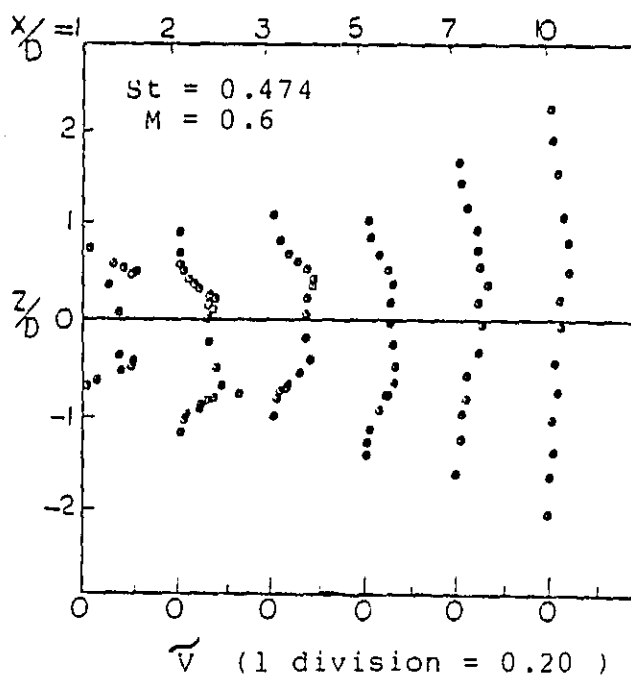
Fig. 9(b). Radial distribution of radial velocity fluctuation full spectrum
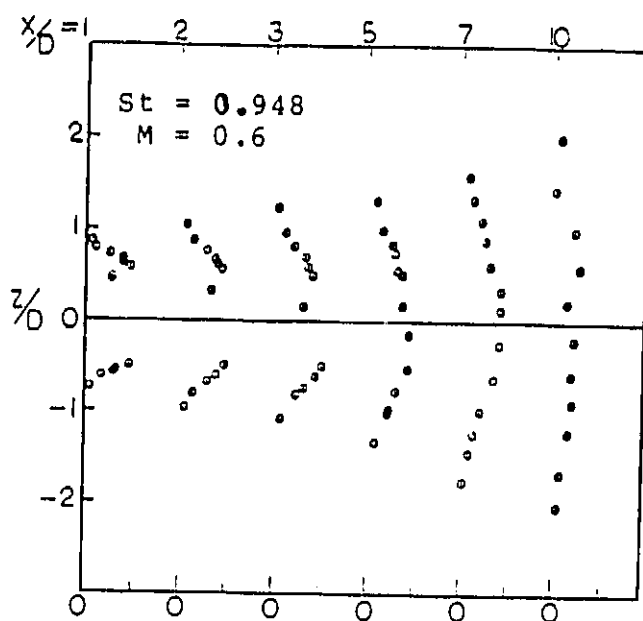
(a) Radial distribution of phase averaged radial velocity fluctuation
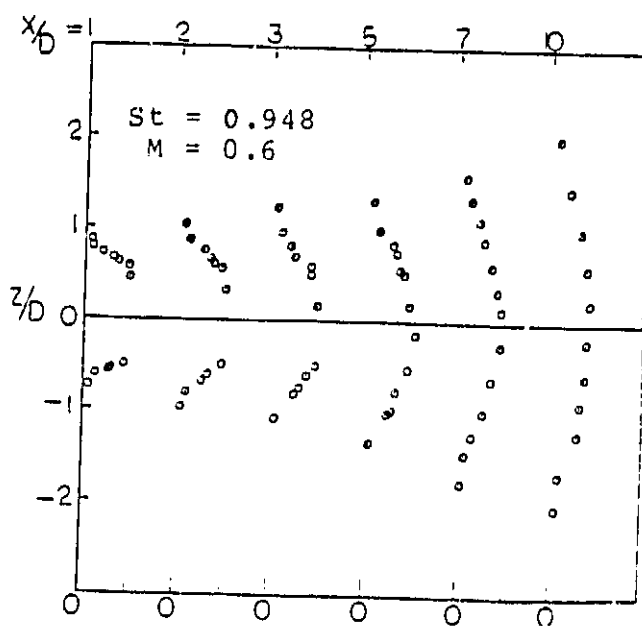
Fig. 10(b)· Radial distribution of radial velocity fluctuation full spectrum
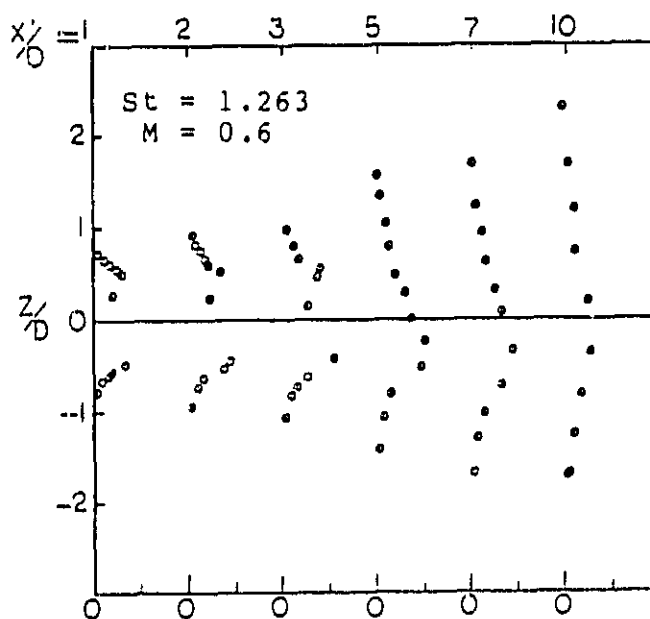
(a) Radial distribution of phase averaged radial veloci-
ty fluctuation
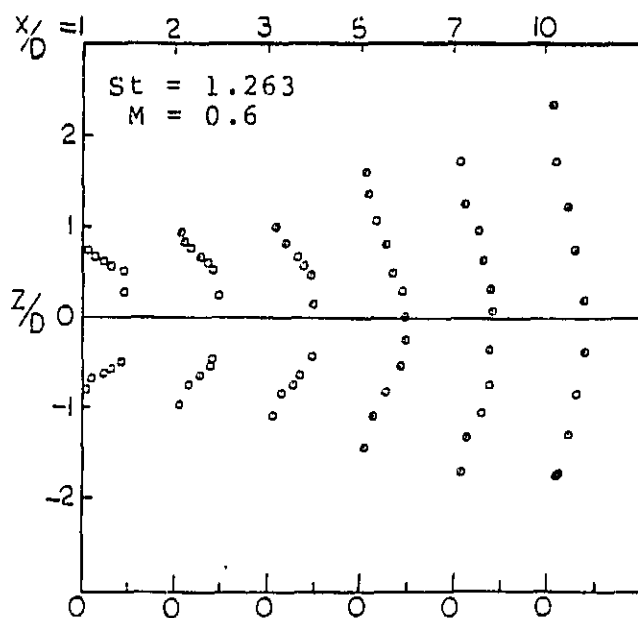
Fig. 11(b). Radial distribution of radial velocity fluc-
tuation full spectrum

axial and radial flow fluctuations at an excitation
frequency of St = 0.474 became fully developed between X/D =
6 and 7.

Figure 9 shows that at the excitation frequency of St
= 0.474, the jet attained its overall maximum amplitude for
the radial fluctuation for both the full wave and the phase
averaged components. Figures 10 and 11 illustrate that as
the excitation frequency increased above St = 0.474, the
maximum overall radial fluctuation amplitude decreased. In
general, the radial velocity fluctuation's radial dependence
compared to the axial mass velocity fluctuations had a lower
amplitude for the full wave and phase averaged fluctuations
and attained a fully developed radial profile sooner.

This difference in amplitude was expected since the
axial fluctuations include not only the axial velocity
fluctuations, but the density fluctuation as well. Figures
7-11 also exhibit that the maximum fluctuation levels of the
radial velocity fluctuation tend toward the centerline of
the jet more rapidly than the maximum mass velocity
fluctuation. The radial location of maximum radial velocity
amplitude was at a radial location of 0.4 for the first
diameter of the flow and then moved outward to Z/D = 0.7 for
the second and third diameters and then moved toward the
centerline at X/D = 5 for both the phase averaged and full
wave components.

The corresponding Reynolds stress profiles are shown

in Figure 12-16. The Reynolds stress profiles possess the
same general radial dependence as the radial velocity
fluctuations profiles for X/D < 5 at all excitation
frequencies. The Reynolds stresses tended to decay faster
in amplitude than the $(\widetilde{\rho u})$ and $(\widetilde{v})$ fluctuations for both the
full wave and phase averaged fluctuation. This indicates
that the coherence of turbulence is decaying as the flow
moves downstream since the correlation between the axial
and radial fluctuations was decaying. The Reynold stress
$(\widetilde{\rho uv})$ was nondimensionlized by the mean mass velocity $(\overline{\rho U})_e$
and mean axial velocity $(\overline{U})_e$ evaluated at the nozzle exit.

In summary, the velocity profiles of the axial mass
velocity fluctuations were different from $(\widetilde{v})$ and $(\widetilde{\rho uv})$ for
both full wave and phase averaged fluctuations. $(\widetilde{v})$ and $(\widetilde{\rho uv})$ fluctuations attained fully developed profiles by the
end of the potential core while the axial mass velocity
profiles were still developing at X/D = 7 to 10 depending
upon the excitation frequency. The axial mass velocity
profiles possessed larger amplitude fluctuations than the
$(\widetilde{v})$ and $(\widetilde{\rho uv})$ fluctuations for both full wave and phase
averaged fluctuations.

3.2 Coherence Level Contours

Characterization of the coherent structures is
valuable since it expands our basic understanding of jet
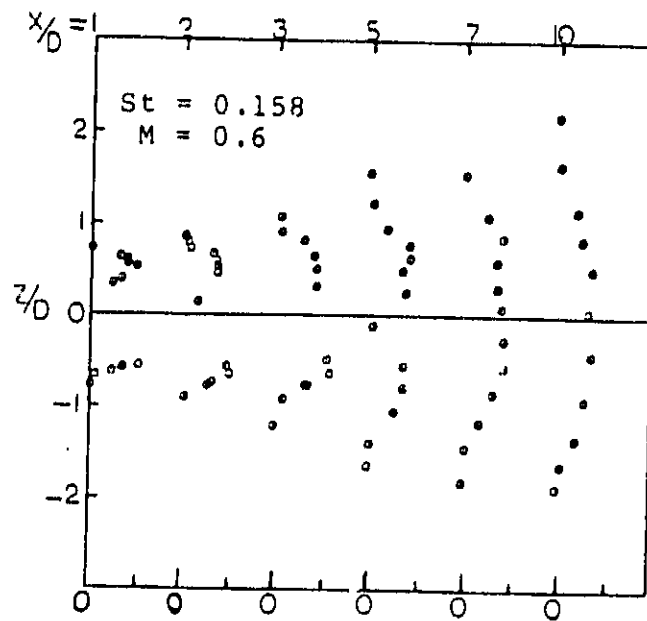
(a) Radial distribution of the phase averaged axial and radial flow fluctuation correlation
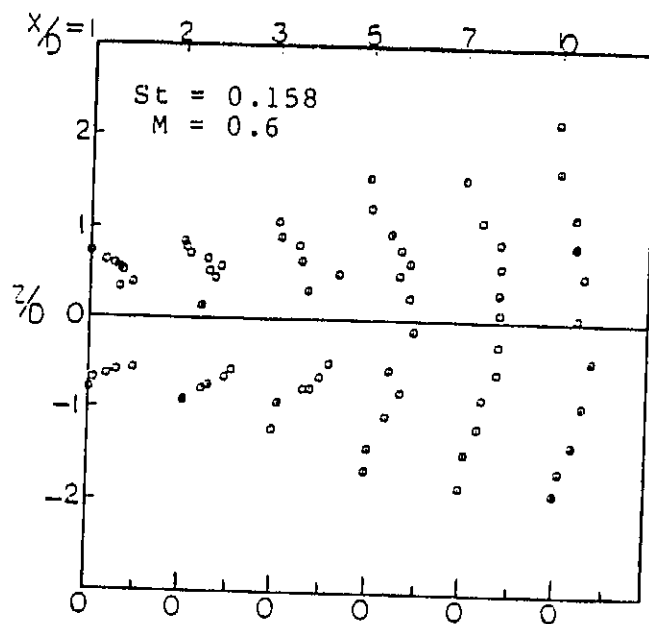
Fig. 12(b). Radial distribution of axial and radial flow fluctuation correlation
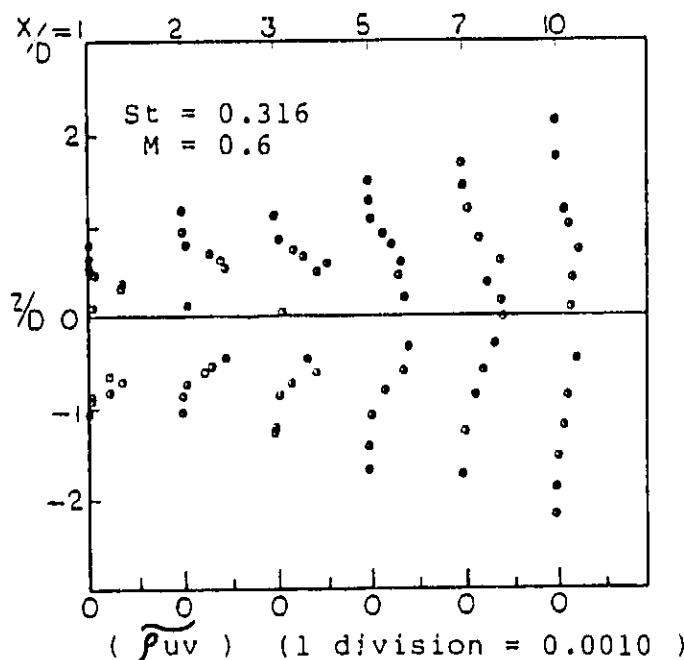
(a) Radial distribution of the phase averaged axial and
radial flow fluctuation correlation
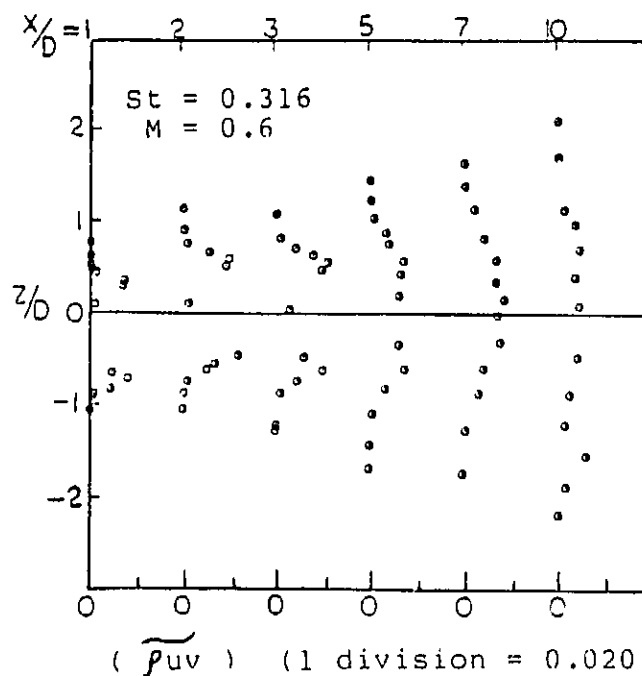
Fig. 13(b). Radial distribution of axial and radial flow
fluctuation correlation
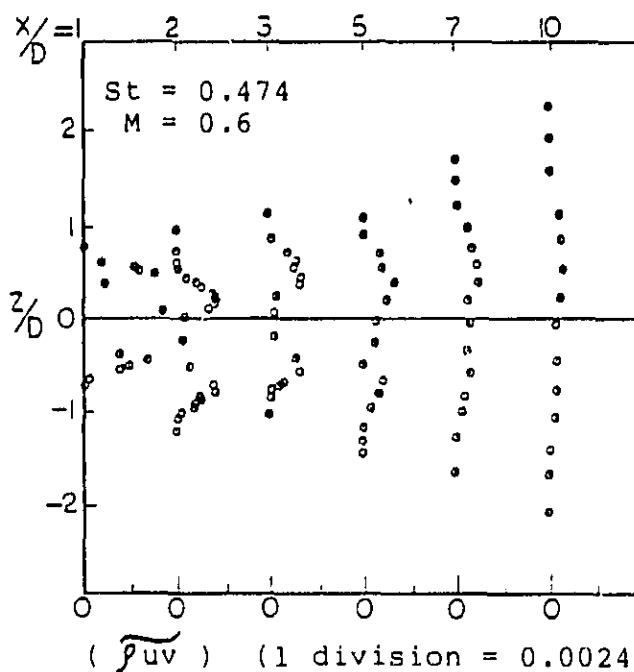
(a) Radial distribution of the phase averaged axial and
radial flow fluctuation correlation

Fig. 14(b). Radial distribution of axial and radial flow
fluctuation correlation
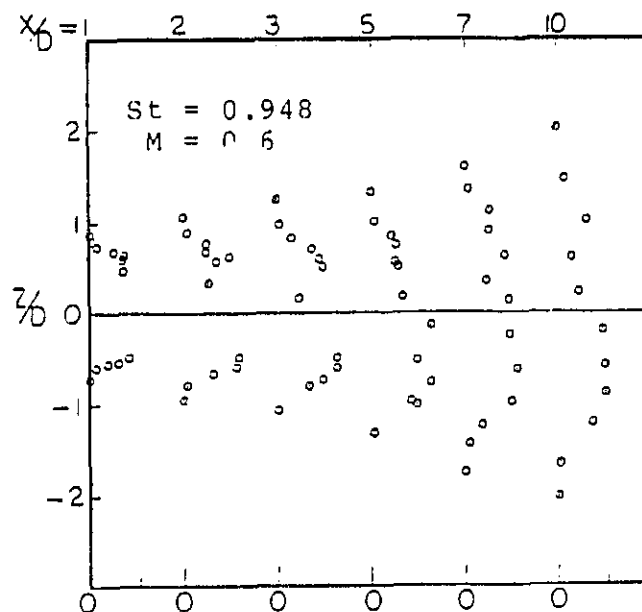
(a) Radial distribution of the phase averaged axial and
radial flow fluctuation correlation

Fig. 15(b). Radial distribution of axial and radial flow
fluctuation correlation
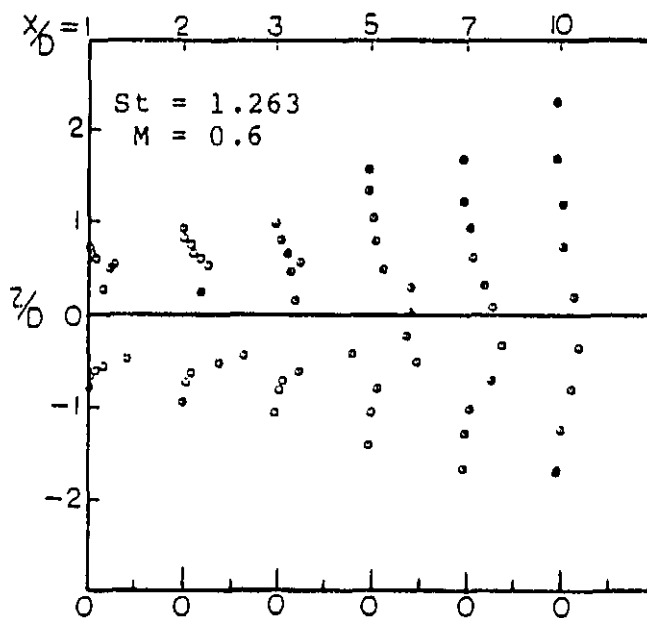
(a) Radial distribution of the phase averaged axial and
    radial flow fluctuation correlation
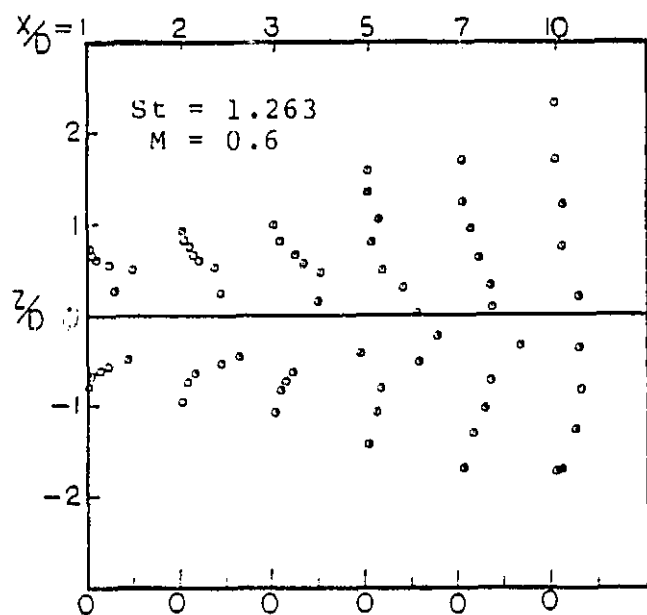
Fig. 16(b). Radial distribution of axial and radial flow
    fluctuation correlation

flowfields. In addition, several theoretical models ([6],
[8], [11] and [17]) suggested that these coherent structures
are of prime importance in the generation of noise. Some of
these theoretical models predicted the development of the
coherent structures present in the flowfield and then use
those results to predict the noise radiated by the jet. One
major problem facing these models is that no extensive
experimental information is available to confirm their
predictions.

Since the coherent structures play an important role
in the generation of noise, the exact percentage of the
overall fluctuations contained in the organized structure at
any location was measured for the Mach number 0.6 jet
exhausting at atmospheric pressure. The fraction of the
axial mass velocity, radial velocity and the correlation of
mass velocity and radial velocity due to organized structure
at excitation frequencies of St = 0.158, 0.316, 0.474, 0.948
and 1.263 (the percent of coherent structure) were obtained
by determining the ratio of the RMS value of the phase
averaged signal to the RMS value of the full wave hot-wire
fluctuation. These measurements were performed at axial
locations of X/D = 1, 2, 3, 5, 7 and 10, and many radial
locations thereby; generating spatial contours of coherence
level for each of the excitation frequencies.

Figures 17-21 show contours of axial mass velocity
fluctuation coherence levels. Figure 17 shows that the
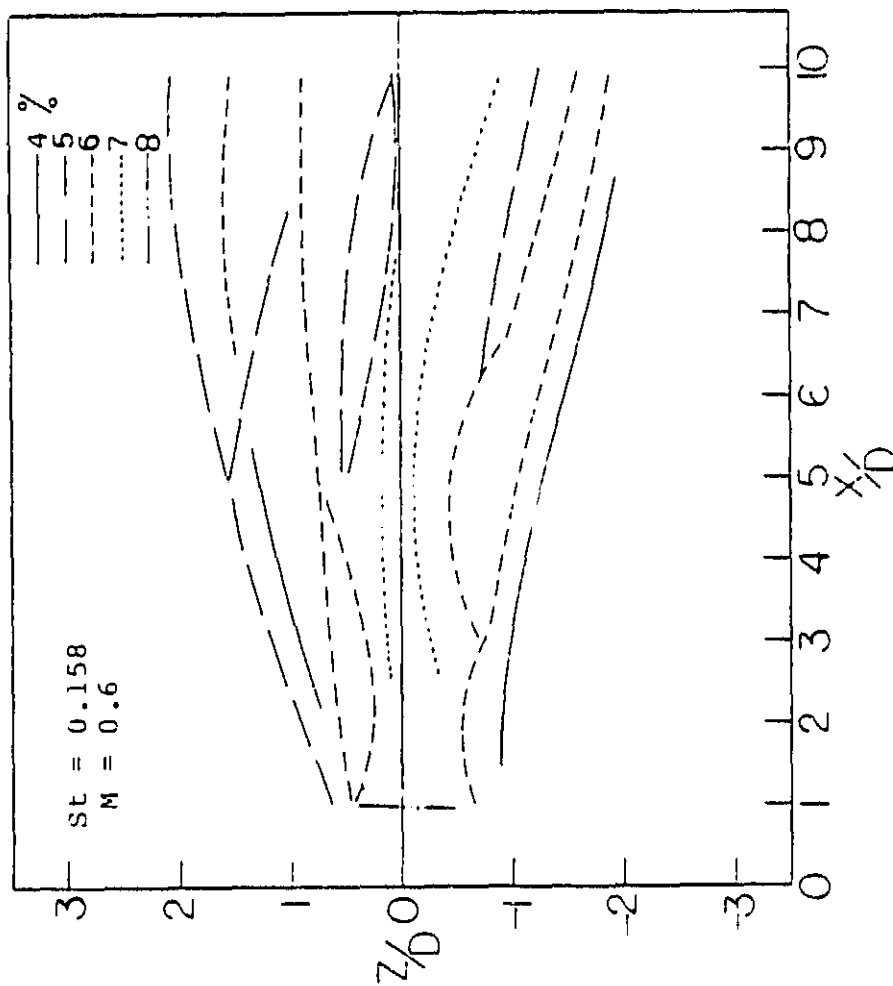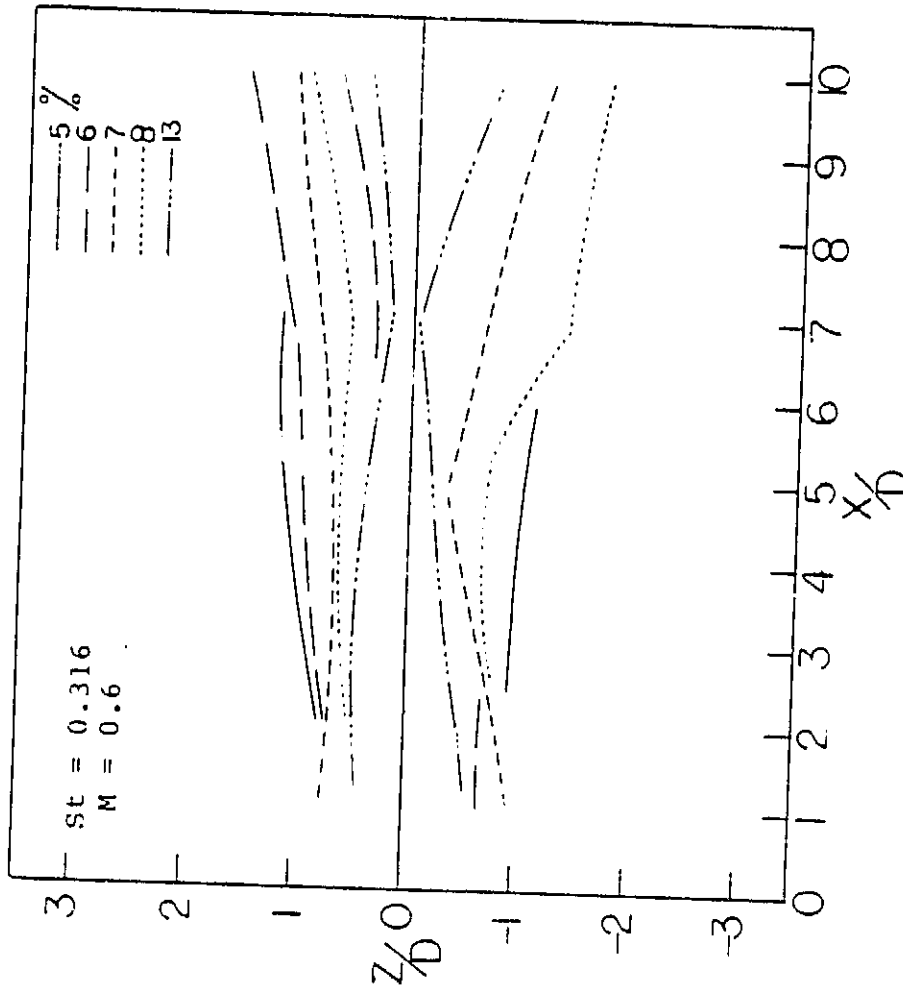
Fig. 17. Contours of coherence levels of phase averaged mass velocity fluctuation
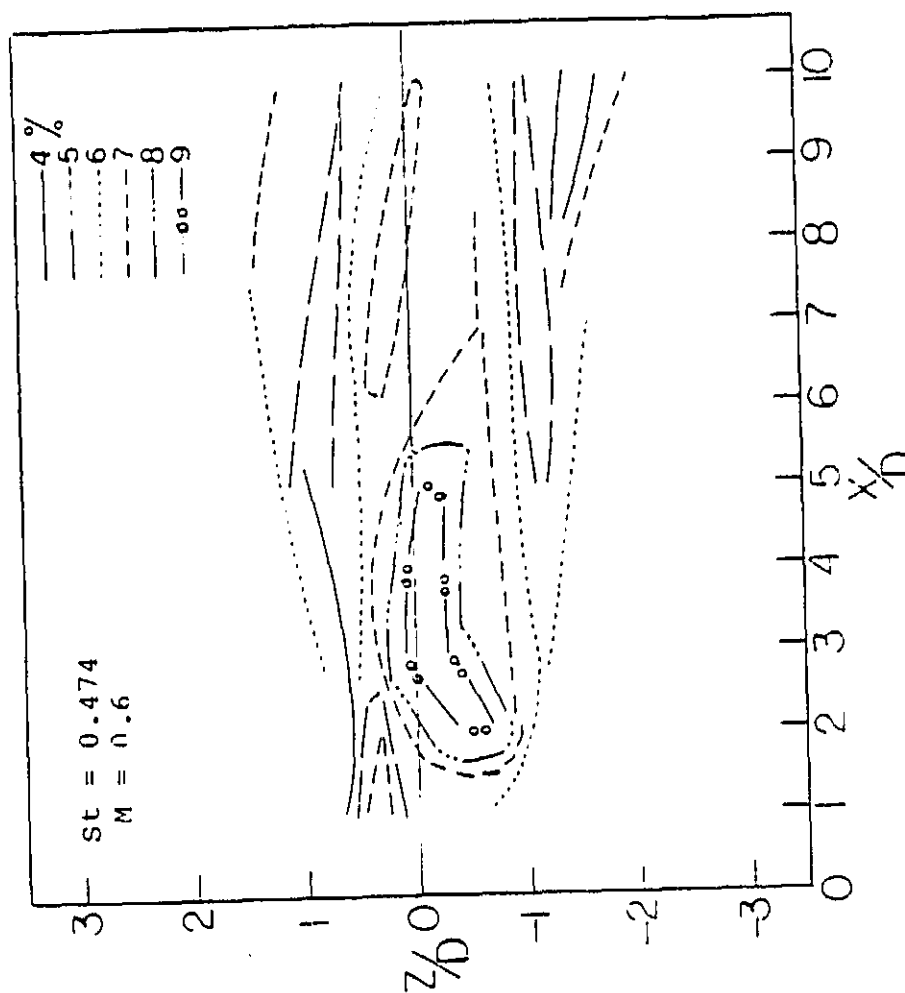
Fig. 18 . Contours of coherence levels of phase averaged mass velocity fluctuation

Fig. 19. Contours of coherence levels of phase averaged mass velocity fluctuation

Fig. 20. Contours of coherence levels of phase averaged mass
velocity fluctuation
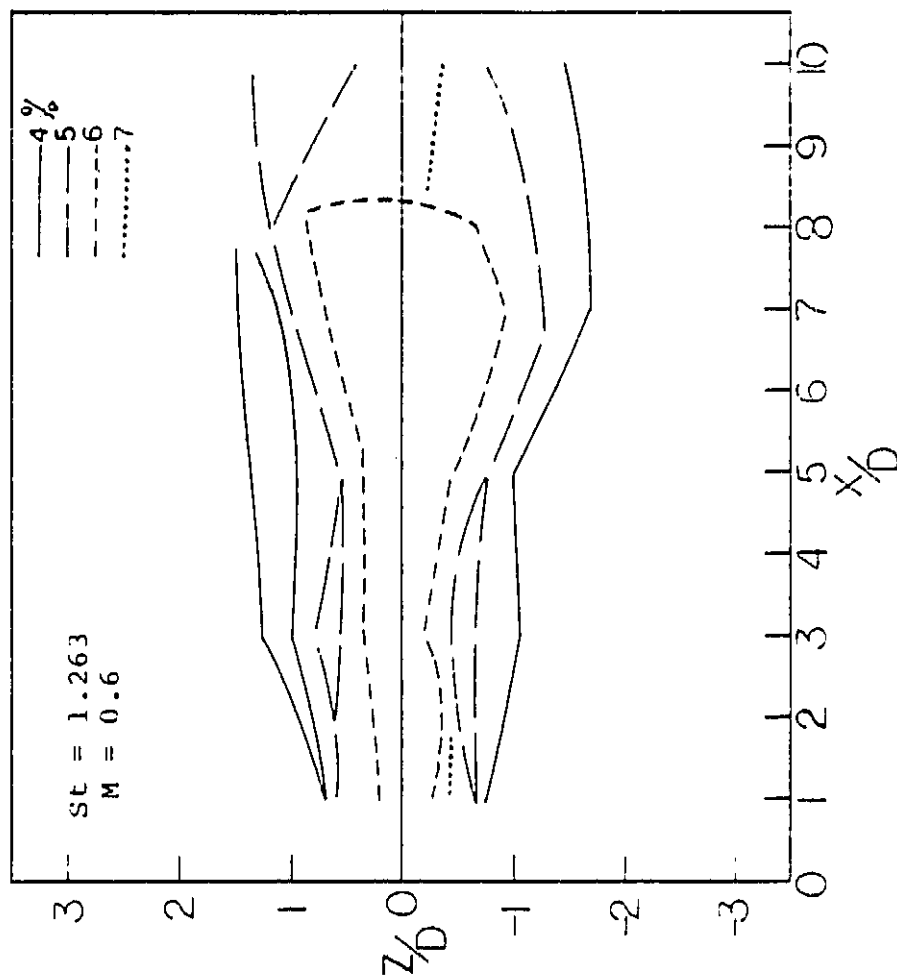
Fig. 21. Contours of coherence levels of phase averaged mass velocity fluctuation

percent of coherent structure varied between 4 and 8 percent for the very low excitation frequency of St = 0.158. The figure also reveals that the coherence level reached a minimum at the edge of the jet as the flow diverged downstream. However, traversing radially across the jet, the percent coherent structure gradually increased through the shear layers and reached the maximum coherency in the center of jet. This trend occurred up to the fifth diameter of the jet, which corresponds to the end of the potential core. After the fifth diameter, the coherency level at the jet centerline gradually decreased as the flow progressed downstream.

Figure 18 illustrates that as the frequency of excitation increased to St = 0.316, the coherency level increased to 13 % at radial locations Z/D = 0.4 through -0.4 and axial location of 1-10 diameters . As the edge of jet diverged downstream, the coherency level of the edge of the jet increased 1 % at X/D = 7. Lines of constant coherency level converged toward the jet center line up to X/D = 7 and then spread out as the jet moves downstream.

As was explained previously, the jet was more responsive and quite unstable at the excitation frequency of St = 0.474. Figure 19 shows that the coherency levels range from 4 to 9 percent. However, the coherency contour levels do not follow a regular trend. At this excitation frequency, the edge of the jet attains a high coherency

level compared to the coherency level in the shear layers. This was observed from X/D = 1 to the end of the potential core. Moving radially inward from the edge of the jet, the coherency levels decreased and reached a minimum in the shear layers. Continuing on toward the centerline, the coherency increased. Beyond the end of the potential core, the coherency at the edge of the jet increased and the coherency at the ce erline decreased as the flow progressed downstream. When the jet was excited at St = 0.474, the highest coherence levels of phas averaged mass velocity fluctuations were attained.

As the frequency increased to St = 0.948, the jet coherency started to follow a more regular and organized pattern and behaved similar to when the jet was excited at St = 0.158 and 0.316. Figure 20 shows that in this case, the centerline from X/D = 1 to X/D = 3 has the highest . coherency of 8 %, but the edge cf the jet contains the lowest coherency. It should be noted that the mass velocity fluctuations had fully developed velocity profiles at X/D = 3. After X/D = 3, the coherency on the centerline drops 2 % and stays the same all through the jet.

Figure 21 illustrates that the phase averaged mass velocity fluctuation coherence levels for a very high excitation frequency of St = 1.263 possessed more organized contour lines than the jet excited at St = 0.948. The edge of the jet contains the lowest coherency level until X/D =

7.5. Moving inward through the shear layers the coherency levels increase up to a maximum of 6 % at the centerline. This high coherency at the centerline continues through X/D = 7.5. After X/D = 7.5 the coherency level of 5 % which was dominate in the shear layers starts to move toward the centerline. Therefore this jet, excited at a very high frequency, has the lowest phase averaged mass velocity fluctuation coherence level.

Morrison and Whitaker [35] observed that this jet produced its maximum noise level when excited at St = 0.474. This corresponds to the case where the coherency level of the axial flow fluctuations is a maximum on the edge of the jet as opposed to on the centerline which was the case for all other excitation frequencies. This ten.'s to reinforce Mollo-Christensen's [28] hypothesis that the organized structures will emitt mor noise since the jet with more coherence on the edge of the jet produced more noise!

Figures 22-26 show that the radial velocity fluctuations possessed higher levels of coherency compared to the axial mass velocity fluctuations. In general, the radial velocity fluctuation coherence contour lines have a more organized pattern than those obtained for the axial mass velocity fluctuations at all excitation frequencies. Figure 22 shows that at a excitation frequency of St = 0.158, the edge of the jet contains a high level of coherency of 14 percent at all axial locations. At X/D = 1
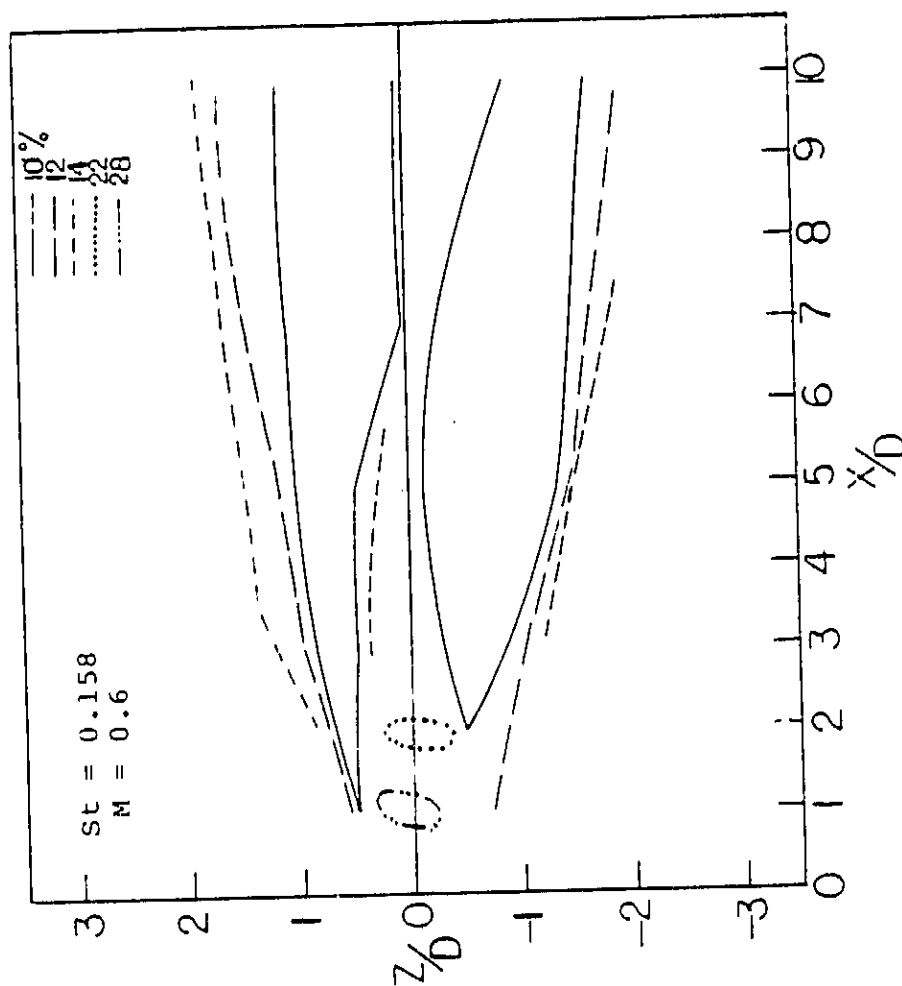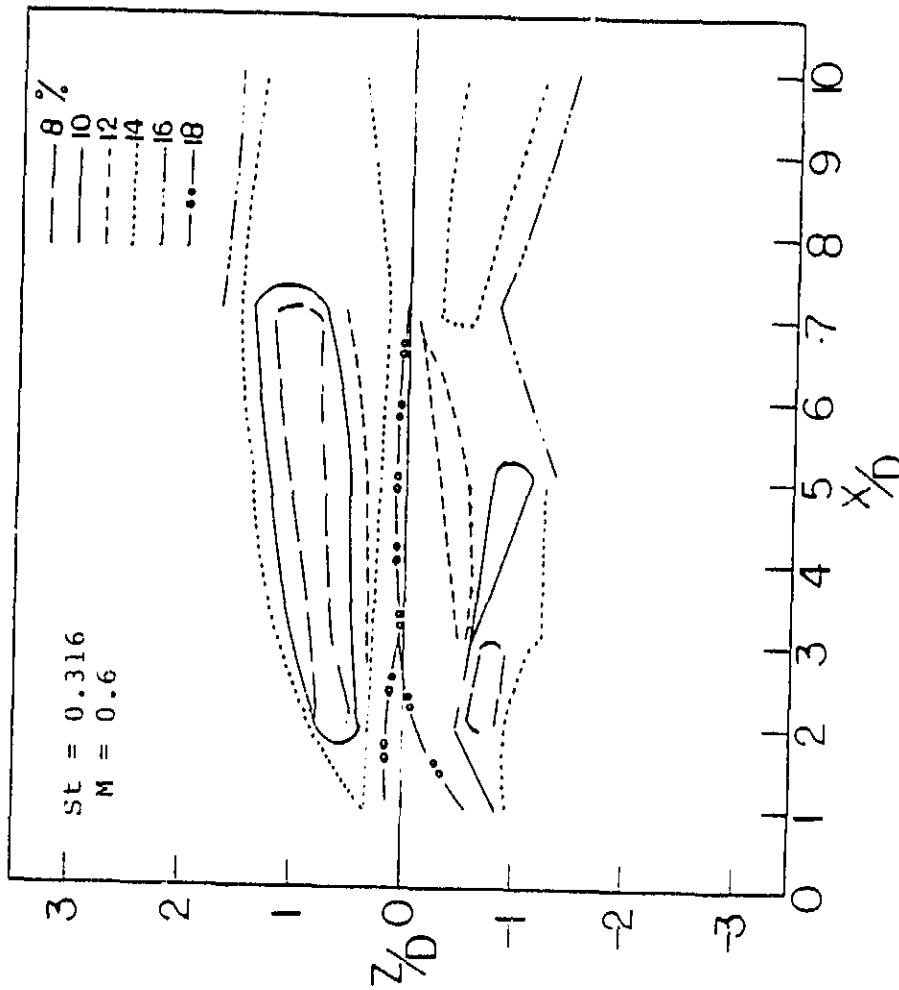
Fig. 22. Contours of coherence levels of phase averaged radial
velocity fluctuation
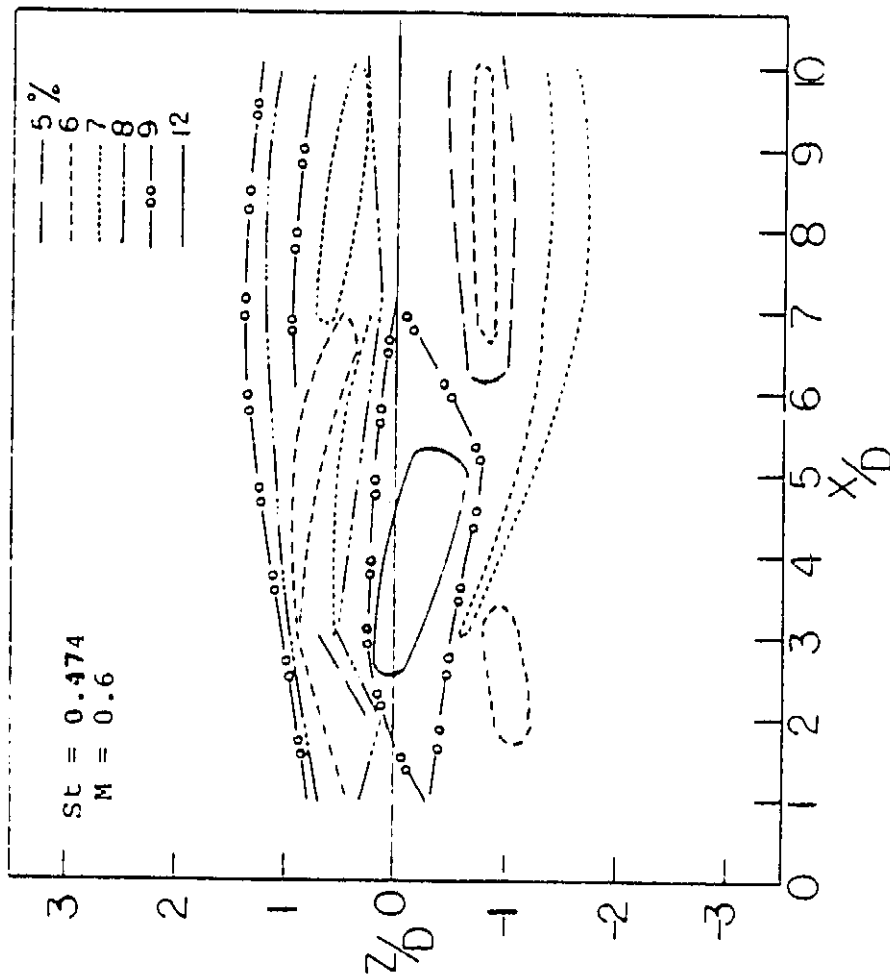
Fig. 23. Contours of coherence levels of phase averaged radial velocity fluctuation

Fig. 24. Contours of coherence levels of phase averaged radial velocity fluctuation

Fig. 25. Contours of coherence levels of phase averaged radial velocity fluctuation
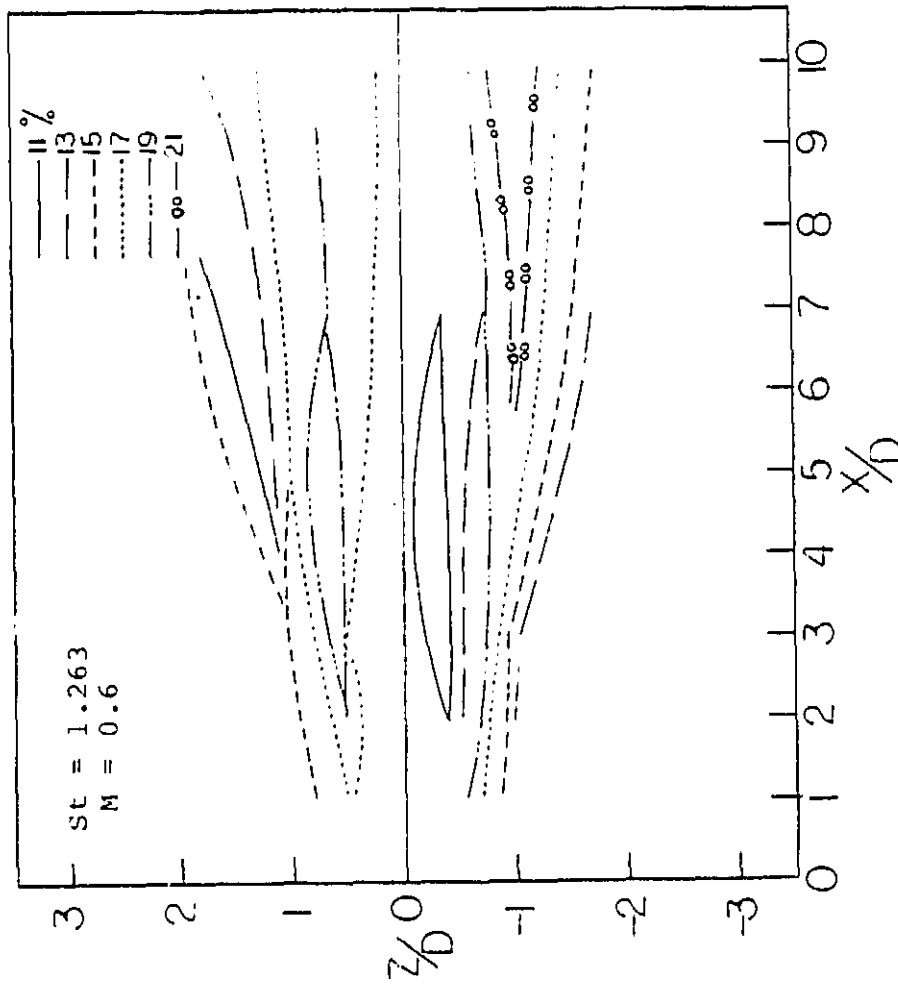
Fig. 26. Contours of coherence levels of phase averaged radial velocity fluctuation

and 2, the jet contains maximum coherency levels of 28 and
22 percent respectivley at the centerline. As the shear
layers grow together at the end of the potential core, the
centerline coherency decreases sharply from 22 to 10
percent. Moving radially inward at X/D = 5, the edge of the
jet has high coherency levels and decreases to a minmum of
10 percent.

Figure 23 shows that for St = 0.316, the jet has a
high coherency of 18 percent at the centerline through X/D =
7.5. Moving radially from the edge of the jet toward the
centerline the coherency level decreases at the shear layers
and increases from the shear layers to the centerline for
X/D = 2 to 7.5. After X/D = 7.5 , the coherency at the edge
of the jet and the centerline start to converge.

Figure 24 shows that the jet excited at St = 0.474
almost exhibits the same radial dependence as the jet
excited at St = 0.316. Figures 25-26 reveal that as
frequency of excitation increased to St = 0.948 and 1.263
the jet has higher overall radial coherency levels than
those obtained at the other excitation freqencies. Figure
26 shows that moving radially in from the edge of the
jet,the coherency level increased at the shear layers and
then decreased to a minimum at the center line.

Figures 27- 29 show the corresponding Reynold's stress
coherency levels. The Reynold's stress components measured
possesed lower coherencies than those obtained for axial
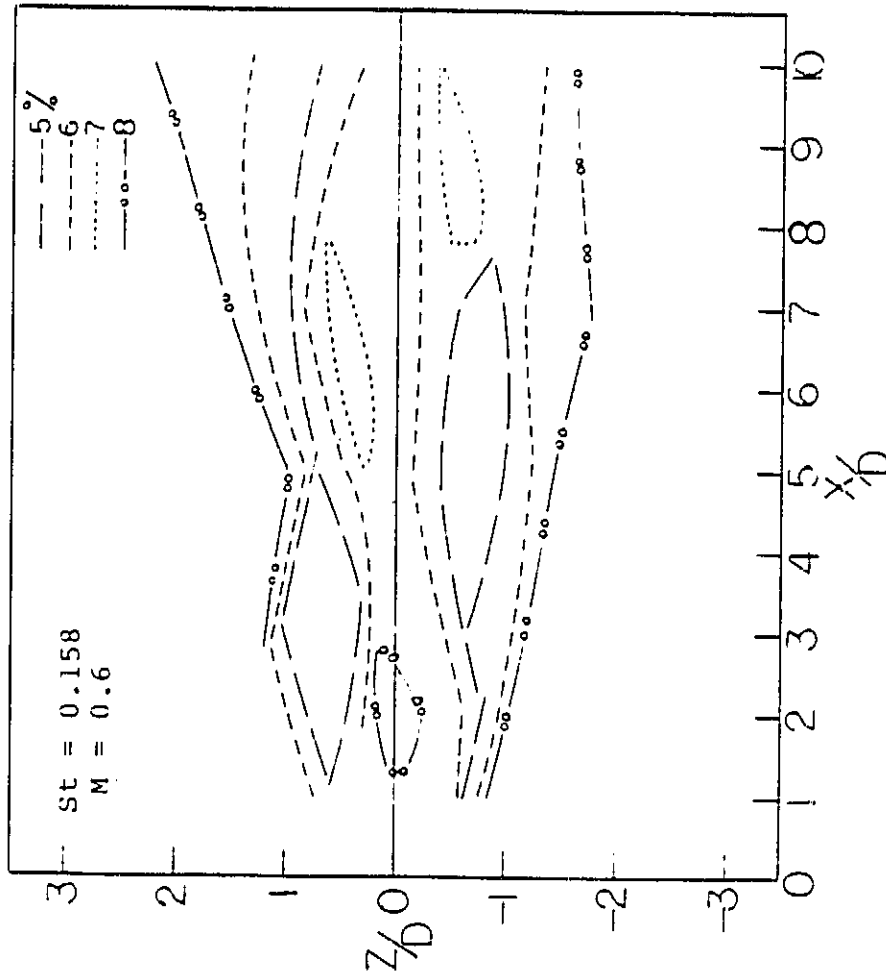
Fig. 27. Contours of coherence levels of phase averaged axial
and radial flow fluctuation correlation
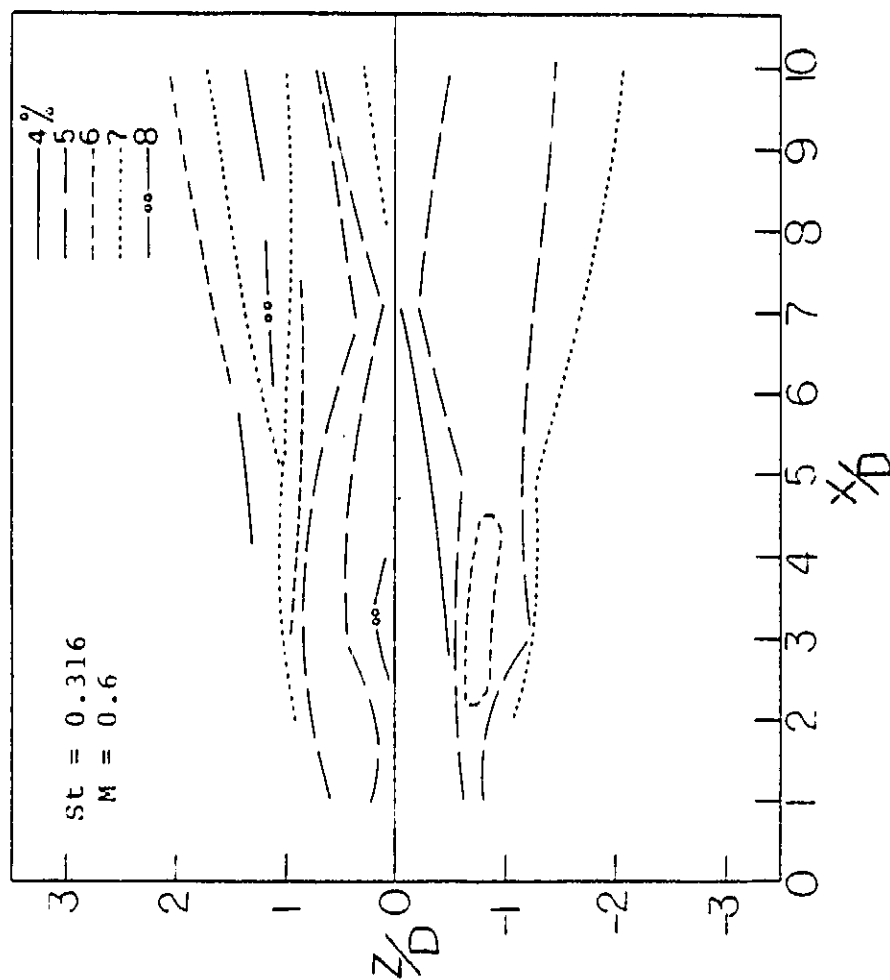
Fig. 28. Contours of coherence levels of phase averaged axial and radial flow fluctuation correlation
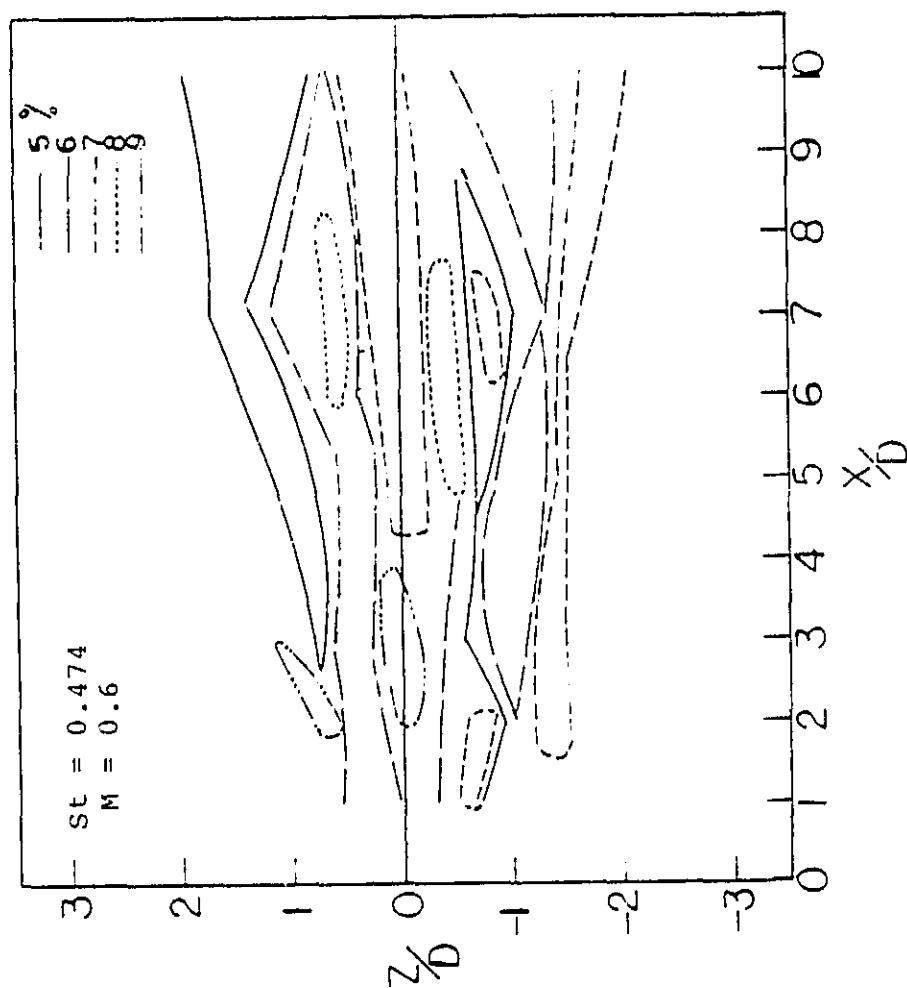
Fig. 29. Contours of coherence levels of phase averaged axial and radial flow fluctuation correlation

mass velocity and radial mass velocity fluctuation. Figure 27 shows that the jet contains a high level of coherency at the edge of jet at all axial locations. Moving radially inward through the shear layers, the coherency level decreased and then slightly increased toward the centerline for the very low excitation frequency of St = 0.158.

Figure 28 shows that as the excitation frequency was increased to St = 0.316, the coherency level of the Reynold's stresses did not change significantly and possessed the same general dependence as the lower frequency. Figure 29 illustrates that for a mid-range excitation frequency of St = 0.474, the jet had a high coherency level at the centerline. But as flow moved downstream, the edge of the jet possessed the lowest coherency for X/D greater than 3. As the excitation frequency increased to St = 0.948 and 1.263 the coherency level data were so dispersed that fitting contour lines between them was impossible.

In summary, the radial velocity fluctuations possessed higher levels of coherence compared to the axial mass velocity and Reynold's stress. The contours showed that the overall coherence of axial mass velocity, radial velocity and Reynold's stresses are very high in the potential core for excitation frequencies of $0.316 \leqslant St \leqslant 0.632$.

3.3 Temporal and Spectral Content of Phase Averaged Flow Fluctuations

Figures 30-36 show the temporal and spectral content of the phase averaged mass velocity fluctuations for an excitation frequency of St = 0.474. The spectrum in Figure 30 shows two discrete peaks centered at St = 0.474 and 1.14 dominating the initial fluctuations at X/D = 1 and Z/D = -0.65. It should be noted that the excitation mechanism input a pulse into the flow and hence contained harmonics. Therefore the presence of this harmonic is not unexpected and may not in ~ate non-linear interactions. The harmonic peak is wider in breadth and lower in amplitude. This broadening maybe be due to the fundamental frequency (St = 0.474) varying slightly hence causing a larger variation in the harmonic.

As the flow progressed downstream to X/D = 3 and Z/D = 0.55 (Figure 31), the coherent structure contained several discrete peaks. These peaks can all be expressed by nf_1 + mf_2 where f_1 = 0.318 and f_2 = 0.474 which n , m = ...-2, -1, 0, 1, 2,....... This type of frequency interaction was observed by Miksad [37] in wakes and was indicative of non-linear interaction.

Time traces recorded at the maximum mass velocity fluctuation level were not quite as periodic as the time traces obtained at the centerline since the jet attained a

Fig. 30. Temporal and Spectral representation of the phase averaged mass velocity fluctuation, $X/D = 1$, $Z/D = -0.56$, $St_{excite} = 0.474$.

Fig. 31. Temporal and Spectral representation of the phase averaged mass velocity fluctuation, $X/D = 3$, $Z/D = 0.55$, $St_{excite} = 0.474$.

Fig. 32. Temporal and Spectral representation of the phase averaged mass velocity fluctuation, X/D = 3 , Z/D = -0.2 , St_{excite} = 0.474.

e
(ALS)

.000E-01

.000E+01   .159E-03   .315E-03   .473E-03   .630E-03

t (sec)

G
(ALS)

0   0.8   1.6   2.4   3.2
                      St
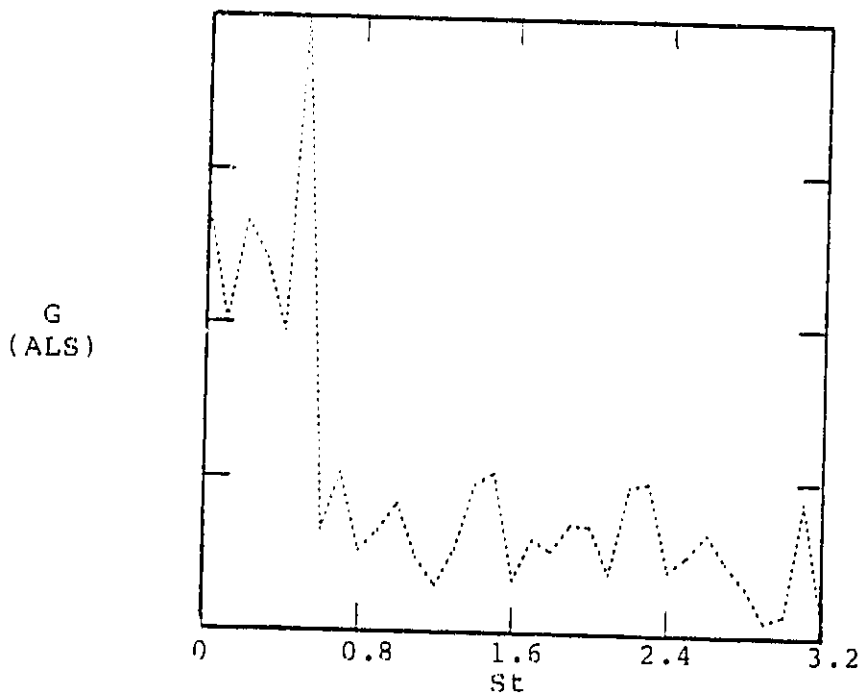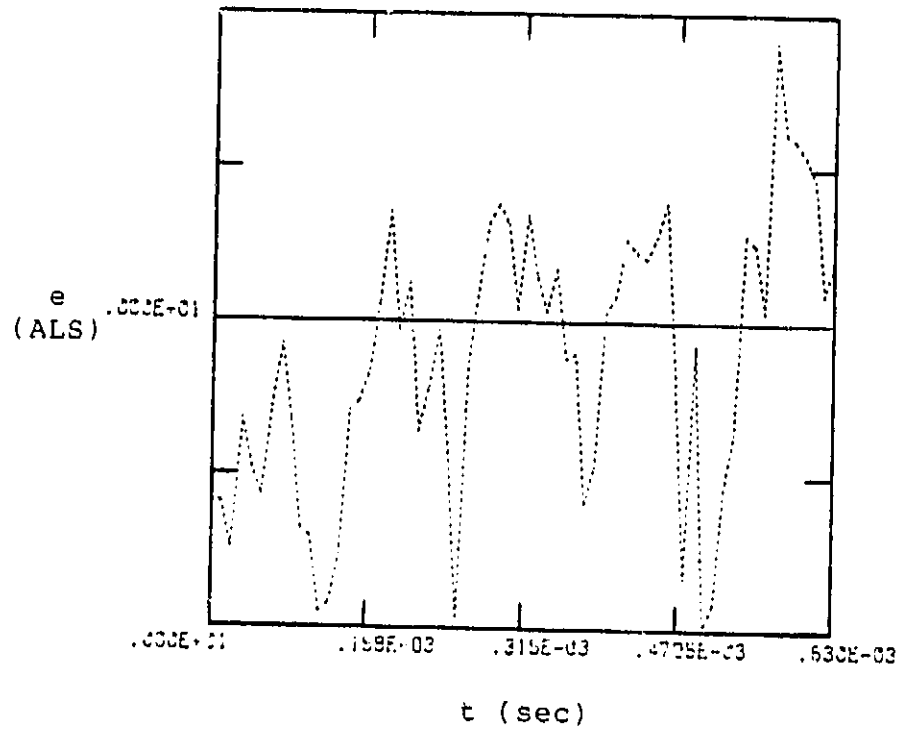
Fig. 33. Temporal and Spectral representation of the
phase averaged mass velocity fluctuation,
X/D = 7 , Z/D = 1.0 , St$_{excite}$ = 0.474.
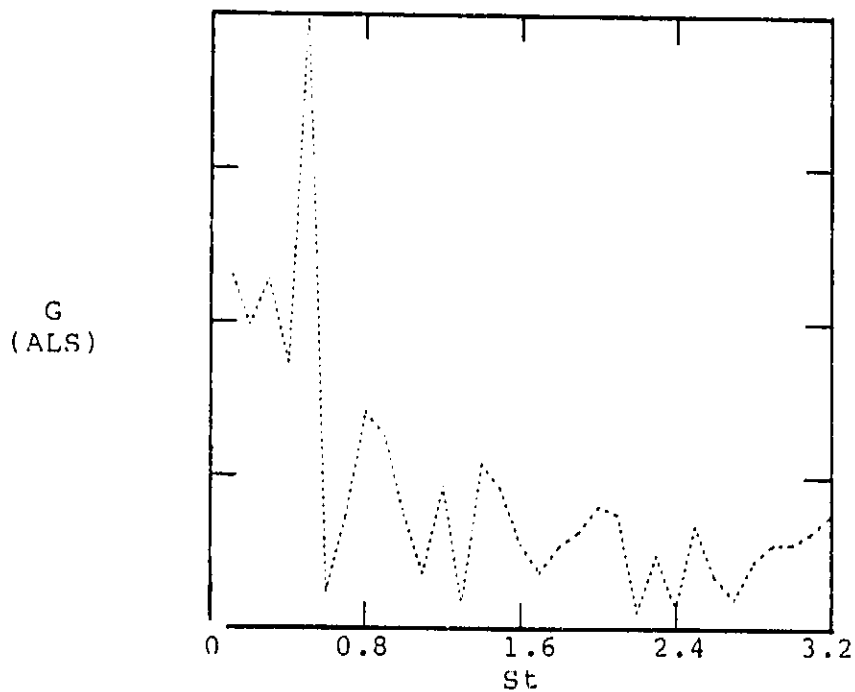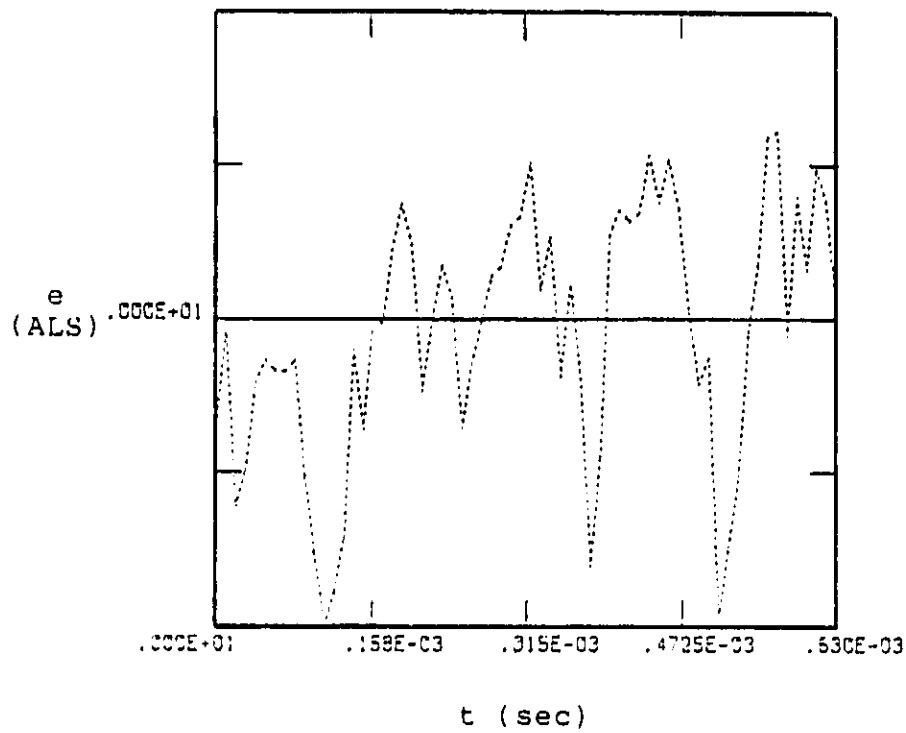
Fig. 34. Temporal and Spectral representation of the phase averaged mass velocity fluctuation, $X/D = 7$, $Z/D = -0.04$, $St_{excite} = 0.474$.
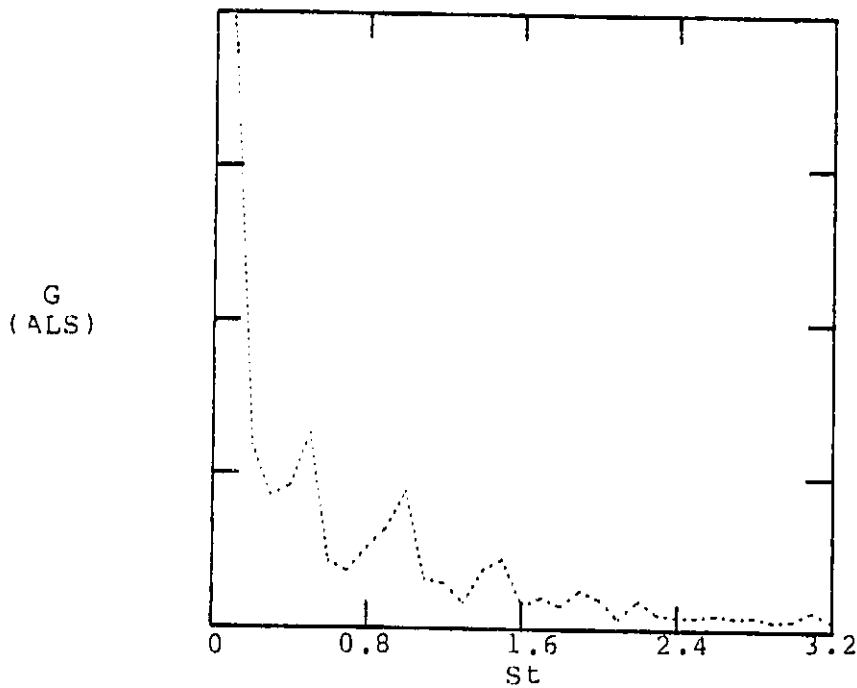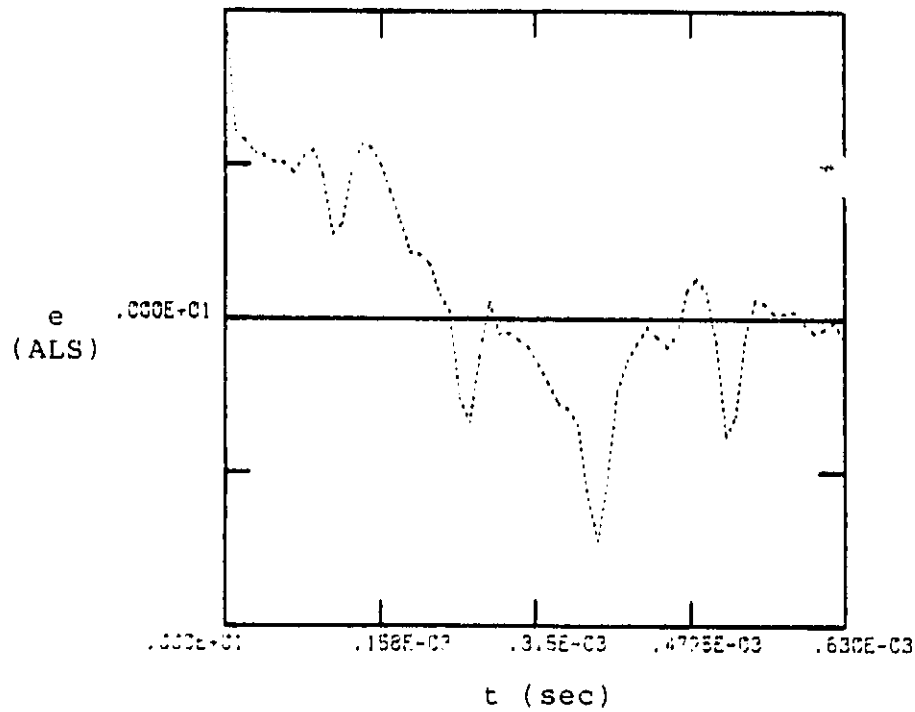
Fig. 35. Temporal and Spectral representation of the
phase average mass velocity fluctuation,
X/D = 10 , Z/D = 0.862 , St_{excite} = 0.474.
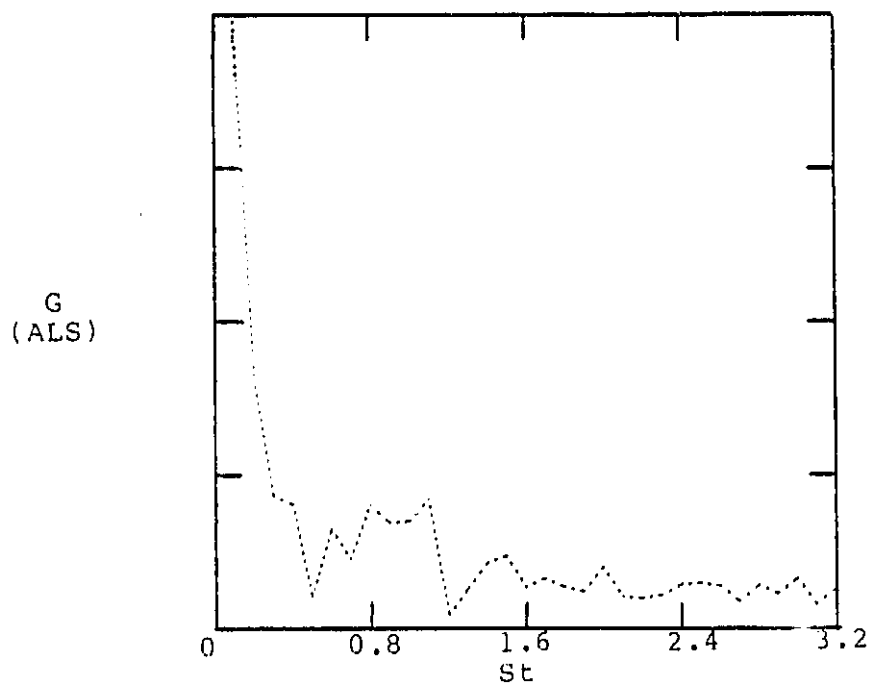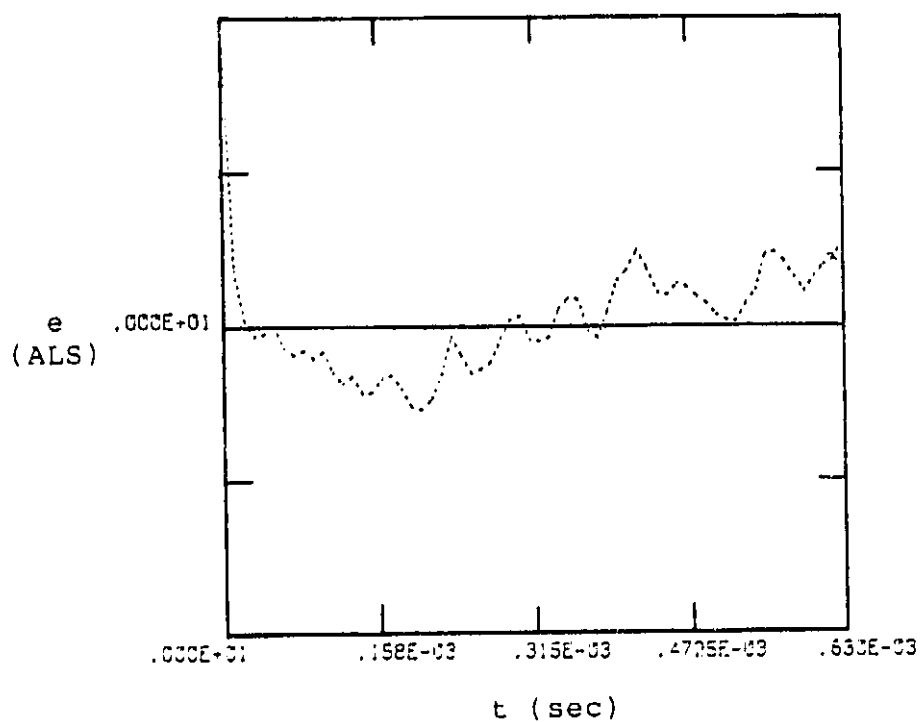
Fig. 36. Temporal and Spectral representation of the
phase averaged mass velocity fluctuation,
X/D = 10 , Z/D = -0.06 , St_{excite} =0.474.

higher coherency level (Figure 19) at the centerline.
Figure 32 shows that at the centerline of the jet for the
same X/D = 3, the coherent structure was periodic with a
fundamental frequency of St = 0.474 with several harmonics
through St = 2.22. As shown in Figure 19, this also was the
location with the highest coherency level. It is important
to note that as the flow progressed downstream, the
fundamental frequency increased in amplitude. Figures 33-34
show that at X/D = 7 the jet contained a periodic time trace
but the large discrete amplitude peaks, except the
fundamental frequency, disappear in the shear layer and at
the centerline of the jet. These fundamental frequencies
centered at 0.474 were followed by several low amplitude
harmonics. At X/D = 10 (Figure 35-36) the jet lost its
periodic time trace and the fundamental frequency sharply
decreased in amplitude. The production of several discrete
frequencies and spectra broadening downstream at X/D = 10
may indicate stages of non-linear spectral interaction.

Figures 37-43 show the temporal and spectral content
of the phase averaged radial velocity fluctuations for the
excitation frequency of St = 0.474 at the same locations as
the previous phase averaged mass velocity fluctuation
measurements. All spectral analyses of phase averaged
radial velocity fluctuations (Figures 37-48) showed that the
fundamental frequency of St = 0.474 with a high amplitude
dominated the entire flowfield from X/D = 1 to 10. This
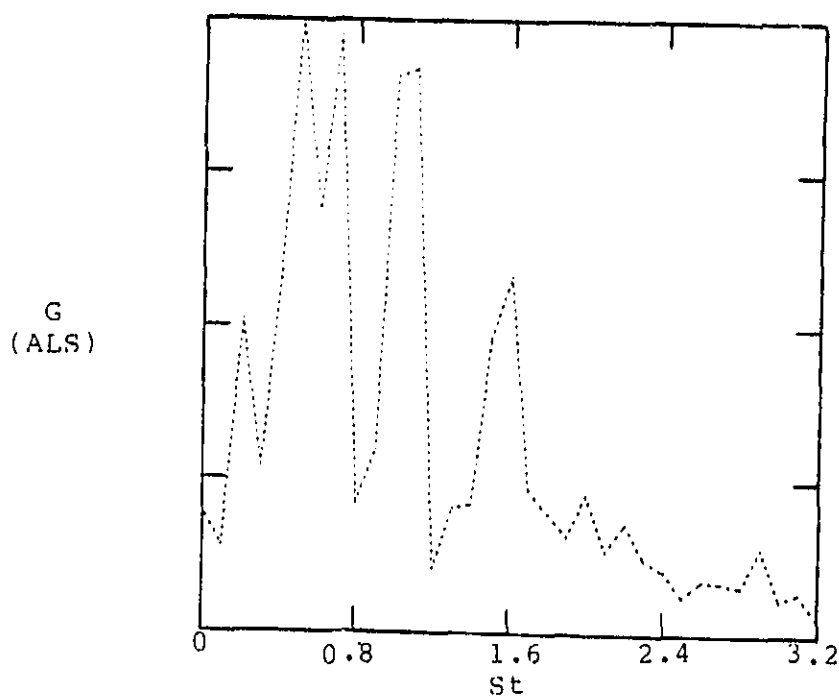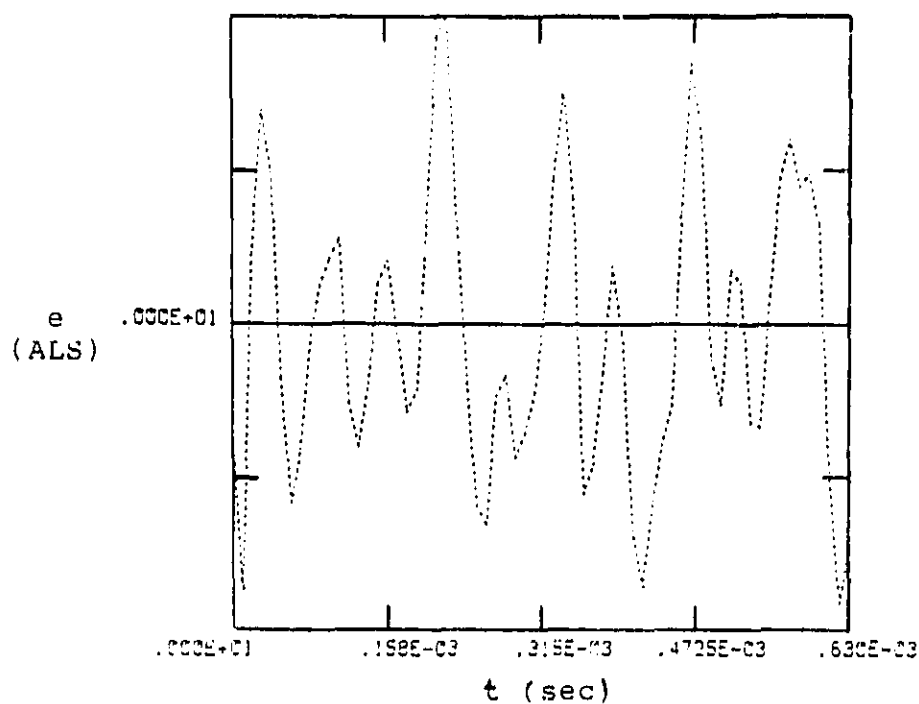
Fig. 37. Temporal and Spectral representation of the phase averaged radial velocity fluctuation, $X/D = 1$, $Z/D = -0.56$, $St_{excite} = 0.474$.

Fig. 38. Temporal and Spectral representation of the phase averaged radial velocity fluctuation, $X/D = 3$, $Z/D = 0.55$, $St_{excite} = 0.474$.

e
(ALS)   .000E+01

.000E+01   .158E-03   .315E-03   .473E-03   .630E-03

t (sec)

G
(ALS)

0   0.8   1.6   2.4   3.2
St
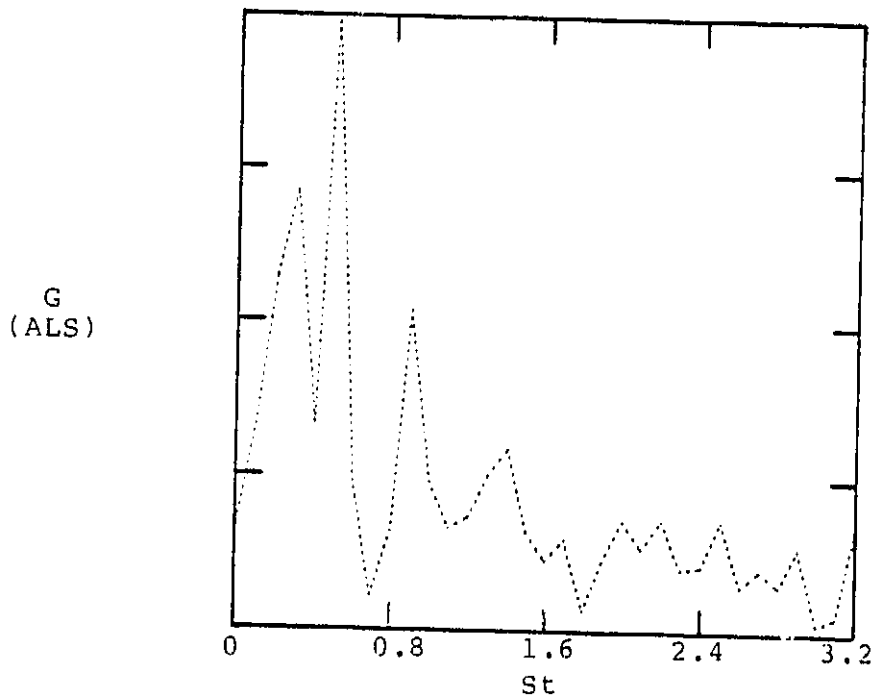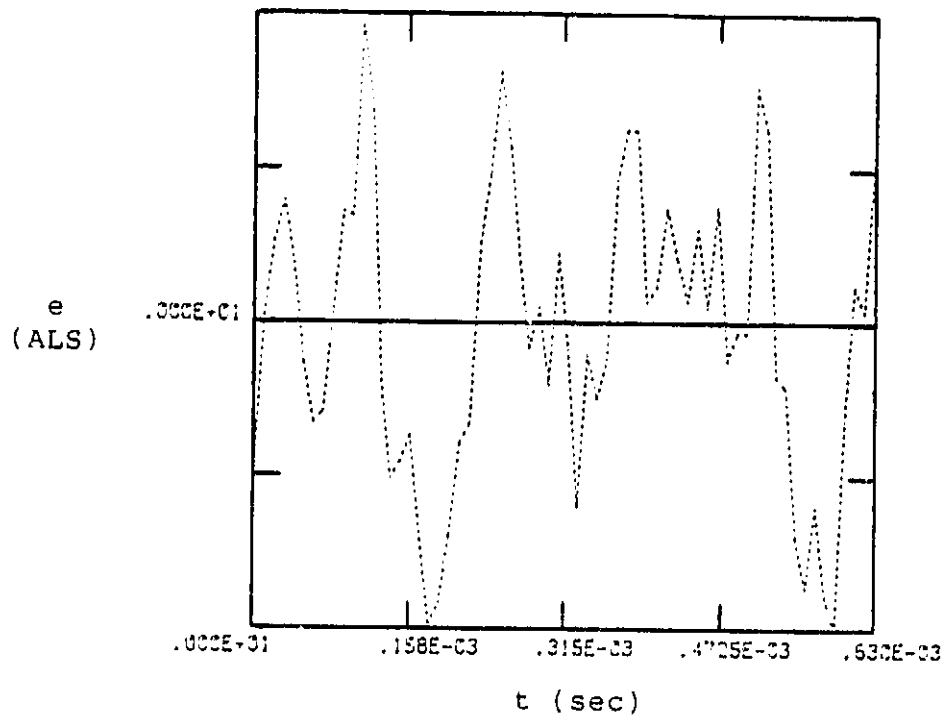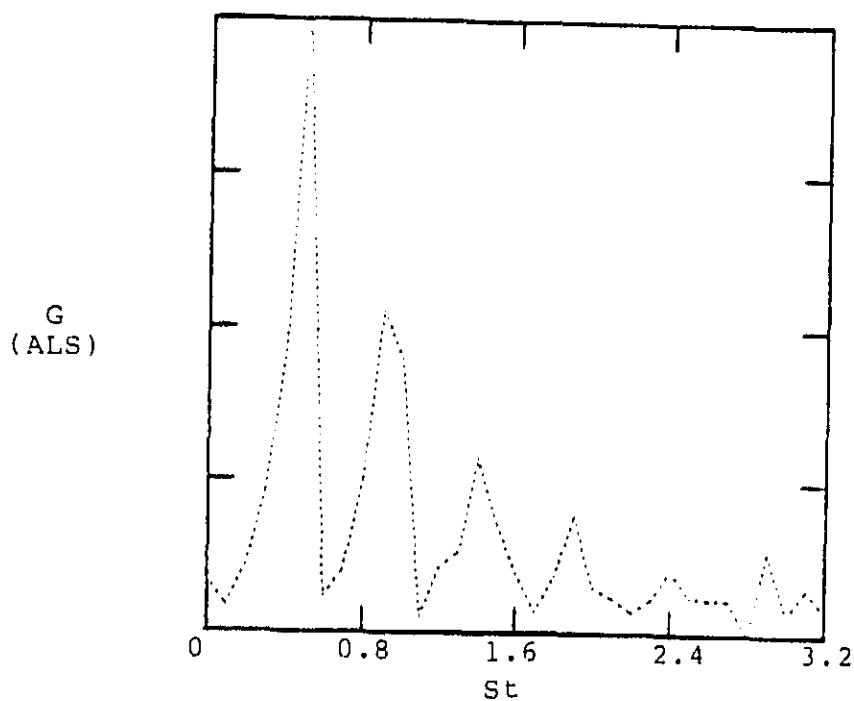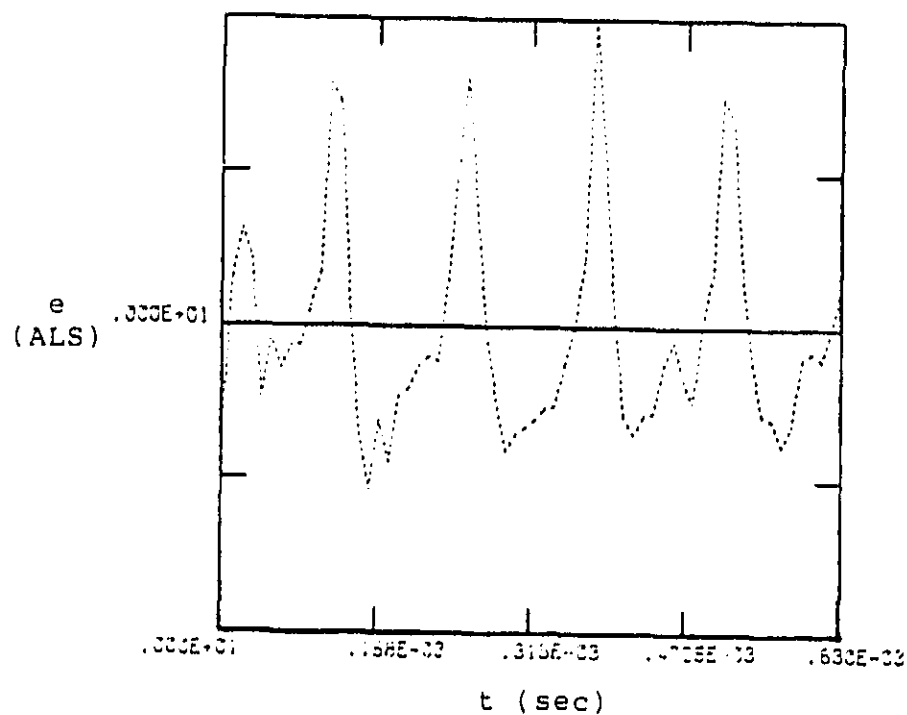
Fig. 39. Temporal and Spectral representation of the
          phase averaged radial velocity fluctuation,
          X/D = 3 , Z/D = -0.2 , St$_{excite}$ = 0.474.
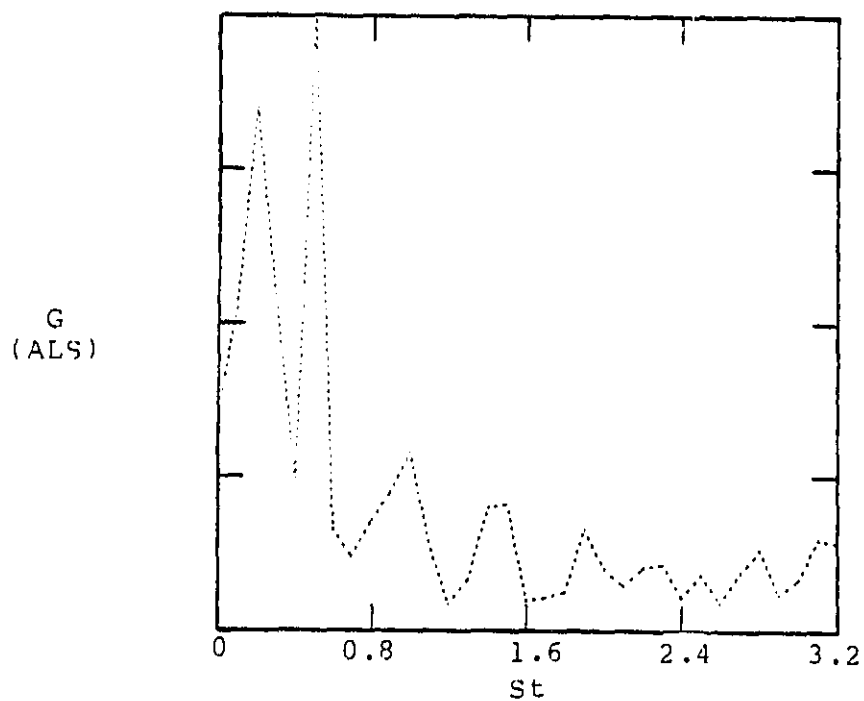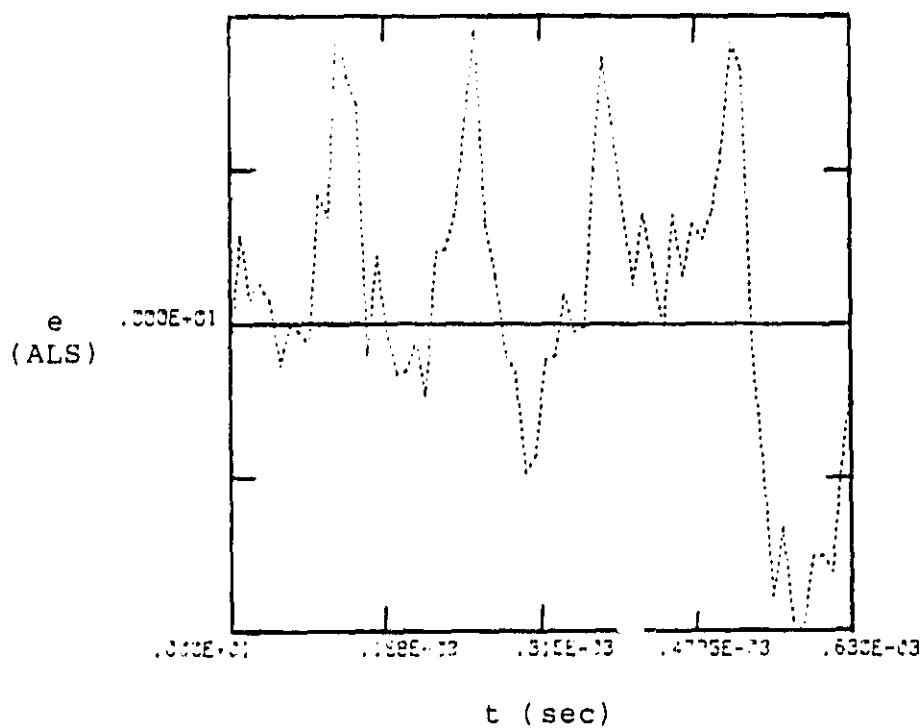
Fig. 40. Temporal and Spectral representation of the phase averaged radial velocity fluctuation, X/D = 7 , Z/D = 1.0 , St_{excite} = 0.474.
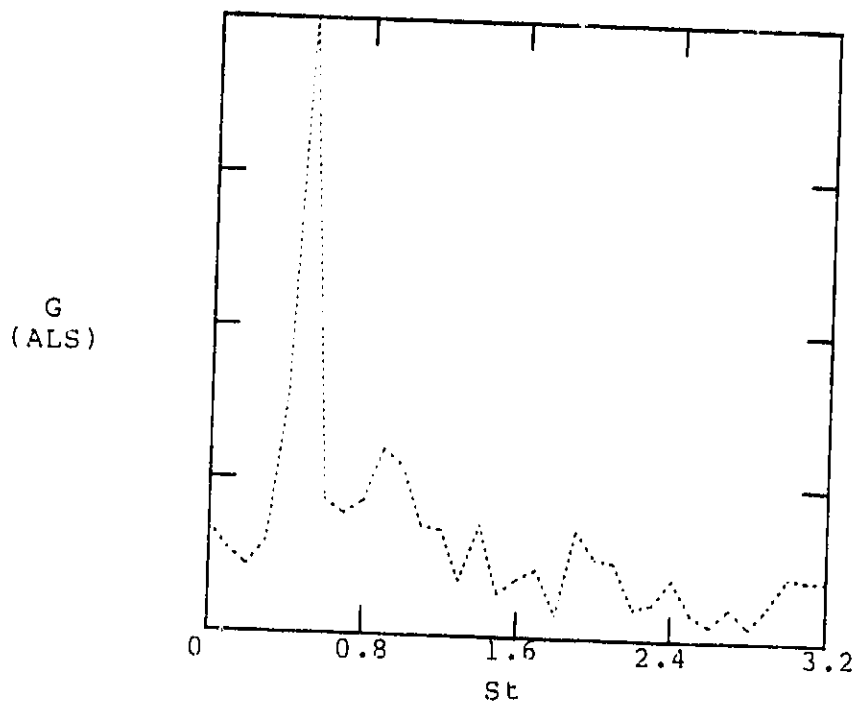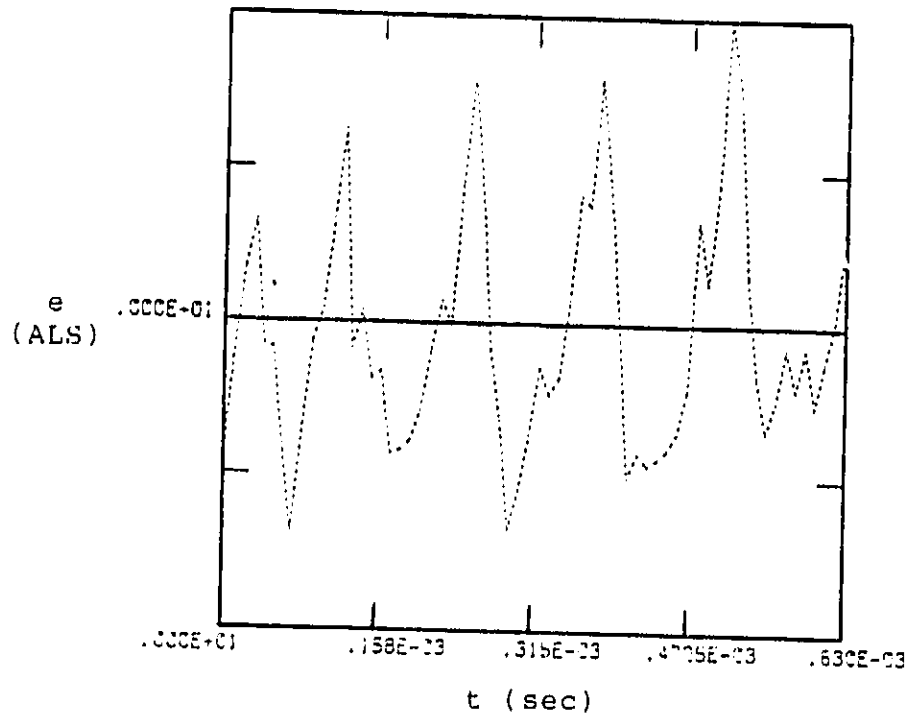
Fig. 41. Temporal and Spectral representation of the phase averaged radial velocity fluctuation, X/D = 7 , Z/D = -0.04 , St_{excite} = 0.474.
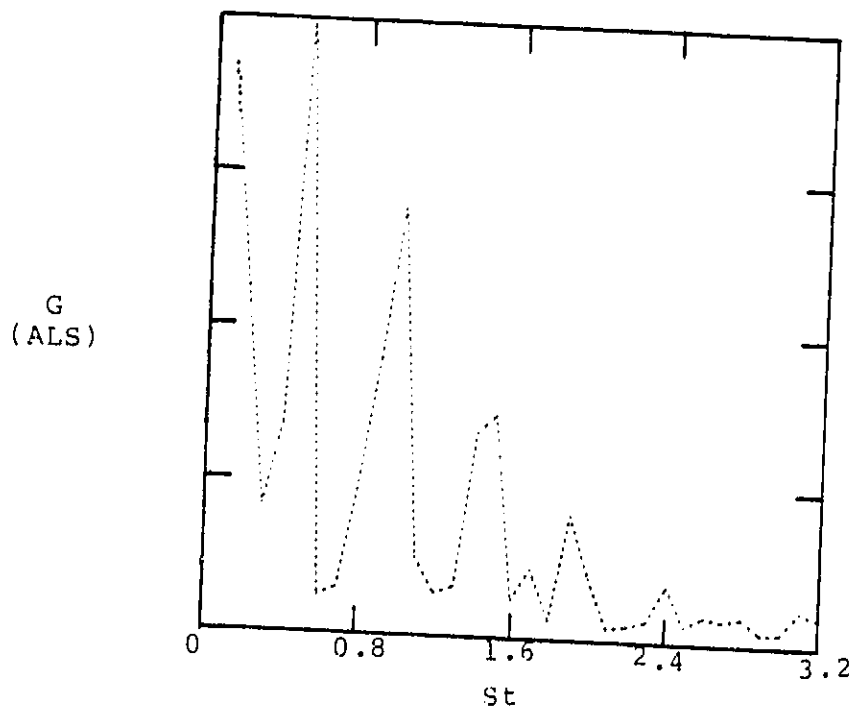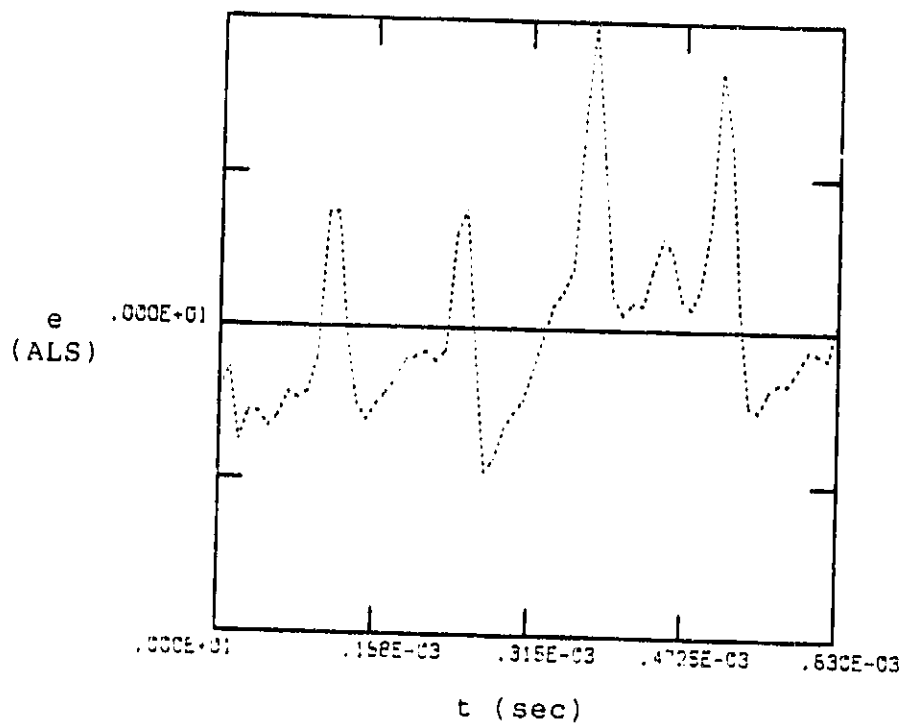
Fig. 42. Tempor l and Spectral representation of the phase averaged radial velocity fluctuation, X/D = 10 , Z/D = 0.862 , $St_{excite} = 0.474$.
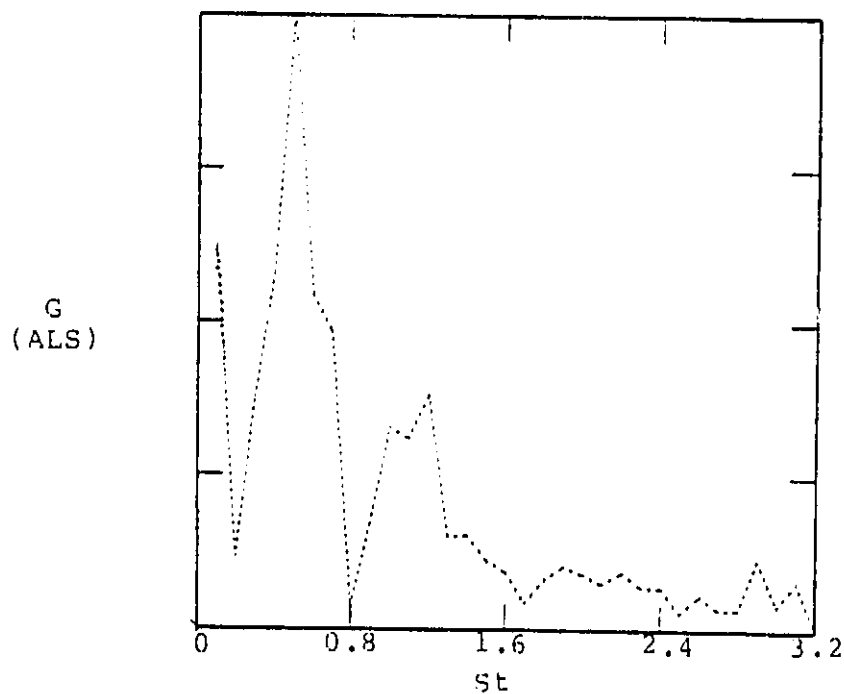
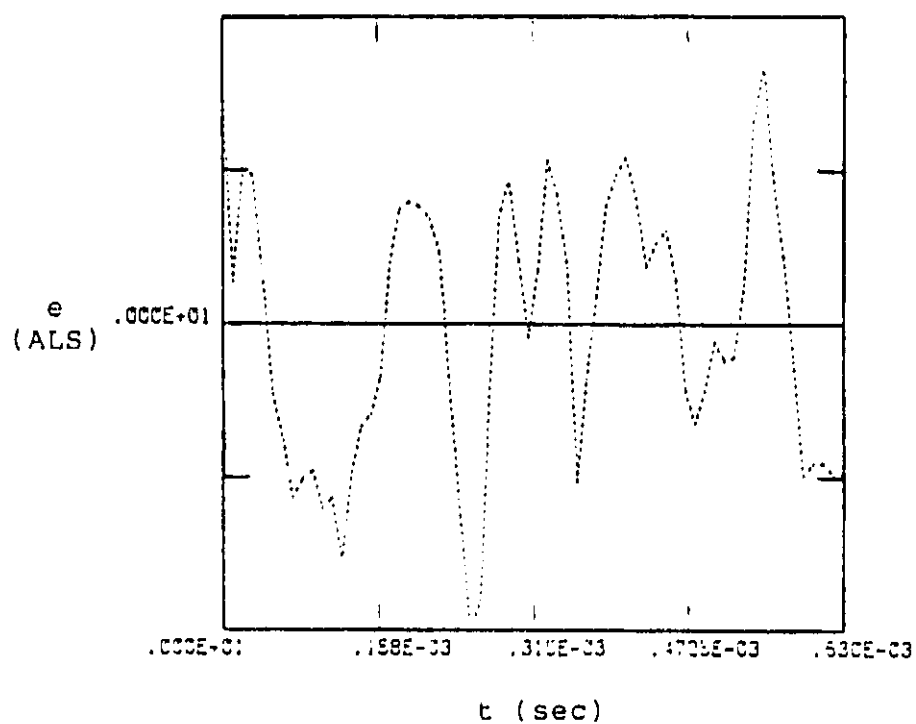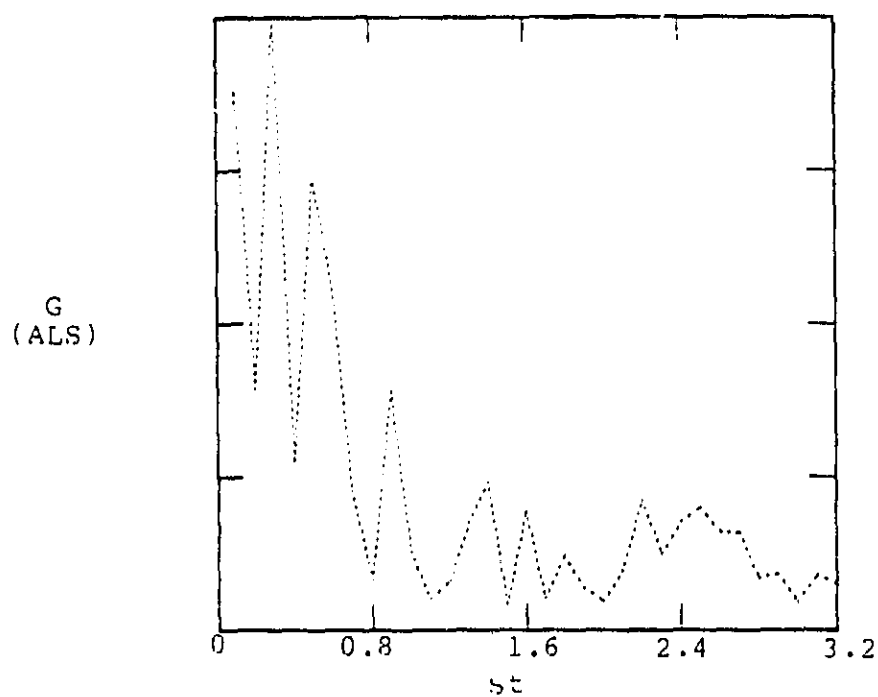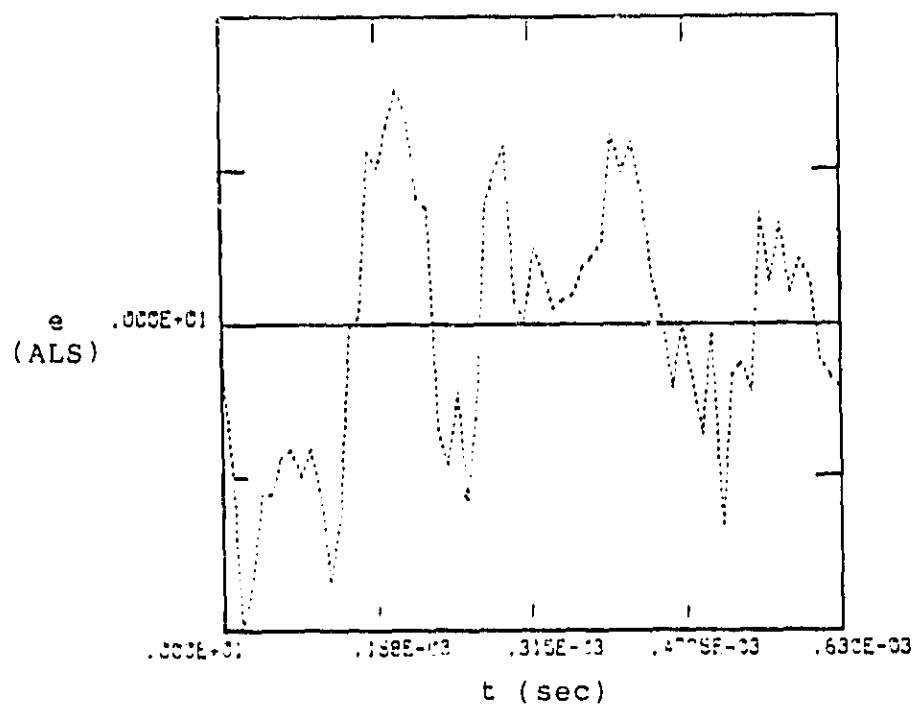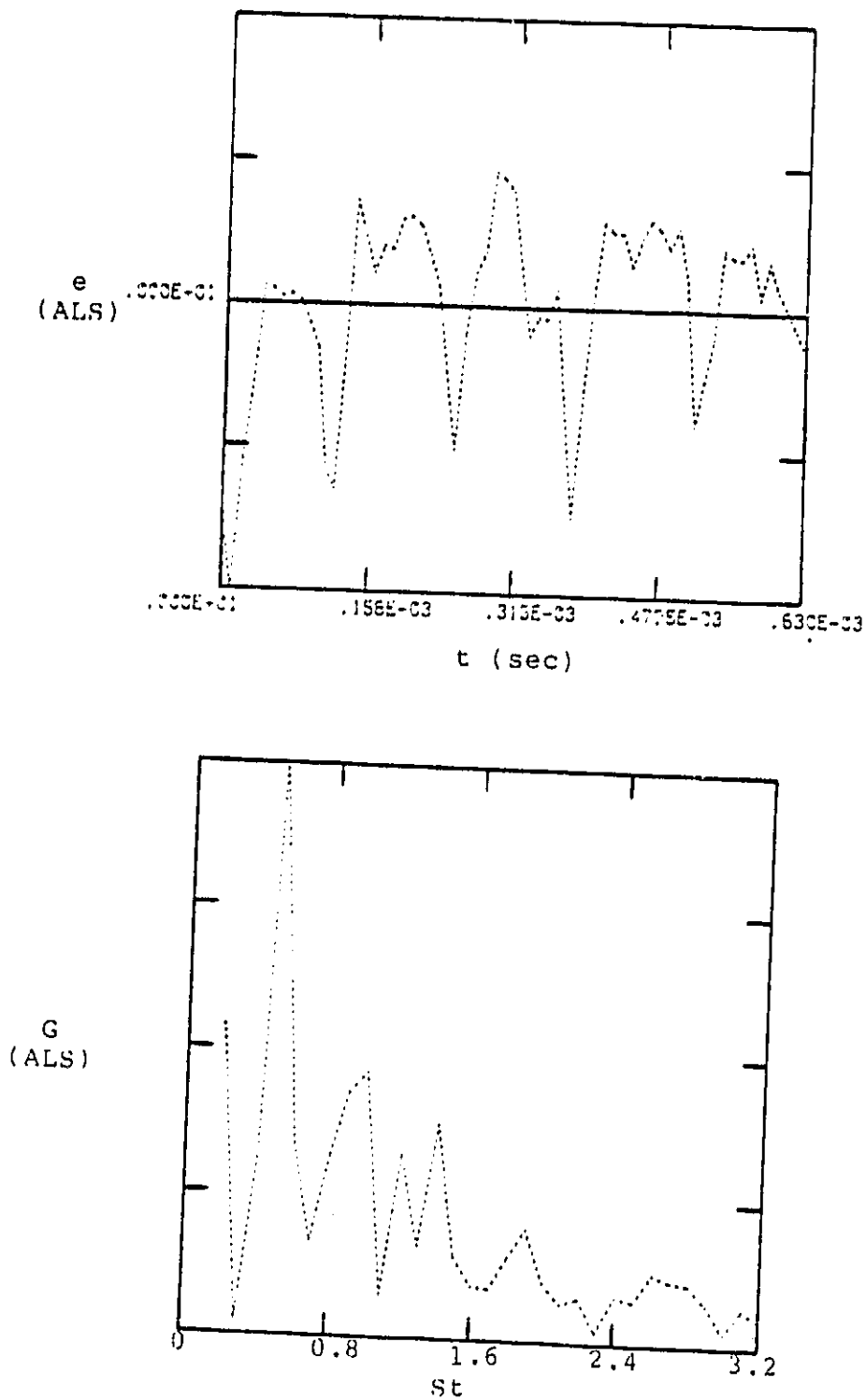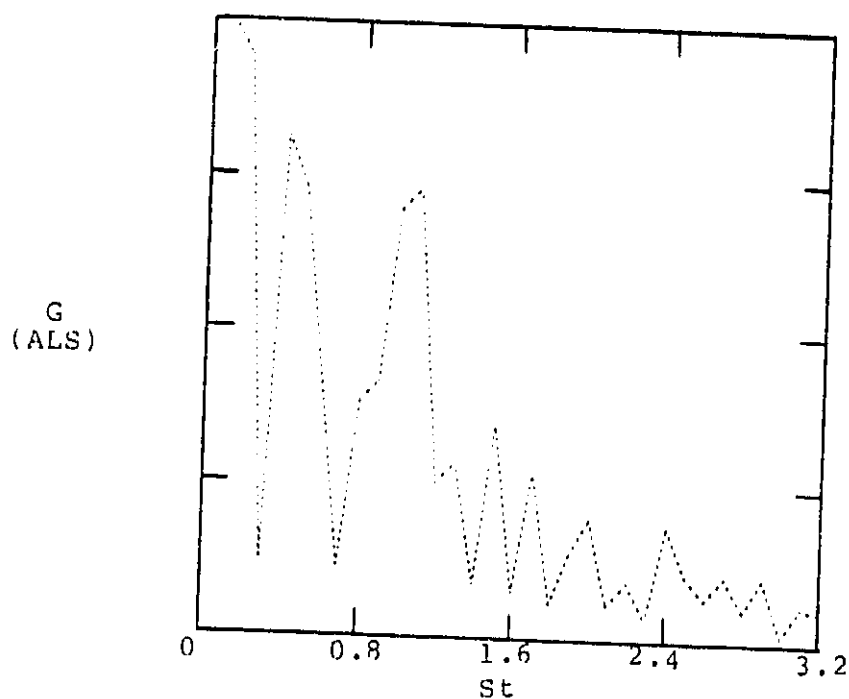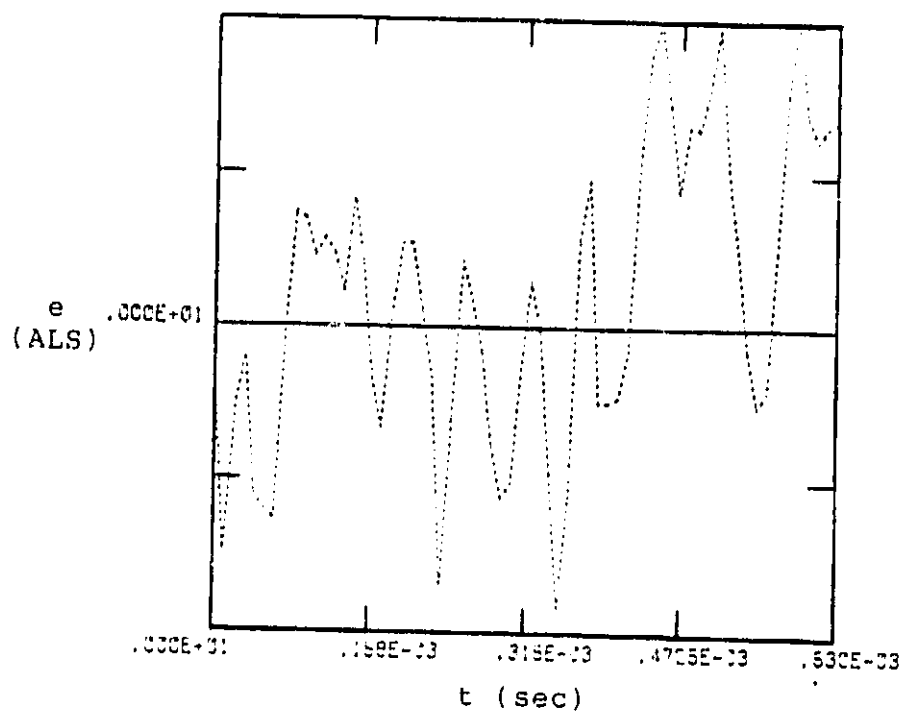Fig. 43. Temporal and Spectral representation of the phase averaged radial velocity fluctuation, $X/D = 10$, $Z/D = -0.06$, $St_{excite} = 0.474$.
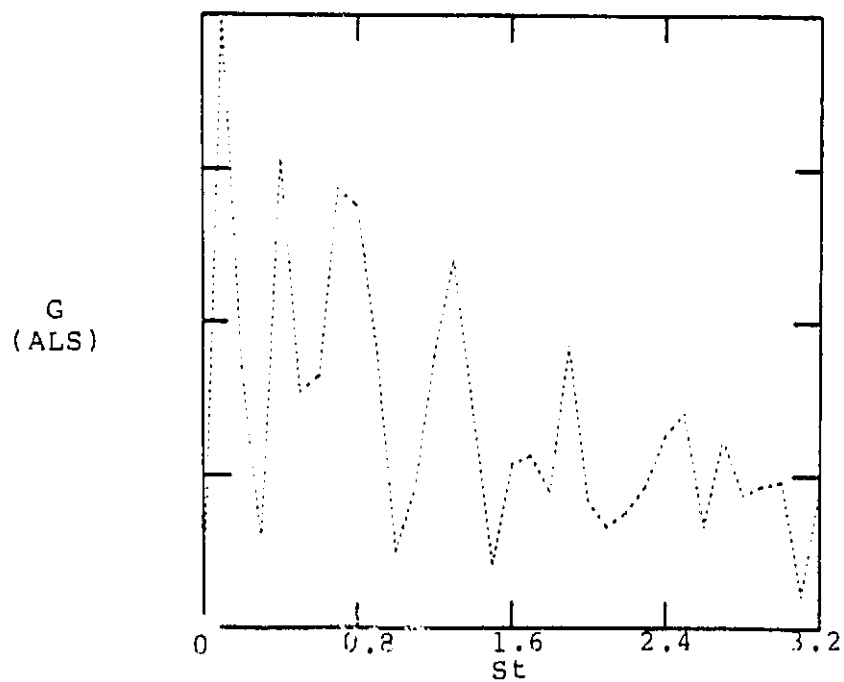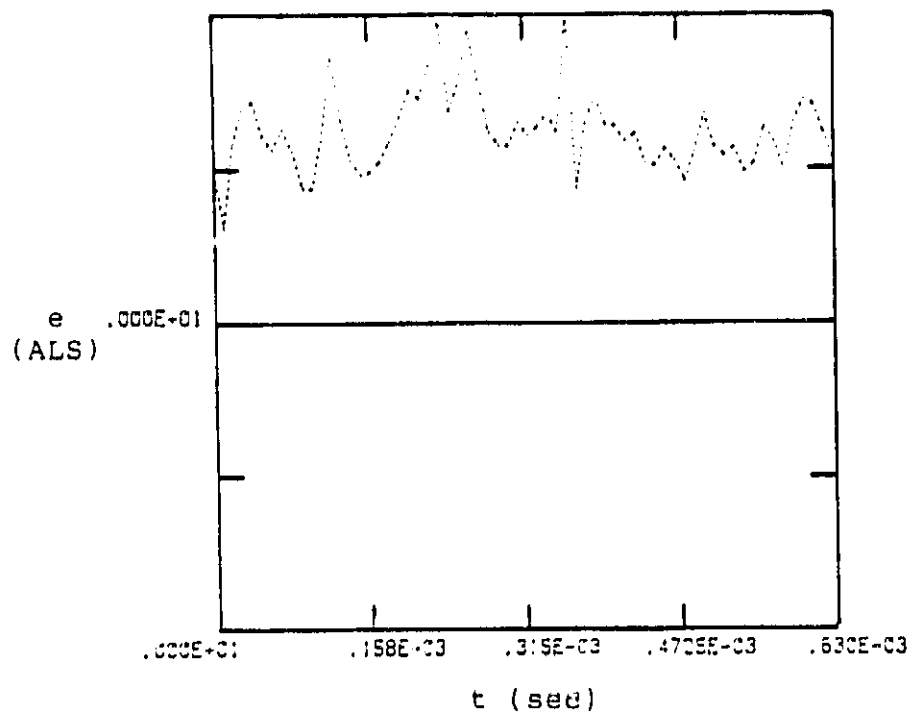
Fig. 44. Temporal and Spectral representation of the
phase averaged axial and radial flow fluct-
uation correlation, $X/D = 1$, $Z/D = -0.56$,
$St_{excite} = 0.474$.
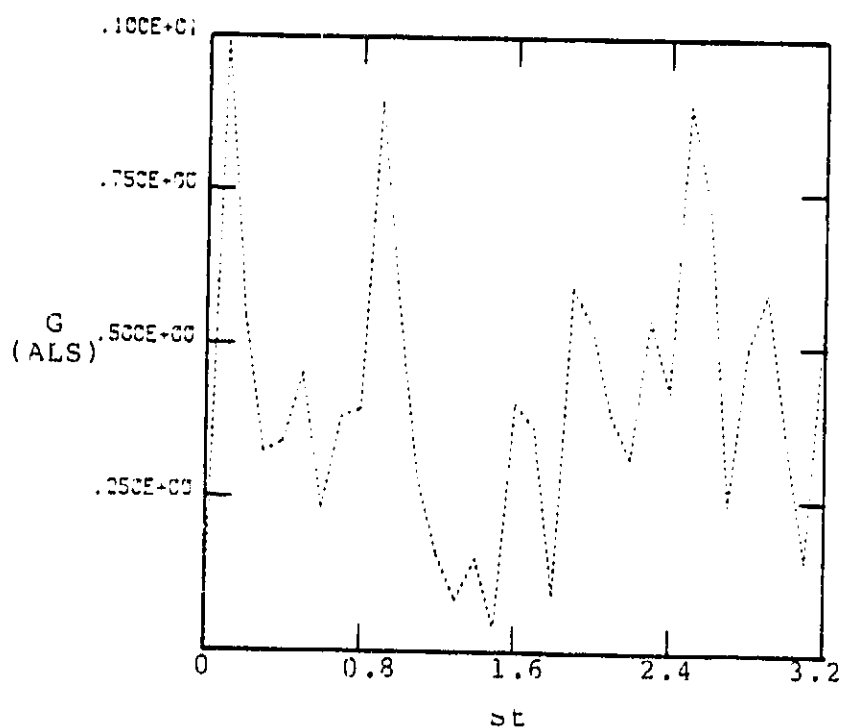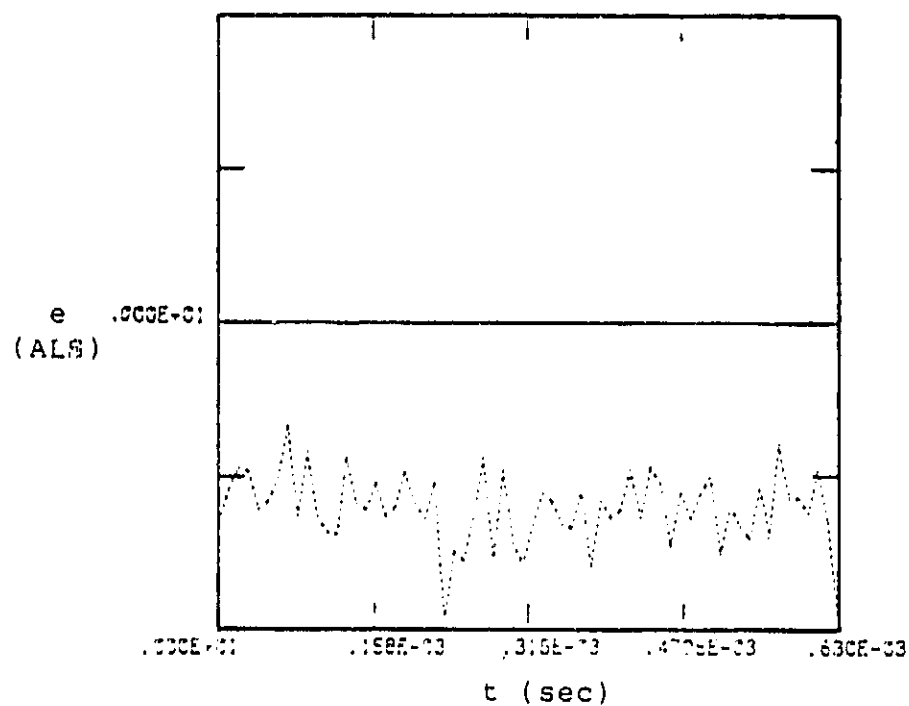
Fig. 45. Temporal and Spectral representation of tne
phase averaged axial and radial flow fluct-
uation correlation, X/D = 3 , Z/D = 0.55 ,
St_{excite}= 0.474.
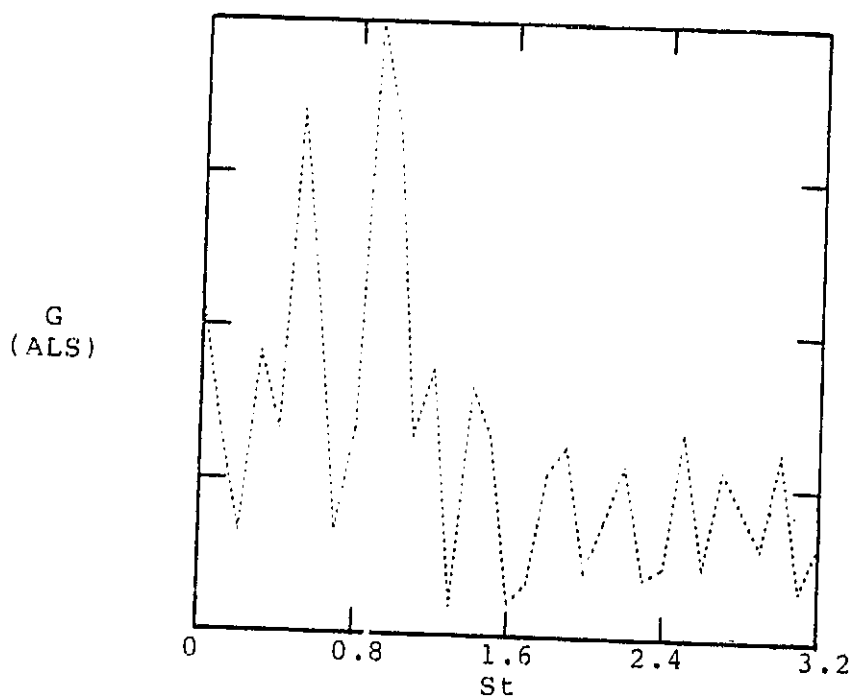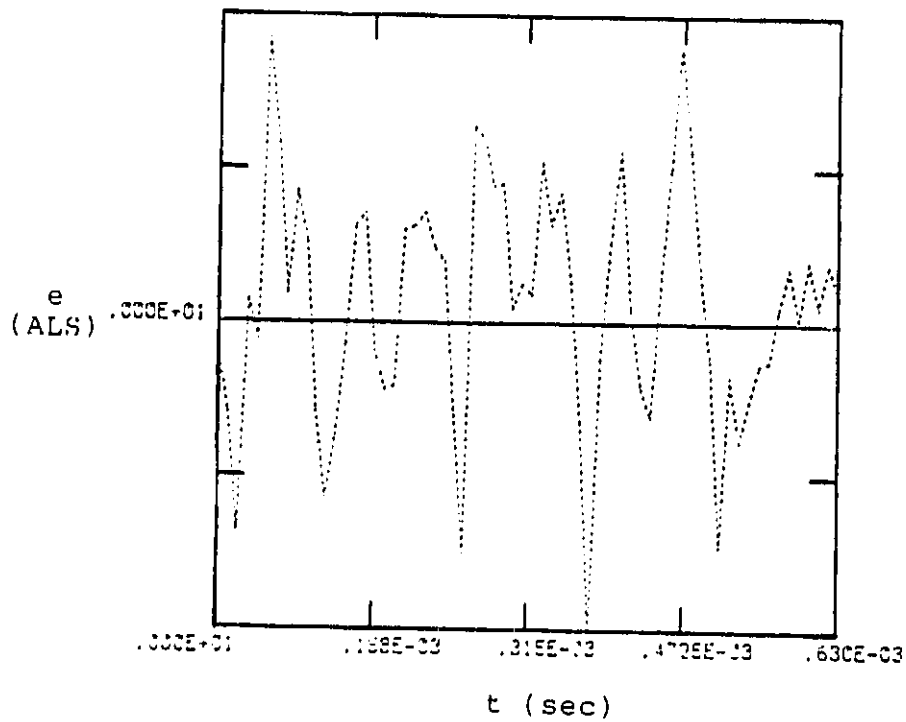
Fig. 46. Temporal and Spectral representation of the
phase averaged axial and radial flow fluct-
uation correlation, X/D = 3 , Z/D = -0.2 ,
St_{excite} = 0.474.
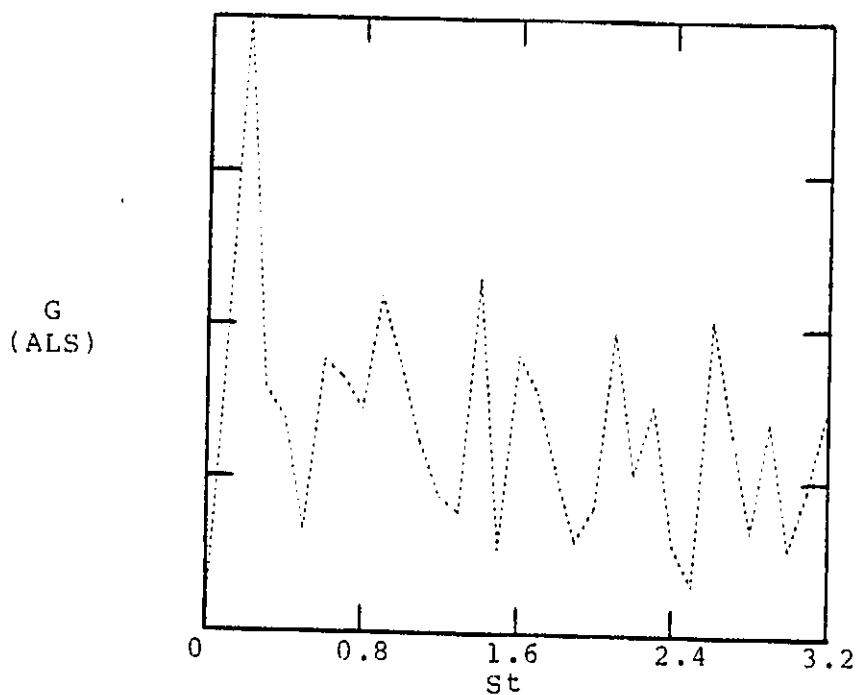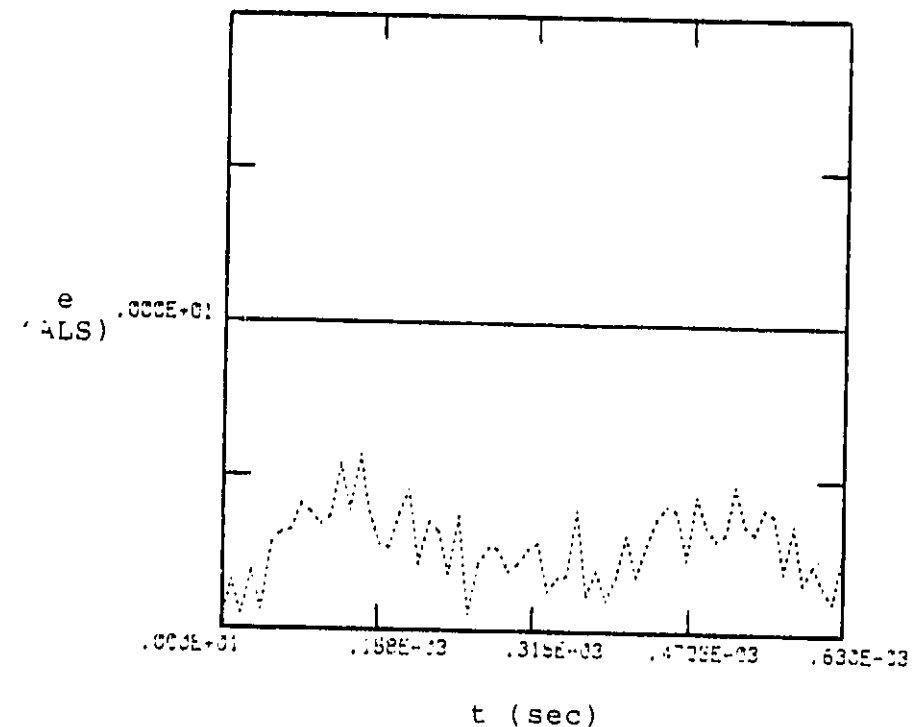
Fig. 47· Temporal and Spectral representation of the
phase averaged axial and radial flow fluct-
uation correlation, X/D = 7 , Z/D = 1.0 ,
St_{excite} = 0.474.
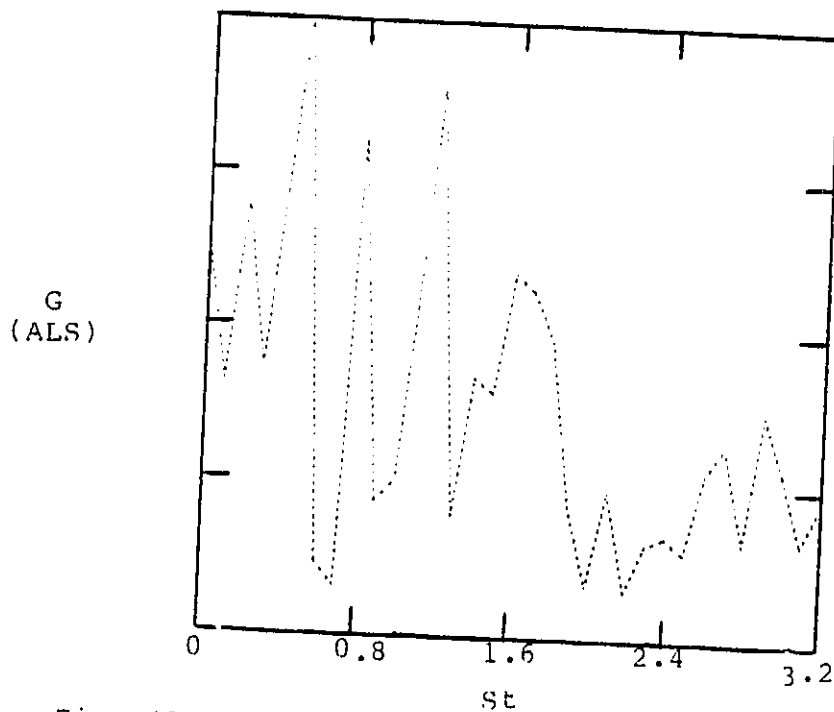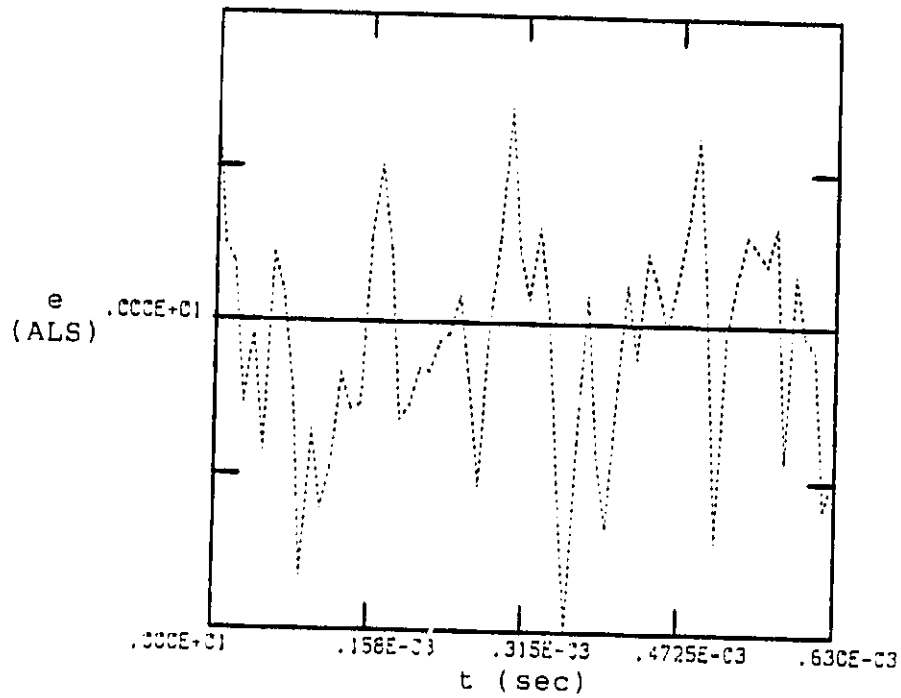
Fig. 48. Temporal and Spectral representation of the
phase averaged axial and radial flow fluct-
uation correlation, X/D = 7 , Z/D = -0.04 ,
St_{excite} = 0.474.

fundamental frequency of St = 0.474 was followed by several relatively high amplitude harmonics with frequencies up to St = 2.35 all through the jet. The spectral content of the mass velocity fluctuations followed the same trend but had a fundamental frequency amplitude peak and this fundamental frequency was followed by a few relatively low amplitude harmonics up to X/D = 7. The temporal representations of radial velocity showed that the radial velocity fluctuations had very periodic time traces all through the jet compared to the mass velocity fluctuation time traces. Comparing the time traces of mass velocity and radial velocity fluctuations, it was evident that the time traces were not in phase with each other. This difference in phase could cause the relatively high amplitude harmonics in Reynolds stress fluctuations; this may explain why there was a high coherency level in the radial velocity fluctuations and Reynold's stresses.

Figure 37 show that at the maximum radial velocity fluctuation amplitude,the jet had three discrete peaks with a relativly low amplitude subharmonic. As the flow progressed downstream (Figure 38-41) to X/D = 3, the subharmonic increased in amplitude for maximum radial velocity fluctuation amplitude and the discrete peaks reduced in amplitude. However, the fundamental frequency amplitude was still higher in amplitude than the other discrete peaks. Moving radially towards the centerline at

X/D = 3, the subharmonic frequency reduced and completely disappeared at the centerline of the jet. In the same region, the fundamental frequency was followed by harmonics. Figures 42-43 exhibit that at X/D = 10 the jet lost its periodicity as compared to the axial locations upstream. At this location, the centerline of the jet had the same high amplitude discrete peak component followed by harmonics for both the Z/D = 0.862 and centerline locations.

Figures 44-50 illustrate the corresponding temporal and spectral content of the phase averaged axial and radial flow fluctuation correlation. Figures 44-45 show that the jet did not have a periodic time trace at the maximum amplitude fluctuation at X/D = 1 and 3, but the spectral content had five discrete peaks. These discrete peaks reduced in amplitude as frequency inceased. Figure 46 shows that at X/D = 3 on the centerline the jet almost had a periodic time trace with a 2/3 subharmonic and a fundamental frequency centered at St = 0.474 and 1.01 respectively. Figures 47-48 show that as the flow moved downstream to X/D = 7 the time trace and spectral content behaved like those obtained at X/D = 3. Figures 49-50 illustrate that at X/D = 10 and a radial location of Z/D = 0.862 and the centerline the jet had a discrete peak centered at St = 0.159 followed by harmonics ranging from St = 0.32 to 2.99.
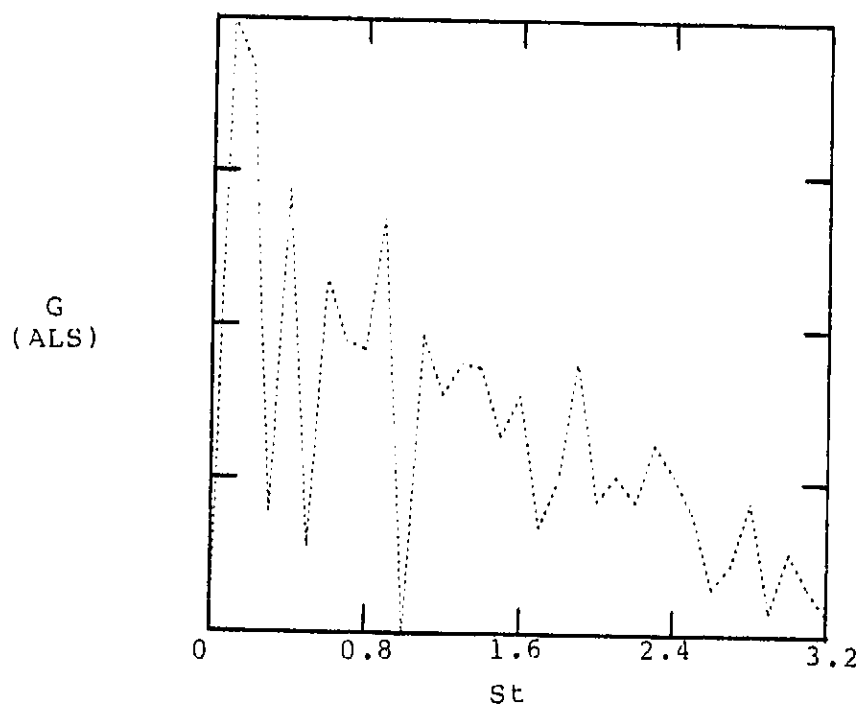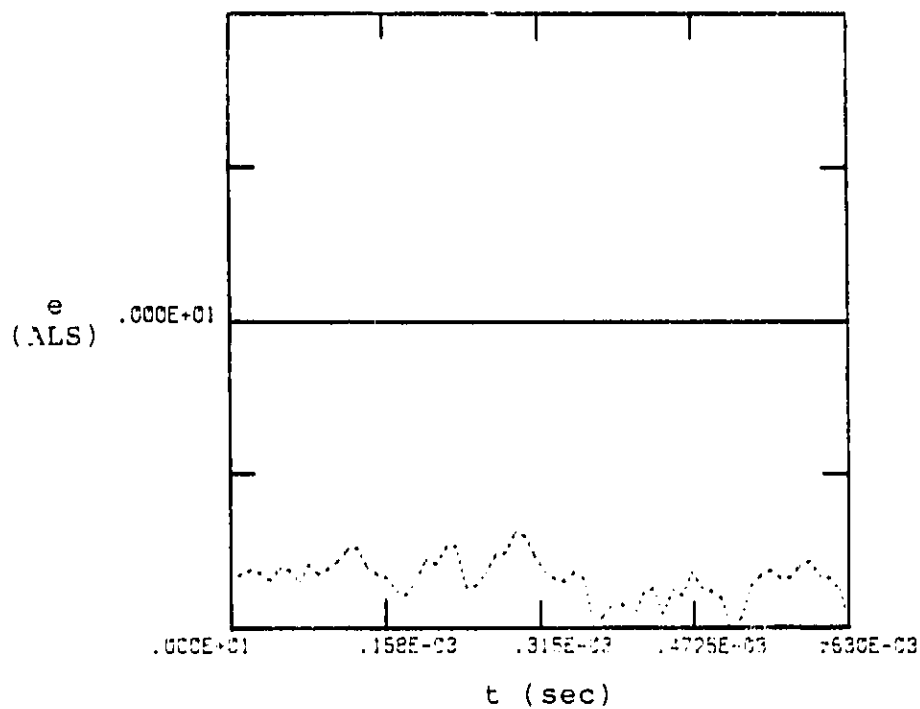
Fig. 49 · Temporal and Spectral representation of the phase averayed axial and radial flow fluctuation correlation, X/D= 10 , Z/D = 0.862 , St_{excite} = 0.474.
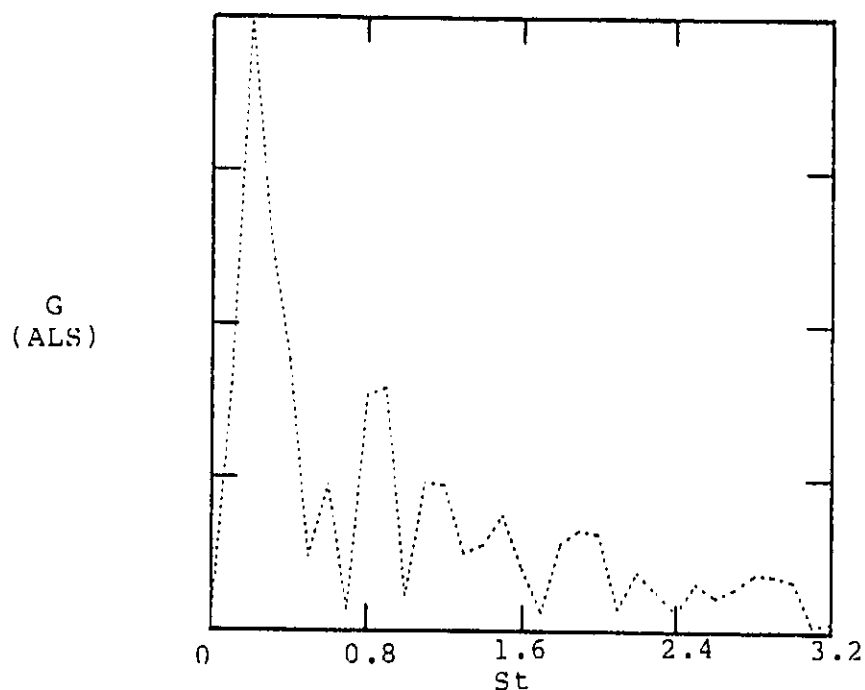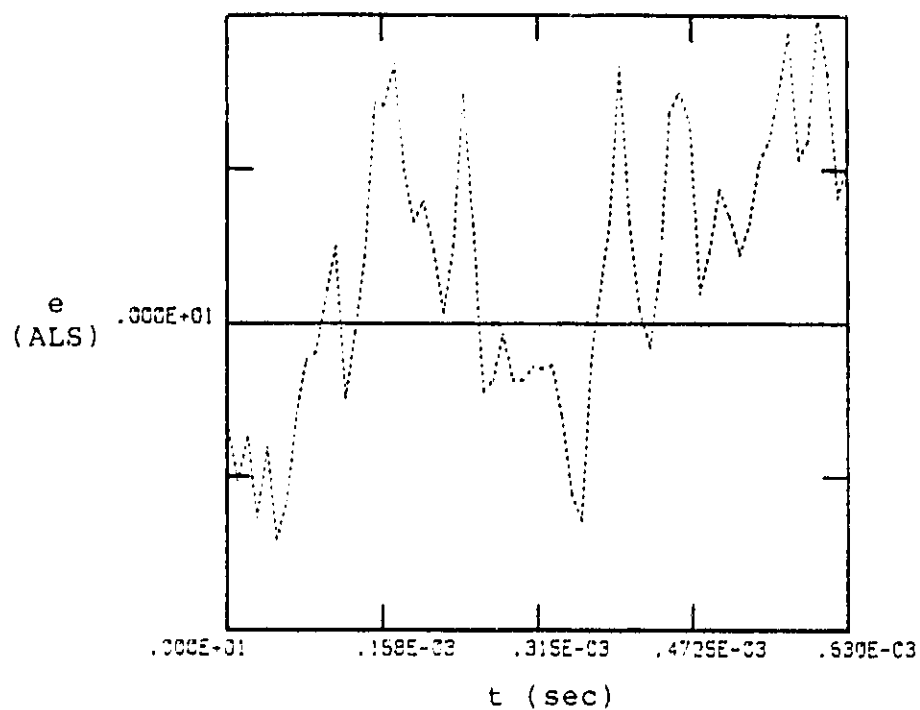
Fig. 50. Temporal and spectral representation of the
phase averaged axial and radial flow fluct-
uation correlation, X/D = 10 , Z/D = -0.06,
St_{excite} = 0.474.

CHAPTER IV

CONCLUSIONS AND RECOMMENDATIONS

4.1 Conclusions

The following conclusions may be drawn from the experimental investigation reported herein.

(1) Mass velocity fluctuation profiles showed that as the excitation frequency increased from St = 0.156 to 0.474, the maximum fluctuation amplitude increased. However, as the excitation frequency increased from St = 0.474 to 1.263, the maximum fluctuation amplitude gradually decreased and the mass velocity profiles developed sooner than the low excitation frequency case.

(2) The overall axial mass velocity fluctuation levels maximized for an excitation frequency of St = 0.474. Therefore, the jet was more responsive to excitation at this frequency since the power input to the exciter was held constant.

(3) The axial mass velocity fluctuations had a higher amplitude than the radial velocity fluctuations and the Reynold's stresses because the axial mass velocity fluctuations include not only the axial velocity fluctuations, but the density fluctuation as well. The Reynold's stresses had the lowest amplitude fluctuation because the correlation between the axial and radial fluctuations decayed faster in amplitude.

(4) The radial velocity fluctuations' radial dependence compared to the axial mass velocity fluctuations had a lower amplitude for the full wave and phase averaged fluctuations and attained a fully developed profile sooner.

(5) The maximum fluctuation levels of the radial velocity fluctuation tend toward the centerline of the jet more rapidly than the maximum mass velocity fluctuations.

(6) The Reynolds stress profiles possess the same general radial dependence as the radial velocity fluctuations profiles for $X/D < 5$ at all excitation frequencies.

(7) The Reynolds stresses tended to decay faster in amplitude than $(\widetilde{\rho u})$ and $(\widetilde{v})$ fluctuations for both the full wave and phased average fluctuations.

(8) The radial velocity fluctuations possessed higher levels of coherence compared to the axial mass velocity and Reynold's stress. The overall coherence of the axial mass velocity, radial velocity, and Reynold's stresses are very high in the potential core for excitation frequencies of $0.316 \leqslant St \leqslant 0.632$. This would suggest that these coherent structures are important in the generation of noise since the jet produced its maximum noise level when excited at these frequencies.

(9) The maximum mass velocity fluctuation levels were not quite as periodic as the time traces obtained at the centerline since the jet attained a higher coherency level

at the centerline.

(10)   The production of several discrete frequencies and spectra broadening as the flow progressed downstream for the axial mass velocity fluctuations at X/D = 10 may indicate stages of non-linear spectral interaction.

(11)   Comparing the time traces of mass velocity and radial velocity fluctuations, it was evident that the time traces were not in phase with each other. This difference in phase could cause the relatively high amplitude harmonics in the Reynold's stress fluctuations; this may explain why there was a high coherency level in the radial velocity fluctuation and Reynold's stresses.

(12)   The corresponding temporal and spectral content of the phase averaged axial and radial flow fluctuation correlation show that the jet did not have a periodic time trace at the maximum amplitude fluctuation at X/D = 1 and 3.

4.2   Recommendations

To futher enhance the state of knowledge in this area, the following studies are recommended:

(1)   Sound pressure level contours of noise that is directly emitted by the coherent structure in the jet should be measured. This set of measurements can provide valuable information about the location and directivity of the coherent noise produced by the jet.

(2)   The Reynolds stress components of the coherent structure should be measured when the jet is not excited. Therefore, two crossed hot wire probes should be used to measure the axial wavelength of the different frequency components being studied. This will help to determine if the artificial exciter is altering these components from the naturally ocurring state.

(3)   The phase relationship between the three different quantities measured by the crossed hot-wire probes $(\widetilde{\rho}u, \widetilde{v}, \bar{\rho}$ $\widetilde{uv})$ should be studied.

(4)   The percentages of the turbulent kinetic energy and turbulence dissipation rate contained in the coherent structure should be measured for the Mach number 0.6 jet.

REFERENCES

1.   Lighthill, M. J., ''On Sound Generated Aerodynamically, I General Theory'', Proc. Roy. Soc., A211 (1952), PP. 546-587.

2.   Lighthill, M. J., ''On Sound Generated Aerodynamically, II Turbulence as a Source of Sound'', Proc. Roy. Soc., A222 (1954), PP. 1-32.

3.   Ffowcs Williams, J. E., ''The Noise From Turbulence Convected at High Speed'', Phil. Trans. Roy. Soc., A255 (1963), PP. 459.

4.   Ribner, H. S., ''The Generation of Sound by Turbulent Jets'', Advances in Applied Mechanics, Vol. 8 (1964), PP. 103-182.

5.   Phillips, O. M., ''On the Generation of Sound by Supersonic Turbulent Shear Layers'', J. Fluid Mech., Vol. 9 (1960), PP. 1-28.

6.   Pao, S. P., and M. V. Lowson., ''Some Applications of Jet Noise Theory'', AIAA Paper No. 70-233, 1970.

7.   Lilley, G. M., P. Morris, and B. J. Tester., ''On the Theory of Jet Noise and its Applications'', AIAA Paper No. 73-987, 1973.

8.   Doak, P. E., ''Analysis of Internally Generated Sound in Continuous Materials: 2. A Critical Review of the Conceptual Adequacy and Physical Scope of Existing Theories of Aerodynamic Noise, with Special Reference to Jet Noise'', Journal of Sound and Vibration., Vol. 25 (1972), PP. 263-335.

9.   Tam, C. K. W., ''On the Noise of Nearly Ideally Expanded Supersonic Jets'', J. Fluid Mech., Vol. 51 (1972), PP. 69-95.

10.   Tam, C. K. W., ''Directional Acoustic Radiation from a Supersonic Jet Generated by Shear Layer Instability'', J. Fluid Mech., Vol. 46 (1971), PP. 757-768.

11.   Tam, C. K. W., ''Supersonic Jet Noise Generated by Large Scale Distubances '', AIAA Paper 73-992, 1973.

12.   Tam, C. K. W., ''Supersonic Jet Noise Generated by Large Scale Disturbances'', J. Sound and Vibration, Vol. 38 (1975), PP. 51-79.

13. Chan, Y. Y., ''Discrete Acoustic Radiation from a High Speed Jet as a Singular Perturbation Problem'', Canadian Aeronautics and Space Journal, Vol. 21 (1975), PP. 221-227.

14. Chan, Y. Y., ''Noise Generated Wavelike Eddies in a Turbulent Jet'', ICAS Paper No. 76-42, 1976

15. Liu, J. T. C., ''Developing Large-Scale Wavelike Eddies and the Near Jet Noise Field'', J. Fluid Mech ., Vol. 62 (1974), PP. 437-464.

16. Morris, P. J., ''The Spatial Viscous Instability of Axisymmetric Jets'', J. Fluid Mech., Vol. 77, Part (1976), PP. 511-529.

17. Morris, P. J., ''Flow Characteristics of a Large-Scale Wavelike Structure of a Supersonic Round Jet'', J. Sound and Vibration, Vol. 53 (1977), PP. 223-244.

18. Winant, C. D. and Browand, F. K., ''Vortex Pairing, the Mechanism of Turbulence Mixing Layer Growth at Moderate Reynolds Numbers'', J. Fluid Mech., Vol. 63 (1974), PP. 237-256.

19. Crow, S. C. and Champagne, F. H., ''Orderly Structure in Jet Turbulenco'', J. Fluid Mech., Vol. 48 (1974), PP. 237-256.

20. Lau, J. C., Fisher, M. J. and Fuchs, H. V., ''The Intrinsic Structure of Turbulent Jets'', J. Sound and Vibration, Vol. 22 (1972), PP. 379-406.

21. McLaughlin, D. K., Morrison, G. L. and Troutt, T. R., ''Experiment on the Instability Waves in a Supersonic Jet and Their Acoustic Radiation'', J. Fluid Mech., Vol. 69 (1976), PP. 73-95.

22. McLaughlin, D. K., Morrison, G. L. and Troutt, T. R., ''Reynolds Number Dependence in Supersonic Jet Noise'', AIAA J., Vol. 15 (1977), PP. 526-532.

23. McLaughlin, D. K., Morrison, G. L. and Troutt, T. R., ''Experiments on the Instability Waves in a Supersonic Jet and Their Acoustic Radiation'', In Proceedings of the Sound Interagency Symposium on University Research in Transportation Noise, Raleigh, North Carolina, June 1974.

24. Morrison, G. L. and McLaughlin, D. K., ''The Instability Process in Low Reynolds Number Supersonic Jets'', AIAA J., Vol. 18 (1980), PP. 793-800.

25. Morrison, G. L. and McLaughlin, D. K., ''The Noise

Generated by Instabilities in Low Reynolds Number Supersonic Jets'', J. Sound and Vibration. Vol. 65 (1979), PP. 177-191.

26. Morrison, G. L., ''Flow Instability and Acoustic Measurements on Low Reynolds Number Supersonic Jets'', Ph.D. Dissertation, Oklahoma State University, 1977.

27. Stromberg, J. L., ''Flowfield and Acoustic Measurements of Low Reynolds Number Jets in a Transonic Range'', M.S. Thesis, Oklahoma State University, 1978.

28. Mollo-Christensen, E., ''Jet Noise and Shear Flow Instability Seen From an Experiment's Viewpoint'', J. Appl. Mech., Vol. 34 (1967), PP. 1-7.

29. Moore, C. J., ''The Role of Shear Layer Instability Waves in Jet Exhaust Noise'', J. Fluid Mech., Vol 80, Part 2 (1977), PP. 321-367.

30. Morrison, G. L. and Whitaker, K. W., ''Mach Number Dependence of the Coherent Structure in High Speed Subsonic Jets'', AIAA. Paper No. 82-49.

31. Browand, F. K. and Laufer, J., ''The Role of Large Scale Structures in the Initial Development of Circular Jets'', Proceeding of the Fourth Biennial Symposium on Turbulence in Liquids, University of Missouri at Rolla. September, 1975.

32. Hussain, A. K., Kleis, S. J., and Sokolov, M., ''A 'Turbulent Spot' in an Axisymmetric Free Shear Layer. Part 2'', J. Fluid Mech., Vol. 98, Part 1 (1980), PP. 97-135.

33. Horstman, C. C. and Rose, W. C., ''Hot-Wire Anemometry in Transonic Flow'', AIAA J., Vol. 15 (1977), PP. 395-401.

34. Johnson, D. A., and Rose, W. C., ''Laser Velocimeter and Hot-wire Anemometer Comparison in a Supersonic Boundary Layer'', AIAA J., Vol. 13, No. 4 (1975), PP. 512-515.

35. Whitaker, K. W., and Morrison, G. L., ''Near Field Acoustic Measurements in Natural and Artificially Excited High Speed Subsonic Jets'', AIAA. Paper No. 83-725.

36. Morrison, G. L., and Wattanachayakul, M., ''Large Scale Structure in a Mach Number 0.7 Jet'', AIAA. Paper No. 81-59.

37. Miksad, R. W., ''Experiments on Non-Linear Interactions in the Transition of a Free Shear Layer'', J. Fluid Mech., Vol. 59 (1973), PP. 1-21.

APPENDIX A

Hot-Wire Data Reduction Technique

A hot-wire data reduction technique similar to that outlined by Horsman and Rose [33] and Johnson and Rose [34] was used in this study. This method let us directly calibrate the sensitivity of the hot-wire to the axial mass velocity and radial velocity for each hot-wire probe used. In this manner, the substantial conduction end losses are accounted for. The sensitivity of the hot-wire to stagnation temperature fluctuations (A_T) is calculated using hot-wire voltage and resistance data recorded at constant flow conditions.

The bridge voltage, E_b, of the hot-wire is comprised of two parts, a fluctuating component, e , and a time averaged mean value, E. An oblique hot-wire responds to axial mass velocity (ρu), stagnation temperature (T_0), and radial velocity (v) fluctuation according to:

$$\frac{e'}{E} = A_m \frac{m'}{\overline{m}} - A_T \frac{T}{T_0} \pm A_v \frac{v'}{u}$$

The sensitivity coefficients A_m, A_T, and A_v can be evaluated as follows:

$$A_m = \frac{\partial \ln E}{\partial \ln(\rho u)} \bigg|_{T_0, R_w, \alpha \text{ constant}}$$

$$A_v = \frac{\partial \ln E}{\partial \alpha} \bigg|_{\rho u, T_0, R_W \text{ constant}}$$

$$A_T = \frac{-\partial \ln E}{\partial \ln T_0} \bigg|_{\rho u, R_W, \alpha \text{ constant}}$$

C-2

both A_m and A_v were evaluated by direct calibration of each wire in the flow using the relations above. Following the method of Horsman and Rose [33] and Johnson and Rose [34] the stagnation temperature sensitivity was evaluated as follows:

$$A_T = \frac{\ln T_W}{\ln R_W} \left[\frac{\ln E}{\ln R_W} + \frac{1}{2} - \frac{R_W}{R_W + R_S} \right] + 0.765 \, A_m - 0.9425$$

The crossed hot-wires were matched so that A_m and A_v were approximately the same for each wire. The output of the two wires were then instantaneously added and subtracted so that the two resulting voltages would be proportional to m'/m and $v'/\overline{U}$. Hence, neglecting stagnation temperature fluctuations:

$$(e_1 - e_2)_{rms} = (E_1 A_{v1} + E_2 A_{v2}) \left(\frac{v'}{\overline{u}} \right)_{rms}$$

$$(e_1 + e_2)_{rms} = (E_1 A_{m1} + E_2 A_{m2}) \, \widetilde{m}$$

where $(e_1 - e_2)_{rms}$ corresponds to radial velocity fluctuations and $(e_1 + e_2)_{rms}$ to axial mass velocity fluctuations.

APPENDIX B

```
C-------> THIS PROGRAM IS WRITTEN FOR EXCITED JET MACH#= .6
      DIMENSION
NAME(6),R1DATA(100),R2DATA(100),R3DATA(100),X(100)
     *,DATA(2,100),XMULT(100)
      WRITE(2,43)
  43
FORMAT(1X,3X,'Z',4X,'E1',4X,'E2',5X,'SUM',5X,'DIFF',5X,
     *'UVRMS',5X,'AM1',5X,'AM2',5X,'MBAR',6X,'M/MBAR',4X,'V/
VBAR',
     *3X,'RHO*UV',4X,'FM/MBAR',4X,'FV/VBAR',3X,'FRHO*UV')
      WRITE(3,66)
  66    FORMAT(' WHAT IS BIO S.RATE,SEC(F10.4),AND EXCITED
FREQUNCY,I6'/)
      READ(3,67)BSR,IFRQ
  67    FORMAT(F10.4,I6)
  111   FORMAT(' BIO SAMPLING RATE=',F10.7)
  112   FORMAT(' EXCITED FREQUNCY=',I6)
      WRITE(3,4)
  4     FORMAT(1X,'WHAT IS THE NAME OF THE FILE TO WRITE
IN?',/)
      READ(3,5)(NAME(I),I=1,6,1)
    5 FORMAT(6A2)
      CALL OPEN(6,NAME,2)
      WRITE(6,111)BSR
C-------> READING SAMPLING RATE
      WRITE(6,112)IFRQ
C-------> READING EXCITATATION FREQUENCY
      DO 900 I=1,100
      X(I)=I
  900   CONTINUE
      DO 333 I=1,100
      R1DATA(I)=0.0
      R2DATA(I)=0.0
      R3DATA(I)=0.0
  333   CONTINUE
      WRITE(3,6)
  6     FORMAT(' WHAT IS THE BIO SENSITIVITY=? (F4.1)',/)
      READ(3,7)BS
  7     FORMAT(F4.1)
      WRITE(6,113)BS
  113   FORMAT(' BIO SENSITIVITY=',F4.1)
      WRITE(3,21)
  21    FORMAT(' HOW MANY TIMES DO YOU WANT TO TRIGGER BIO',/)
---------> NUMBER OF TRIGGERING OF TIMES BIOMATION
      READ(3,22)NN
  22    FORMAT(I3)
      CALL DC(1.,1000,DC1)
      CALL DC(2.,1000,DC2)
---------> READING DC VALUE
```

```
      DO 334 KK=1,NN
      WRITE(3,888)KK
  888 FORMAT(' SAMPLE NUMBER ',I3)
      CALL SUBBI2(DATA)
      DO 23 I=1,100
      R1DATA(I)=DATA(1,I)+R1DATA(I)
      R2DATA(I)=DATA(2,I)+R2DATA(I)
   23 CONTINUE
      SUM1=0.
      SUM2=0.
      DO 24 I=1,100
      SUM1=SUM1+DATA(1,I)
      SUM2=SUM2+DATA(2,I)
   24 CONTINUE
      SUM1=SUM1/100.
      SUM2=SUM2/100.
      DO 25 I=1,100
      XMULT(I)=(DATA(1,I)-SUM1)*(DATA(2,I)-SUM2)*(BS/256.)**
    2
   25 R3DATA(I)=XMULT(I)+R3DATA(I)
      IF(KK.GT.10)GO TO 26
--------> FINDING RMS VALUE
      CALL RMSV(ANS,XMULT,100)
      XSUM=ANS+XSUM
   26 CONTINUE
  334 CONTINUE
      SUM1=0.0
      SUM2=0.0
      DO 10 I=1,100
      SUM1=SUM1+R1DATA(I)
      SUM2=SUM2+R2DATA(I)
   10 CONTINUE
      AVE1=SUM1/100.
      AVE2=SUM2/100.
      WRITE(3,392)AVE1,AVE2
  392 FORMAT(' AVE1=',E11.4,' AVE2=',E11.4)
      DO 20 I=1,100
      R1DATA(I)=(R1DATA(I)-AVE1)*BS/256.
      R2DATA(I)=(R2DATA(I)-AVE2)*BS/256.
   20 CONTINUE
      E2=DC2
      E1=DC1
      WRITE(3,18)E1,E2
   18 FORMAT(' E1=',F4.2,' E2=',F4.2)
      IF(E2.GT.5.0)GO TO 1000
      IF(E2.GT.4.5)GO TO 1002
      A20=2.61437
      A21=0.31366
      A22=-0.012717
      GO TO 1001
 1000 A20=4.2398
      A21=0.03529
```

```
      A22=-0 000185
      GO TO 1001
 1002 A20=3.7868
      A21=0.071825
      A22=-.0009514
 1001 CONTINUE
      IF(E1.GT.5.)GO TO 1003
      IF(E1.GT.4.5)GO TO 1004
      A10=2.61437
      A11=0.31366
      A12=-0.012717
      GO TO 1005
 1003 A10=4.2398
      A11=0.03529
      A12=-0.000185
      GO TO 1005
 1004 A10=3.7868
      A11=0.071825
      A12=-0.0009514
 1005 CONTINUE
--------> FINDING HOT-WIRE COEFFICIENT
      DISC=A11*A11-4.*A12*(A10-E1)
      RM1=(-1.*A11+SQRT(DISC))/(2.*A12)
      DISC=A21*A21-4.*A22*(A20-E2)
      RM2=(-1.*A21+SQRT(DISC))/(2.*A22)
      AM1=(RM1*(A11+2.*A12*RM1)/(A10+A11*RM1+A12*RM1*RM1))
      AM2=((RM2*(A21+2.*A22*RM2))/(A20+A21*RM2+A22*RM2*RM2))

      AV1=-0.077114
      AV2=0.0727741
      R1XMAX=0.0
      R1XMIN=0.0
      R2XMAX=0.0
      R2XMIN=0.0
      R3XMAX=0.0
      R3XMIN=0.0
      DO 222 I=1,100
      R1DATA(I)=R1DATA(I)/KK
      IF(R1DATA(I).GT.R1XMAX)R1XMAX=R1DATA(I)
      IF(R1DATA(I).LT.R1XMIN)R1XMIN=R1DATA(I)
      R2DATA(I)=R2DATA(I)/KK
      IF(R2DATA(I).GT.R2XMAX)R2XMAX=R2DATA(I)
      IF(R2DATA(I).LT.R2XMIN)R2XMIN=R2DATA(I)
      R3DATA(I)=R3DATA(I)/KK
      IF(R3DATA(I).GT.R3XMAX)R3XMAX=R3DATA(I)
      IF(R3DATA(I).LT.R3XMIN)R3XMIN=R3DATA(I)
 222  CONTINUE
----------> PLOT ON CRT
      CALL CRT(X,R1DATA,R1XMAX,R1XMIN,100.,1.,100)
      PAUSE
      CALL CRT(X,R2DATA,R2XMAX,R2XMIN,100.,1.,100)
      PAUSE
```

```
      CALL CRT(X,R3DATA,R3XMAX,R3XMIN,100.,1.,100)
      PAUSE
      CALL RMSV(SUMRMS,R1DATA,100)
      CALL RMSV(DIFRMS,R2DATA,100)
      CALL RMSV(UVRMS,R3DATA,100)
      RHOU=(RM1+RM2)/2.
      TWIM=SUMRMS/(E1*AM1+E2*AM2)
      VPRIMU=DIFRMS/(E2*AV2-E1*AV1)
      RUOUV=UVRMS/((E1*AM1+E2*AM2)*(E2*AV2-E1*AV1))
      WRITE(3,527)
  527 FORMAT(' WHAT IS VALUE OF (SUMFRU,SUMFV,F8.4,)',/)
      READ(3,528)SUMFRU,SUMFV
  528 FORMAT(2F8.5)
      SUMFUV=XSUM/10.
      FVPRIM=SUMFV/(E2*AV2-E1*AV1)
      FTWIM=SUMFRU/(E1*AM1+E2*AM2)
      FRUOUV=SUMFUV/((E1*AM1+E2*AM2)*(E2*AV2-E1*AV1))
      WRITE(3,288)
  288 FORMAT(' WHAT IS THE LOCATION OF (X),(Y),(Z),6.3',/)
      READ(3,289)X1,Y,Z
  289 FORMAT(3F7.3)
      WRITE(6,290)X1,Y,Z
  290 FORMAT(' X=',F7.3,' Y=',F7.3,' Z=',F7.3)
      WRITE(3,28)
  28  FORMAT(' WHAT IS THE STAG PO ("HG,F4.2),AND TO
     (I2)',/)
      READ(3,29)PO,ITO
  29  FORMAT(F6.3,I2)
      WRITE(6,45)PO,ITO
  45  FORMAT(' PO=',F6.3,' TEMP=',I2)
      WRITE(6,30)E1,E2
  30  FORMAT(' DC1=',E11.4,' DC2=',E11.4)
      WRITE(6,32)AM1,AM2
  32  FORMAT(' AM1=',E11.4,' AM2=',E11.4)
      WRITE(6,34)RHOU
  34  FORMAT(' RHOU AVE=',E11.4)
      WRITE(6,42)RUOUV
  42  FORMAT(' RUOUV=',E11.4)
      WRITE(6,35)TWIM,VPRIMU
  35  FORMAT(' RHOU PRIME(RMS)/RHOU AVE=',E11.4,' VPRIME RMS
     */VAVE=',E11.4)
      WRITE(6,39)FTWIM,FVPRIM,FRUOUV
  39  FORMAT(' FRHOU PRIME/RHOU AVE=',E11.4,'
     FVPRIME/VAVE',E11.4
     *,' FRUOUV=',E11.4)
      WRITE(2,44)Z,E1,E2,SUMRMS,DIFRMS,UVRMS,AM1,AM2,RHOU,TW
     IM,
     *VPRIMU,RUOUV,FTWIM,FVPRIM,FRUOUV
  44
FORMAT(1X,F6.3,1X,F5.3,1X,F5.3,1X,F6.4,3X,F6.4,2X,F7.4,2X,
     *F7.5,1X,F7.5,2X,F8.3,4X,F7.5,1X,F7.5,F10.5,4X,F7.5,4X,
     F7.5,
```

```
      *2X,F8.5)
       WRITE(3,8888)
 8888 FORMAT(' READY TO WRITE DATA ON DISK')
       WRITE(6,37)(R1DATA(I),R2DATA(I),R3DATA(I),I=1,100,1)
 37    FORMAT(1X,6E11.4)
       ENDFILE 6
       STOP
       END

C***************************************************************
C       THIS PROGRAM USES THE FAST FOURIER TRANSFORM ALGOR-  *
C  ITTHM AND IT MUST BE CALLED FROM MAIN PROGRAM.            *
C***************************************************************
       SUBROUTINE FFT(XREAL,XIMAG,N,NU)
       DIMENSION XREAL(N),XIMAG(N)
       N2=N/2
       NU1=NU-1
       K=0
       DO 100 L=1,NU
 102   DO 101 I=1,N2
       P=IBITR(K/2**NU1,NU)
       ARG=6.283185*P/FLOAT(N)
       C=COS(ARG)
       S=SIN(ARG)
       K1=K+1
       K1N2=K1+N2
       TREAL=XREAL(K1N2)*C+XIMAG(K1N2)*S
       TIMAG=XIMAG(K1N2)*C-XREAL(K1N2)*S
       XREAL(K1N2)=XREAL(K1)-TREAL
       XIMAG(K1N2)=XIMAG(K1)-TIMAG
       XREAL(K1)=XREAL(K1)+TREAL
       XIMAG(K1)=XIMAG(K1)+TIMAG
 101   K=K+1
       K=K+N2
       IF(K.LT.N)GO TO 102
       K=0
       NU1=NU1-1
 100   N2=N2/2
       DO 103 K=1,N
       I=IBITR(K-1,NU)+1
       IF(I.LE.K)GO TO 103
       TREAL=XREAL(K)
       TIMAG=XIMAG(K)
       XREAL(K)=XREAL(I)
       XIMAG(K)=XIMAG(I)
       XREAL(I)=TREAL
       XIMAG(I)=TIMAG
 103   CONTINUE
       RETURN
       END
       FUNCTION IBITR(J,NU)
       J1=J
```

```
        IBITR=0
        DO 200 I=1,NU
        J2=J1/2
        IBITR=IBITR*2+(J1-2*J2)
  200   J1=J2
        RETURN
        END

        SUBROUTINE DC(CH,NUM,DATA)
        DATA=0.0
        DO 1 I=1,NUM,1
        CALL ATOD(CH,X)
        DATA=DATA+X
    1   CONTINUE
        DATA=DATA/NUM
        RETURN
        END

        SUBROUTINE SUBBI2(DATA)
C DATA IS AN ARRAY (2,2048) WHICH CONTAINS THE SAMPLED DATA
FROM THE
C TWO (1 AND 2) DIFFERENT CHANNELS. IT IS AN INTEGER ARRAY
IN ORDER TO MINIMIZE
C STORAGE USAGE.
C IJ = NUMBER OF CHANNELS TO BE RECORDED
C NUM = NUMBER OF DATA POINTS PER CHANNEL
C THIS PROGRAM MUST HAVE THE SAMPLE RATE SET ON THE
BIOMATION.
C THIS PROGRAM IS TO CONTROL THE BIOMATION 2805 WAVE FORM
DIGITIZER
        DIMENSION DATA(2,100)
C SET ARM, OPT AND WDC HIGH AND CBEN LOW
        CALL OUT(32,56)
C ARM THE DIGITIZER TO TAKE DATA
        CALL OUT(32,48)
        CALL OUT(32,56)
        WRITE(3,100)
  100   FORMAT(' BIOMATION HAS BEEN ARMED')
C SEE WHEN RECORD AND FLAG GO LOW SAYING DATA IS READY
   10   J=INP(32)
        IF(J-4)10,11,10
   11   CONTINUE
C DATA HAS BEEN RECORDED NOW SELECT A CHANNEL AND TRANSFER
ITS DATA
        WRITE(3,101)
  101   FORMAT(' DATA HAS BEEN RECORDED')
        IJ=2
        DO 13 K=1,IJ,1
        KK=K-1+56
        CALL OUT(32,KK)
        WRITE(3,989)KK
  989   FORMAT(I5)
```

```
C SET OPT LOW SO THE BIOMATION WILL START TO TRANSMIT DATA
      KKK=KK-16
      CALL OUT(32,KKK)
      DO 14 JK=1,200,1
   15 J=INP(32)
      IF(J.EQ.14)GO TO 16
      GO TO 15
   16 CONTINUE
      LMN=INP(40)
      IF(LMN.LT.0)LMN=LMN+255
      DATA(K,JK)=FLOAT(LMN)
C REQUEST A NEW WORD BY PULSING WDC
      KKK=KKK-32
      CALL OUT(32,KKK)
      KKK=KKK+32
      CALL OUT(32,KKK)
   14 CONTINUE
C SET OPT HIGH SO NEW CHANNEL CAN BE SELECTED
      KKK=KKK+16
      CALL OUT(32,KKK)
   13 CONTINUE
      RETURN
      END


      SUBROUTINE RMSV(RMS,DATA,N)
C*********** (N) IS NUMBER OF DATA POINT
      DIMENSION DATA(100)
      SUM=0.0
      DO 1 I=1,N
      SUM=SUM+DATA(I)
    1     CONTINUE
      DC=SUM/N
      R=0.0
      DO 2 I=1,N
      R=R+((DATA(I)-DC)**2)
    2     CONTINUE
      R=R**0.5
      RMS=R/(N**0.5)
      RETURN
      END
```

VITA

Saied Emamai the son of Mr&Mrs Hassan Agha Emami was born on ████████ ███ in ██████ ███. He received his high school education at Khamenee'poor School, Tehran, Iran.

He received a AA degree in elementry Engineering from Weaterford College in May 1977. He received also a Bachelor degree in Mechnical Engineering from Texas A&M University in May 1981. He intends to remain at Teaxas A&M University after earning his degree of Master of Science to work towards his degree of Doctor of Philosophy in Mechanical Engineering. His permanent address is:

Saied Emami

c/o Wanda Ballow

1300 Brierwood

Weatherford, Texas 76086

Ph: 817 - 594 - 6667